MISFIT ACCOMMODATION IN THIN FILMS OF Ni/Cu AS MEASURED BY MAGNETIC ANISOTROPY

by

HEATHER ELIZABETH INGLEFIELD

B. S. in Physics and Psychology
Bates College 1989

SUBMITTED TO THE DEPARTMENT OF MATERIALS SCIENCE AND ENGINEERING IN PARTIAL FULFILLMENT OF THE REQUIREMENTS FOR THE DEGREE OF

DOCTOR OF PHILOSOPHY

at the

MASSACHUSETTS INSTITUTE OF TECHNOLOGY

June, 1995

Author.....
Department of Materials Science and Engineering
May 5, 1995

Certified
by.....
Carl V. Thompson
Professor of Electronic Materials
Thesis Supervisor

Accepted
by.....
Carl V. Thompson
Professor of Electronic Materials
Chair, Departmental Committee on Graduate Students

MISFIT ACCOMMODATION IN EPITAXIAL Ni/Cu AS MEASURED BY MAGNETIC ANISOTROPY

by

Heather Elizabeth Inglefield

Submitted to the Department of Materials Science and Engineering on May 5, 1995 in partial fulfillment of the requirements for the degree of Doctor Of Philosophy in Materials Science

ABSTRACT

The measurement of misfit strain and misfit accommodation in Ni/Cu (001) has been made in conjunction with measurements of magnetic anisotropy in order to explore the possibility of using anisotropy measurements as a convenient *in situ* method of strain evaluation in magnetic thin films. Epitaxial Ni films with thickness ranging between 10Å and 200Å were deposited using e-beam evaporation under UHV conditions on epitaxial Cu films grown on NaCl and Si substrates. Misfit dislocation content was characterized using transmission electron microscopy (TEM). Ni film strain was measured *ex situ* using substrate curvature measurements. Magnetic properties were determined qualitatively *in situ* using the magneto-optic Kerr effect. Magnetic anisotropy energy was measured *ex situ* using vibrating sample magnetometry. Microscopy results indicate the presence of two types of misfit dislocation at the Ni/Cu interface, 60° dislocations with Burgers vector inclined to the interface plane, and 90° dislocations with Burgers vector lying in the plane of the interface. Average dislocation spacing was measured using TEM, and was found to decrease with increasing Ni thickness. Strain measurements indicated that the increased misfit dislocation content resulted in a decrease in strain. *In situ* magnetic characterization showed that, for low Ni thicknesses (high strain), the preferred magnetization direction was perpendicular to the plane of the film. At higher thicknesses (lower strain) the preferred direction was in the plane of the film. *Ex situ* quantitative measurement of magnetic anisotropy energy confirmed this result. The anisotropy measurements, combined with strain measurements, were analyzed using a modified version of the Neél pair interaction model. From this analysis, values for the surface magnetocrystalline and surface magnetoelastic anisotropy energies were determined. A quantitative relationship between strain and magnetic anisotropy has therefore been established which is useful for *in situ* study of the strain and strain evolution in these films through magnetic characterization.

Thesis Supervisor: Carl V. Thompson
Professor of Electronic Materials

TABLE OF CONTENTS

LIST OF FIGURES

LIST OF TABLES

ACKNOWLEDGEMENTS

There are many I wish to thank without whom this thesis would not have been possible.

First and foremost, I wish to thank my advisor, Carl Thompson, for his guidance and encouragement during my graduate career. He has taught me much about the art of scientific research. I also am grateful to my co-advisor Bob O'Handley for his advice, good humor, and exciting and illuminating scientific discussions.

I wish to thank the other members of my committee, L. C. Kimerling and John Vander Sande, for their advice.

Craig Ballentine and Jerry Floro taught me all the intricacies of working with vacuum deposition systems. For this I am exceedingly grateful.

I thank my partner in this work, Gabriel Bochi for his insight into the magnetic properties of thin films, and in particular, the use of the modified Neél model to describe magnetic anisotropy in Ni/Cu (001).

I thank K. Das Chowdhury for his work in the analysis of the Cu/Si interface and his helpful discussions on TEM technique.

The members of the CMSE have been an invaluable resource to me during my time here at MIT, including, but not limited to, Mike Frongillo, Tony Garrat-Read, Fred Wilson, Libby Shaw, Rich Perilli, Tim McClure, and Pat Kearney.

I would also like to thank the members of the submicron materials research group, as well as all the friends I have made while at MIT. There are far too many to list here. These are the people that have made graduate school fun.

I wish to acknowledge the love and support of my parents, who as professionals have been a source of inspiration to me.

Finally, I wish to thank Jeff, who will soon become my husband, for loving me and believing in me throughout this whole ordeal.

1. CHAPTER 1: MISFIT AND MAGNETIC PROPERTIES

1.1 INTRODUCTION

The presence of misfit strain and the relief of that strain through the formation of misfit dislocations can have significant effects on materials properties and performance. The electronic properties of semiconductor materials are strongly affected by dislocations at the interface. For instance, the presence of misfit dislocations can increase the carrier mobility in $In_xGa_{1-x}As/GaAs$ strained layer superlattices by 500%.[1] Additionally, metastable strained layers can have properties which are useful in certain kinds of devices.[2] It is necessary, therefore, to thoroughly understand misfit and misfit accommodation through dislocation formation in order to determine the conditions under which it is possible to deposit a metastable, undislocated strained layer, and to determine the extent to which dislocations relief misfit strain. One other type of material property which is strongly affected by misfit strain is magnetic anisotropy. The exact nature of this influence has to date been poorly understood. In conjunction with this work, a phenomelogical model defining the relationship between misfit strain and magnetic anisotropy has been developed.[3]

Dislocation formation and strain relief have been studied extensively *ex situ* using a variety of techniques, most commonly electron microscopy. The kinetics of the process have been studied by Hull and coworkers *ex situ* by annealing samples in a transmission electron microscope (TEM) and monitoring dislocation motion.[4] The development of an *in situ* technique would be highly advantageous. In most cases, misfit

accommodation occurs during growth, with only some additional strain relief upon *ex situ* annealing. Additionally, *ex situ* studies are complicated by such factors as contamination and oxidation.

A few *in situ* techniques have been developed to date for the study of misfit dislocation formation. Whaley and Cohen[2] measured the surface lattice constant of InGaAs/GaAs films using RHEED to determine strain due to misfit. They were able to determine the lattice constant to within 0.003Å, and thus resolve the strain to within 0.05%. This technique was also used by Springholtz, *et al.*[5] in conjunction with STM to measure misfit relaxation in EuTe/PbTe (111). Celii *et al.*[6] used scattering of laser light to measure relaxation in InGaAs/GaAs. All these techniques have limitations, however. Measurement of lattice constant via RHEED cannot be performed during deposition due to oscillations in the intensity of the diffraction spots that occurs during growth. Additionally, it requires a smooth surface (sharper diffraction spots) for high precision. The use of STM and light scattering depend on the fact that, in films with very smooth surfaces, the presence of misfit dislocations is accompanied by the formation of surface steps, with the step density equal to the misfit dislocation density. It is therefore an indirect measure of misfit accommodation. Again, an otherwise smooth surface is required. If there are other factors affecting the surface roughness, these methods are invalid.

The goal of this thesis is to develop magnetic characterization as an *in situ* tool for the study of misfit accommodation by defining the relationship between anisotropy energy and strain. The relationship between magnetic anisotropy and strain make the measurement of magnetic hysteresis a useful tool for the analysis of strain and strain relaxation in magnetic thin films. The technique has advantages over the ones discussed above in that it can be used for ultrathin films, and is sensitive only to changes in the Ni layer. It could also be performed during deposition. In the experiments described in this thesis, the *in situ* measurement of the magneto-optic Kerr effect has been used in conjunction with extensive *ex situ* analysis to study misfit strain accommodation and magnetic anisotropy energy in Ni/Cu epitaxial thin films.

This document will first describe the characterization of strain in Ni/Cu (100) as a function of Ni thickness as measured by substrate curvature. Detailed microscopy that

shows misfit dislocations as being the primary means of misfit accommodation will be outlined. These measurements are then used in conjunction with *in situ* and *ex situ* measurements of magnetic anisotropy energy to determine quantitatively the relationship between strain and magnetic anisotropy. After establishing this relationship, work is described showing how magnetic anisotropy energy can be used to characterized the strain behavior of the Ni/Cu system under different strain conditions.

1.2 BACKGROUND

Misfit refers to the degree of difference between the lattice constants of the substrate and of the epitaxial layer, denoted η where $\eta = \frac{a_e - a_s}{a_e}$, where a_e and a_s are the lattice constants of the epitaxial layer and substrate, respectively. The presence of misfit induces a strain in the film equal to η due to the fact that the atomic positions of the epitaxial layer will tend to align with those of the substrate at the interface. Initially, all this strain will be elastic. The entire epitaxial film will be tetragonally distorted and the total strain energy will increase with film thickness. Above some critical thickness h_C, it becomes energetically favorable to relieve some of this strain by creating dislocations at the interface. The presence of dislocations allows the atoms to position themselves close to the substrate atoms at the interface, while atoms away from the interface are relaxed, approaching the bulk spacing. This idea is illustrated in Figure 1.1. Here when the term "misfit dislocation" is used, it indicates only those dislocations or portions of dislocations which are at the interface and act to relieve misfit. In order for a dislocation to relieve misfit between two layers, Burgers vector must project a non-zero length in the plane of the interface and perpendicular to the dislocation line.

The system studied was Ni/Cu (100). This system has a misfit of 2.6%, which must be accommodated by either elastic deformation (coherent film and substrate) or plastic deformation (mostly in the form of misfit dislocations). A goal of this work has been to characterize the formation of the dislocated interface. In order to achieve this goal, the structure of the interface has been observed directly using transmission electron microscopy, and the residual elastic strain has been measured indirectly using a number

of techniques. The primary means of measuring strain has been through the measurement of the bending of the substrate in response to that strain. In addition, strain has been measured in some samples by measuring the spacing of moiré fringes observed in TEM.

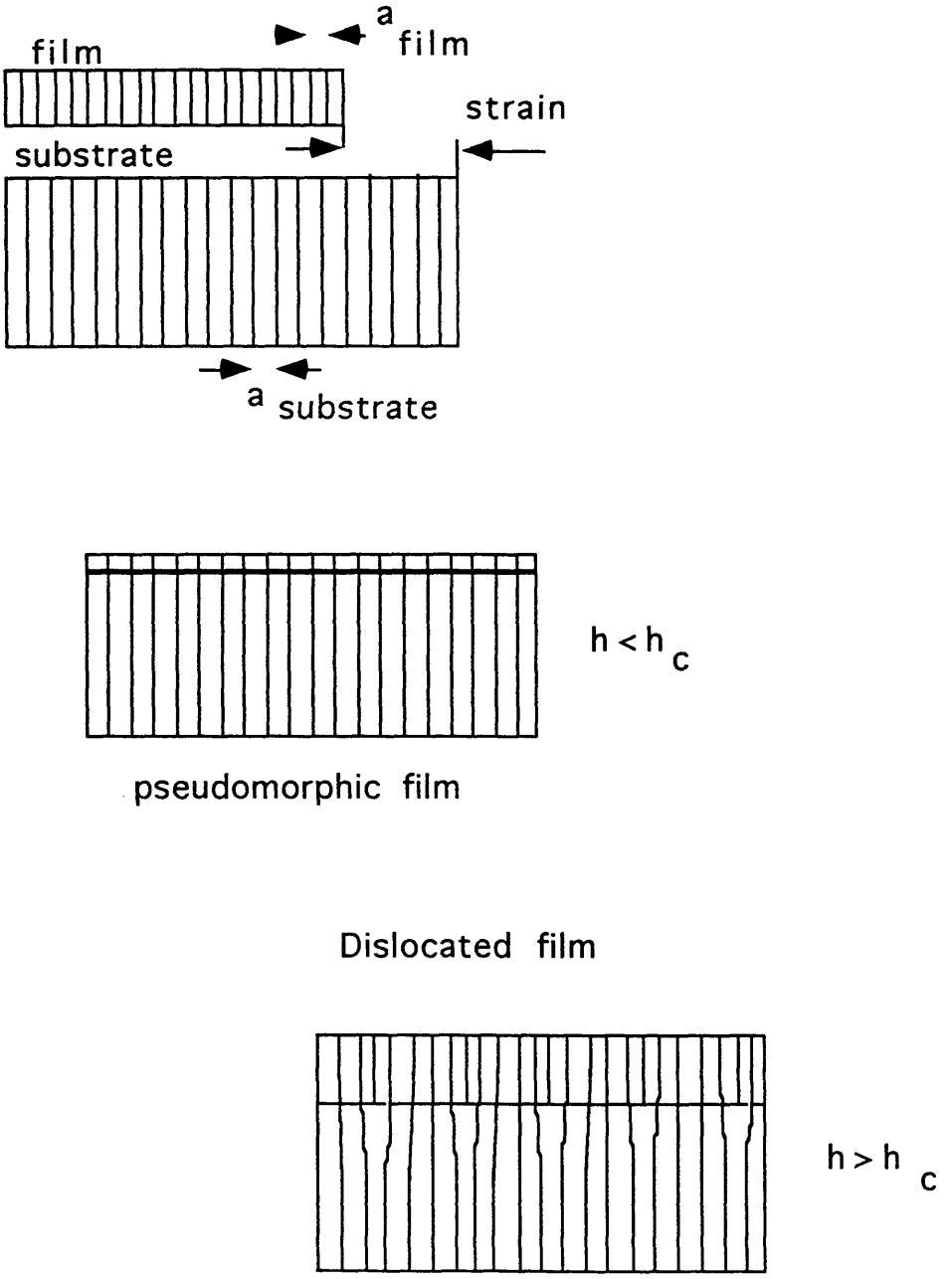

Figure 1.1 Illustration of misfit dislocation formation

By far the most unique measurement of strain in this system has been the measurement of magnetic anisotropy. It is known that magnetic properties, particularly magnetic anisotropy, are strongly affected by strain. This relationship has been exploited in this work as a way of monitoring strain *in situ* using the magneto-optic Kerr effect. The results of this work clearly show that magnetic anisotropy is a useful way of measuring misfit strain in epitaxial thin films of magnetic materials.

1.3 THE Ni/Cu (100) SYSTEM

The nickel/copper epitaxial system has been studied extensively by various researchers.[7,8,9,10,11,12,13,14,15] Nickel and copper are both fcc metals with lattice constants of 3.542Å and 3.615Å respectively, giving a misfit for the (100) orientation of 2.6%. With this small, but significant misfit, Ni grows pseudomorphically on Cu fairly easily, but the system is under a measureable strain at low thicknesses. One other important property of the Ni-Cu system is that while the two metals are effectively completely miscible, forming no intermetallic compounds. The diffusion coefficients at the temperatures reached in these experiments do not exceed 10^{-28} cm^2/s, so it is likely that there will exist a relatively sharp interface which will be easy to model.

Epitaxy of Ni on Cu is fairly easy to acheive, and occurs for deposition at room temperature in UHV. In the (100) orientation, an orthogonal grid of dislocations forms at the interface for sufficiently thick Ni layers. The dislocation lines lie along <110> directions. The measured critical thickness for dislocation formation is very close to the theoretical thermodynamic limit, about 15Å.[10]

The magnetic properties of the Ni/Cu system have been studied as well.[16,17,18,19] It has been shown that the Curie temperature decreases with decreasing Ni thickness, and approaches room temperature at about 2 monolayers.[20] Naik, et. al.[21] found that 50Å Ni on a Cu(100) substrate had a tendency to show anisotropy perpendicular to the film. Although these findings have affected this research, the strength of the magnetic anisotropy has not been reported. Measurements of the anisotropy of the Ni film are part of the main focus of this work. Bulk Ni is known to have strong magnetoelastic

properties relative to the strength of the magnetic anisotropy, making it easier to determine strain effects on the M-H loop. This property, along with the 2.6% misfit with respect to Cu, which allows Ni to grow epitaxially on Cu, but with a measurable amount of strain, make the Ni/Cu system ideal for this work.

This project is unique in that it combines magnetic characterization of Ni/Cu with extensive microstructural analysis. In general, interpretation of magnetic anisotropy in thin films has been based on the phenomelogical Neél model described later in this chapter. In this study, this type of analysis is made more complete with the additional information gained from the structural characterization.

1.4 MISFIT

1.4.1 Thermodynamics of misfit—the Matthew's Blakeslee model

The presence of misfit dislocations in a heteroepitaxial film can be explained from a thermodynamic perspective. Calculating the critical thickness and dislocation density as a function of thickness is a matter of balancing strain energy with dislocation energy. This method was originally proposed by Matthews et al.[22] The derivation given here follows a straightforward form of this analysis by Tsao. [23] The energy per unit area for a strained layer is

$$\mathbf{U}_{\mathbf{coh}} = 2Mh\varepsilon^2 \tag{1.1}$$

where M is the biaxial modulus, and h is the film thickness. The strain is equal to

$$\varepsilon = \eta - \rho b \cos\lambda \tag{1.2}$$

where ρ is the linear dislocation density, b is the Burgers vector, and λ is the angle between **b** and the direction normal to the dislocation line in the plane of the interface. In other words, the edge component of the Burgers vector that lies in the interface plane

acts to relieve misfit. It is possible to imagine this edge component as an extra half-plane of atoms inserted into the film at the interface as seen in Figure 1.1. As can be seen from this equation, the component of the misfit dislocations lying in the plane of the film acts directly to reduce the overall strain. A comparison of Equations (1.1) and (1.2) shows that, when there are no dislocations present, the strain energy increases linearly with film thickness.

The energy per unit length associated with the formation of a dislocation is given by

$$\mathbf{U}_{edg} = \frac{\mu b_{edg}^2}{4\pi(1-\nu)} \ln\left(\frac{R}{r_0}\right) \tag{1.3}$$

and

$$\mathbf{U}_{scr} = \frac{\mu b_{scr}}{4\pi} \ln\left(\frac{R}{r_0}\right) \tag{1.4}$$

for an edge and screw dislocation respectively, where μ is the shear modulus of the film, ν is Poisson's ratio, and r_0 and R are the inner and outer radii of the cylindrical strain field surrounding the dislocation line. The inner radius represents the distance at which continuum elastic theory breaks down. It is often estimated as b/4. The outer radius, in the case of a thin film, is the thickness h. For the general case of a mixed dislocation,

$$\mathbf{U}_{dis} = \rho \frac{\mu b^2}{4\pi(1+\nu)} \ln\left(\frac{4h}{b}\right) \tag{1.5}$$

The dislocation density which gives the lowest energy can be determined from minimization of the derivative of the total energy

$$\mathbf{U}_{tot} = \mathbf{U}_{coh} + 2\,\mathbf{U}_{dis} \tag{1.6}$$

giving

$$\rho = \left(\frac{\eta}{b\cos\lambda}\right) - \frac{\left(1-\nu\cos^2\beta\right)}{8\pi h\cos^2\lambda(1+\nu)}\ln\left(\frac{4h}{b}\right) \qquad (1.7)$$

Combining equations 1.2 and 1.5 gives the dependence of strain on film thickness:

$$\varepsilon = \frac{b}{8\pi\cos\lambda}\frac{\left(1-\nu\cos^2\beta\right)}{(1+\nu)}\ln\left(\frac{4h}{b}\right). \qquad (1.8)$$

The density of dislocations needed to relieve misfit in the film therfore increases (or, alternatively, the spacing between them decreases) as a function of film thickness, resulting in a decrease in strain, as shown in Figure 1.2.

There is a critical thickness at which the dislocations begin to form which can be determined by setting equation (1.7) equal to zero giving

$$h_c = \frac{b}{8\pi\eta(1+\nu)}\ln\left(\frac{4h_c}{b}\right). \qquad (1.9)$$

Similarly, equation (1.7) can be solved to give a critical misfit for a given thickness:

$$f_c = \frac{b}{8\pi h\cos\lambda}\left(\frac{1-\nu\cos^2\beta}{1+\nu}\right)\ln\left(\frac{4h}{b}\right). \qquad (1.10)$$

This approach is based on some broad assumptions. In particular, it assumes that dislocations are evenly spaced. Due to the higher strain, dislocations will have a tendency to form near where other dislocations already exist, resulting in some degree of clustering of dislocations. This effect has been seen clearly in our films and is shown in plan-view TEM micrographs. The energy of a system of randomly spaced dislocations can be calculated by sequentially adding the effects of each surrounding dislocation as has been illustrated by Dodson.[24]

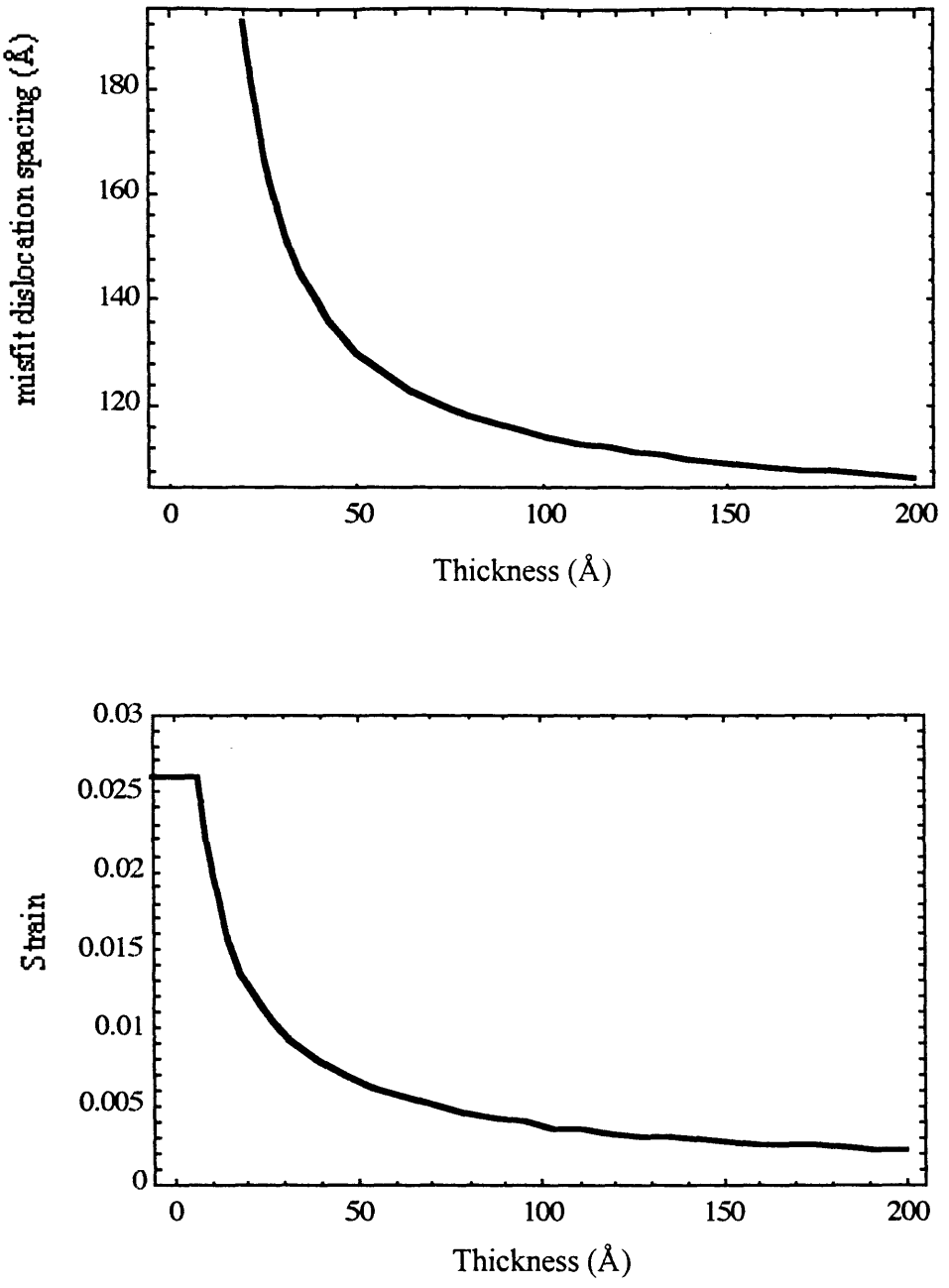

Figure 1.2 Misfit dislocation spacing and misfit strain vs. thickness according to Matthews-Blakeslee model

Another major assumption in this theory is that dislocations are the only mechanism for strain relief in the growing film. It has been shown that diffusion[25] and

surface roughness[26] can act to relieve strain in epitaxial films. The model is useful, however, since dislocation formation tends to be the primary mechanism for strain relief.

1.4.2 Kinetics of misfit accommodation

The thermodynamics of misfit accommodation is fairly well understood. Experimentally, however, a thermodynamically equilibrated state is rarely observed. It is clear then that the accommodation of misfit is limited by kinetic constraints. For a dislocation to relieve misfit at the interface it must first be formed, and then it must arrive at the interface through glide.[27] Equations (1.5) and (1.1) show the energy required to form dislocations and the strain energy of the film. In order to calulate the kinetic behavior of the system, we need to translate these energies into a driving force for misfit accommodation. The driving force is the stress driving dislocation motion.[23]

$$\sigma_{exc} = \sigma_{coh} - \sigma_{dis} \tag{1.11}$$

$$= 2\mu\left(\frac{1+\nu}{1-\nu}\varepsilon - \frac{1-\nu\cos^2\beta}{4\pi(1-\nu)}\frac{\ln(4h/b)}{h/b}\right) . \tag{1.12}$$

The primary mechanism for the formation of misfit dislocations is glide in the interface of existing threading dislocations. Threading dislocations present in the substrate are continued in the film as it is deposited. The stress in the film causes the dislocation to bend as shown in Figure 1.3 and leaves a misfit dislocation as it moves. The portion of the dislocation in the substrate remains stationary since the force on it is much smaller than in the film and in the opposite direction. To a first order approximation, therefore, the relaxation rate is proportional to the glide velocity and the threading dislocation density

$$\frac{\partial\gamma}{\partial t} = Nbv\cos\lambda \ , \tag{1.13}$$

where γ is the amount of strain relief, η - ε, N is the total number of threading dislocations and v is the dislocation glide velocity

$$v = B\exp\left(-\frac{U}{kT}\right)\left(\frac{\sigma_{eff}}{\sigma_0}\right)^{1.2} \tag{1.14}$$

where U is the activation energy for dislocation motion and σ_{eff} is the shear stress normalized in the direction of motion.

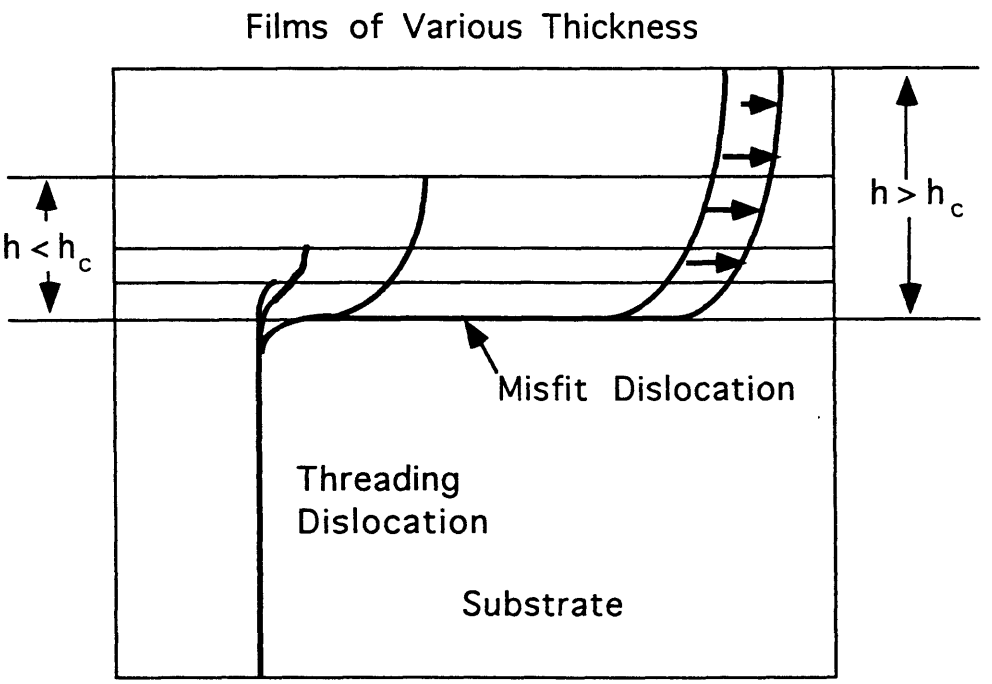

Figure 1.3 Bending of a threading dislocation to form a misfit dislocation

A more complete model for misfit accommodation has been proposed by Dodson and Tsao[27] which includes a number of other factors which become important in epitaxial systems. Nucleation of dislocations must be considered for systems in which the threading dislocation density is very low, as is the case for most semiconductor systems. They propose that this nucleation takes place through the formation of

dislocation "half-loops" at the surface of the film and by multiplication of existing dislocations. The model also takes into account pinning of dislocations by other dislocation segments as the threading dislocation moves through the film. The relaxation rate is then

$$\frac{d\gamma}{dt} = \frac{\sigma_{exc}^2(\gamma)}{\mu^2}\left(\Gamma_g e^{-Q_g/kT} + \Gamma_c e^{-Q_c/kT}\right)(\gamma + \gamma_0) \ , \qquad (1.15)$$

where Γ_g and Γ_c are glide and climb rate prefactors, Q_g and Q_c are glide and climb activation energies, and γ_0 is a constant source term.

1.5 MAGNETISM

The response of a ferromagnetic material to misfit strain is described by a strain dependent magnetic anisotropy called magnetostriction or magnetoelastic coupling. Anisotropy is simply the energy difference between magnetization in one direction and in another. A material with a high anisotropy will tend to have a magnetization which points along certain directions or easy axes. In order to understand magnetic anisotropy, particularly as it relates to heteroepitaxial thin films, we first need to review some general characteristics of ferromagnetic materials. The information contained in this section is taken primarily from *The Physics of Magnetism* by Chikazumi.[28]

1.5.1 Ferromagnetism: Exchange energy

In any material, electrons orbiting around atomic nucleii give rise to an atomic magnetic moment **m**. In a ferromagnetic material, each magnetic moment is in a lower energy state when aligned parallel to the moments of its neighboring atoms, resulting in a net magnetization **M** in the material. The energy associated with the allignment of neighboring spins is known as the exchange energy. It can be expressed as

$$E_{ex} = A_x(\nabla\phi)^2 \ , \qquad (1.16)$$

where A_X is the exchange constant, and ϕ is the angle between the moments at two adjascent sites.

Competition between the exchange energy, which acts to align all the moments within a sample, and magnetostatic energy, which acts to reduce the strength of magnetic poles at the surface, leads to the formation of magnetic domains. Domains are regions where the magnetization is uniform. Separating the domains are domain walls, and it is the motion of these walls that gives rise to the familiar ferromagnetic hysteresis loop. The magnetic induction **B** due to a sample is $\mu_0\mathbf{M}$. If a magnetic field is present, it will also contribute to the induction and **B** is then given by $\mu_0(\mathbf{H} + \mathbf{M})$. In examining magnetic hysteresis and related properties, one can therefore plot **B** vs. **H** or **M** vs. **H**, whichever is more convenient.

The basic shape of a hysteresis curve is shown in Figure 1.4. As a positive field is applied, the magnetization within the sample increases through movement of domain walls and actual rotation of magnetization within domains so that the magnetization in the sample becomes stronger in the direction of the applied field. Eventually, the entire sample (all the individual moments) is magnetized in the direction of the applied field and **M** reaches a maximum. This maximum is the saturation magnetization M_S. If **H** is then removed, the sample may have a tendency to stay magnetized due to the exchange energy, particularly if the applied field direction is an easy axis. The magnetization remaining in the film when H goes back to zero is the remanence, M_r. If the field is reversed, M will begin to change to the opposite direction. The applied field strength for which the magnetization goes back to zero is the coercivity H_C. These are the components of a typical hysteresis loop as shown in Figure 1.4. A loop that is more square (higher M_r) indicates that **H** is along an easy axis. It will be more difficult to demagnetize a sample that is magnetized along its easy axis. If the field is applied in a hard direction, the sample will have a tendency to demagnetize itself.

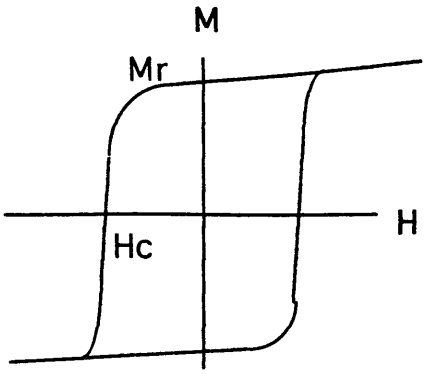

Figure 1.4 A typical magnetic hysteresis curve

1.5.2 Magnetostatic anisotropy

The magnetostatic anisotropy, also known as the shape anisotropy, is the dependence of the magnetization direction on the macroscopic shape of the specimen. When a specimen is magnetized, "magnetic poles" are generated at its ends which, in turn, result in a magnetic field opposing the applied field. This field is known as the demagnetizing field $\mathbf{H}_d$, where

$$\mathbf{H}_d = -N_d\mathbf{M}. \tag{1.17}$$

N_d is the demagnetizing factor and is dependent on the sample geometry. In the case of a thin film, N_d is equal to zero when **M** is in the plane of the film, and one with M perpendicular to the film. The magnetostatic energy is therefore

$$E_{ms} = 2\pi N_d M_s^2. \tag{1.18}$$

For Ni, $2\pi M_s^2 = 1.5 \times 10^6$ erg/cm^3.

1.5.3 Magnetocrystalline anisotropy

Within a magnetic crystal, the anisotropy energy will depend on the direction relative to the crystallographic axes. This effect is due to coupling between the electron spin and its orbit around the nucleus. When an atom is bonded within a crystal, the 3d shell is distorted and the orbital angular momentum is dependent on the direction of magnetization, giving rise to an anisotropy. The magnetocrystalline anisotropy energy can be expanded in terms of the direction cosines of the magnetization with respect to the crystallographic axes of the material. For a cubic crystal the lowest order terms are:

$$E_a = K_0 + K_1\left(\alpha_1^2\alpha_2^2 + \alpha_2^2\alpha_3^2 + \alpha_3^2\alpha_1^2\right) + K_2\alpha_1^2\alpha_2^2\alpha_3^2 + \cdots \qquad (1.19)$$

If $K_1 > 0$ the easy axes are in the <100> directions; if $K_1 < 0$, the easy axes are the <111> directions. For Ni, $K_1 = -4.5 \times 10^4$ erg/cm^3 and the easy axes are in the <111> directions.

1.5.4 Magnetoelastic anisotropy

In addition to magnetostatic energy and magnetocrystalline energy, there exists a magnetoelastic energy which effects the anisotropy of a sample. When a sample is magnetized, it undergoes a magnetostriction, an elastic distortion in response to the magnetization equal to $\lambda = \frac{dl}{l}$. Likewise, an applied stress can cause a change in the anisotropy energy. This phenomenon is known as piezomagnetism. It is also due to the spin-orbit interaction as described above. Its expansion in terms of the crystallographic direction cosines for cubic systems is

$$E_{me} = B_1\left(e_{11}\alpha_1^2 + e_{22}\alpha_2^2 + e_{33}\alpha_3^2\right) + 2B_2\left(e_{12}\alpha_1\alpha_2 + e_{23}\alpha_2\alpha_3 + e_{13}\alpha_1\alpha_3\right) + \cdots \qquad (1.20)$$

In the case of a biaxial misfit strain along principle crystal axes, the second term goes to zero. This energy is discussed in more detail in the next section.

1.5.5 Pair model of magnetic anisotropy

The phenomenon of magnetic anisotropy can be interpreted in terms of interactions between atomic pairs in a crystal. Specifically, it is dependent on the orientation of the magnetic moment relative to the bond direction. This analysis was used by Néel to describe anisotropy due to reduced local symmetry (e.g. at a surface or interface),[29] and described in detail by Chuang.[30] The total pair energy can be expressed as a Legendre polynomial expansion:

$$w(r,\psi) = G(r) + L(r)\left(\cos^2\psi - \frac{1}{3}\right) + Q(r)\left(\cos^4\psi - \frac{6}{7}\cos^2\psi - \frac{3}{35}\right) + \cdots \quad (1.21)$$

where r is the atomic pair distance and ψ is the angle between **m** and the bond direction, as shown in Figure 1.5.

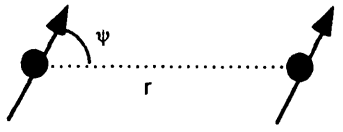

Figure 1.5 Magnetic dipole

In the above equation, G(r) includes exchange energy and other isotropic effects and does not contribute to magnetic anisotropy. The overall anisotropy energy can be calculated by adding w(r, ψ) for all pairs of atoms in the material. The Néel model accounts for anisotropy due to strain by taking into account the strain induced changes in r and ψ. Accordingly, the coefficients in the expansion can be expanded in terms of the bond strain:

$$L_i(r) = L_i(r_0) + \frac{dL}{dR}\cdot\varepsilon\cdot r_0 + \cdots \quad (1.22)$$

and

$$Q_i(r) = Q_i(r_0) + \frac{dQ}{dr} \cdot \varepsilon \cdot r_0 + \cdots , \tag{1.23}$$

where i =1 refers to nearest neighbors, i =2 referse to second-nearest neighbors, etc. We assume that only nearest neighbor interactions are significant (i = 1). For an fcc crystal,

$$Q(r_0) = K_1, \tag{1.24}$$

$$3L(r_0) + \frac{1}{2}\frac{dL}{dR} r_0 = B_1, \tag{1.25}$$

and

$$2L(r_0) + \frac{dL}{dr} r_0 = B_2. \tag{1.26}$$

For Ni, Q(r0) = -4.5 x 10^4 erg/cm^3, L(r0) = 9.75 x 10^6 erg/cm^3, $\frac{dL}{dr}$ = 6.55 x 10^8 erg/cm^3. The strain in the film (assuming a uniform biaxial misfit strain) is

$$\varepsilon = \varepsilon_0 \begin{pmatrix} 1 & 0 & 0 \\ 0 & 1 & 0 \\ 0 & 0 & \frac{-2\nu}{1-\nu} \end{pmatrix}.$$

Neél modified the pair interaction model by taking into account the missing nearest neighbors at the surfaces of the film by adding the w(r, ψ) over these atoms. The w(r, ψ) then must be added over atoms at an interface with a non-magnetic material (in this case, the Cu substrate). Chuang[30] computed these energies for an fcc crystal strained biaxially in the plane. The interaction energies for these atoms are defined as $L^{f-s}(r_1)$ and $\frac{dL^{f-s}}{dr}(r_1)$, etc., where f and s refer to the film and substrate, respectively. To determine the relative effect of bulk anisotropy and surface anisotropy, we express the energy as

$$E_{film} = E_{bulk} - 2\frac{E_{surface}}{h} + 2\frac{E_{interface}}{h} \tag{1.27}$$

where E_{bulk} is in units of energy per unit volume, and $E_{surface}$ is in units of energy per unit area. The Néel model assumes both surfaces (interface and free surface) are magnetically identical. Chuang[30] calculated these energies for an fcc (100) oriented crystal under biaxial strain to be

$$E_{bulk} = -2B_1\varepsilon_0 \cos^2\theta = -\left(6\varepsilon_0 L(r_0) + \varepsilon_0 \frac{dL}{dr} r_0\right)\cos^2\theta, \tag{1.28}$$

and

$$E_{surface} = \left(\frac{1}{2}L^{f-s}(r_0) - 3\varepsilon_0 L^{f-s}(r_0)\right)\cos^2\theta \tag{1.29}$$

(For an unstrained crystal, E_{bulk} is simply the bulk magnetocrystalline anisotropy energy). Similarly, the first term in Equation (1.30) is K^s, the surface magnetocrystalline term, and the second term is B^s, the surface magnetoelastic term. Note that the model predicts that B^s is opposite in sign and a factor of 6 greater than K^s.

The Neél model, then, gives the bulk and surface magnetocrystalline and magnetoelastic energies. As can be seen from the values given above, the bulk magnetocrystalline anisotropy is small relative to other effects on anisotropy, and so can be ignored in this analysis. So the total anisotropy energy, including the magnetostatic term, is

$$E_a = K^{eff} \sin^2\theta, \tag{1.30}$$

where

$$K^{eff} = 2\pi M_s^2 - 2\left(B_1 + \frac{B^s}{h}\right)\varepsilon_0 - 2\frac{K^s}{h}. \tag{1.31}$$

1.6 SUMMARY

The information presented here illustrates the practical aspects of using MOKE data to measure strain in Ni/Cu films. Strain measurements and microstructural analysis were performed in tandem with magnetic characterization in order to determine the surface magnetic constants. Once these are determined, we are able to establish quantitatively the relationship between strain and magnetic anisotropy energy. Knowing this relationship allows the use of MOKE as a powerful *in situ* tool for measurement of strain. This instrument will be discussed in the context of misfit strain and misfit accommodation through dislocation formation. It is hoped that the ability to measure strain precisely and accurately during deposition and during *in situ* anneal will give new insight into the kinetics of misfit accommodation, particularly in metallic thin films.

2. CHAPTER 2: SAMPLE FABRICATION

All films in this work were deposited using electron-beam evaporation under ultra-high vacuum (UHV) conditions. In order to study misfit accommodation, it is necessary to achieve high epitaxial quality. The models used in this work assume a perfectly epitaxial film free of impurities. A UHV environment produces samples closest to this ideal.

2.1 GROWTH IN BALZERS SYSTEM

A series of films was deposited in a Balzers UMS 500 UHV electron-beam evaporation system. The system has two hearths for evaporation of two different source materials. It is pumped using a mechanical roughing pump, turbo pump and titanium sublimation pump, all manufactured by Balzers, to a background pressure of about 10^{-10} Torr. The pressure is monitored before and during depostion with an ion guage with partial pressure of residual gases measured using a quadropole mass spectrometer. The sample stage is capable of both heating and cooling. The system is equipped with a RHEED (reflection high energy electron diffraction) system for surface analysis.

In order to study the Ni/Cu interface, a high quality single crystal Cu substrate is needed. The easiest and most practical way to obtain one is by depositing a relatively thick Cu film epitaxially on a single crystal substrate in the chamber prior to depostion

of the Ni. In this way, it is possible to ensure a surface of high purity and good crystalline quality that is free of native oxide. It is necessary to make the Cu layer thick so that the surface is relaxed and relatively defect-free. In this case, the substrate chosen was NaCl. NaCl with {100} type surfaces is relatively easy to obtain and Cu is known to grow epitaxially on this surface. Using NaCl also facilitates TEM sample preparation because the film can be floated off in water, eliminating the need for mechanical dimpling and ion milling.

The depostion procedure was as follows: first the NaCl was cleaved in air along {100} planes, into pieces 1 cm^2 in size. These pieces were then loaded into the vacuum chamber and the chamber was pumped down. The chamber was then baked overnight at 200°C for a minimum of 16 hours. During the bakeout, the substrate temperature was maintained at ~350°C. The chamber was then cooled and the sublimation pump cycled to obtain a background pressure in the 10^{-10} Torr range.

Once the background pressure was low enough, the Cu film could be deposited. The substrate temperature was maintained at 300°C during depostion. The Cu was deposited using e-beam evaporation at a rate of 1-2 Å/s, as measured by a quartz crystal oscillator, to a total thickness of 1000Å. The crystal structure of the Cu surface was then checked for crystalline quality and surface roughness using RHEED. The Cu/NaCl was cooled prior to depostion of the Ni to 50-60°C by cooling the substrate plate with a liquid nitrogen feed-through. The RHEED pattern was observed again at this temperature to ensure no change in surface structure. The Ni was deposited at 0-1Å/s to a total thickness of between 20 and 200Å. The RHEED pattern of the Ni surface was observed.

2.2 GROWTH IN A MOLECULAR BEAM EPITAXY SYSTEM

Most of the films used in this study were deposited in a Perkin Elmer MBE system. A rough diagram of the deposition chamber is shown in Figure 2.1. This system is pumped using a CTI cryopump and Perkin Elmer ion pump as well as a Ti sublimation pump. The background pressure that can be achieved is approximately 3 x

10^{-11} Torr. The system is equipped with a load-lock introduction chamber also pumped by a (smaller) CTI cryopump. Roughing for both these chambers is accomplished using a venturi pump and four Perkin Elmer sorbtion pumps. The lack of any oil-based pumps contributes to the purity of the vacuum. This deposition system has many additional features. We have the ability to heat the sample both in the introduction chamber and in the deposition chamber itself to 1000°C. The temperature of the substate is monitored by means of a type K thermocouple. Pressure in both chambers is monitored by an ion guage and a Spectramass residual gas analyzer. The sample stage in the main chamber has many degrees of freedom which have been found to be useful in these experiments. The sample can be rotated azimuthally, both manually and electronically. This feature can be used to ensure a uniform film thickness by rotating the sample continuously during deposition. The sample can also be rotated axially to allow positioning for different in situ analyses. While in the deposition position, the sample can be analysed using RHEED. The sample can be repositioned for Auger analysis, and MOKE (magneto-optic Kerr effect) measurements. The chamber is equipped with two hearths for source material. These were filled with Ni and Cu.

The substrate used for these depositions was (001) oriented Si wafers. There were several reasons for this choice. First, the MBE was structurally designed to accommodate three inch wafers. Also, unlike NaCl, the presence of Si does not adversely effect the quality of the vacuum. NaCl tends to dissociate upon heating in vacuum and introduce contamination to a UHV chamber. Si provides an optically flat surface, ideal for Kerr effect measurements, which require the measurement of the polarization direction of a beam reflected off the magnetized surface of the sample. Si is also the best choice for measurement of film stress through wafer bending, to be discussed in detail later, both because of the optically flat surface and because of the fact that Si can be purchased as wafers as thin as 100 μm. A thinner substrate means greater bending in response to an applied stress, making the stress in the film more measureable. The two major difficulties associated with using Si as a substrate for Cu are difficulty in making TEM samples, which must be done using mehcanical dimpling and ion milling, and the formation of copper silicide at the interface, a phenomenon which is discussed in detail in the Appendix.

Prior to deposition, the Si wafers were processed using an HF dip to remove native oxide and provide a smooth, crystaline surface. Deoposition is by electron beam evaporation of 99.999% pure source material. The substrates were not intentionally

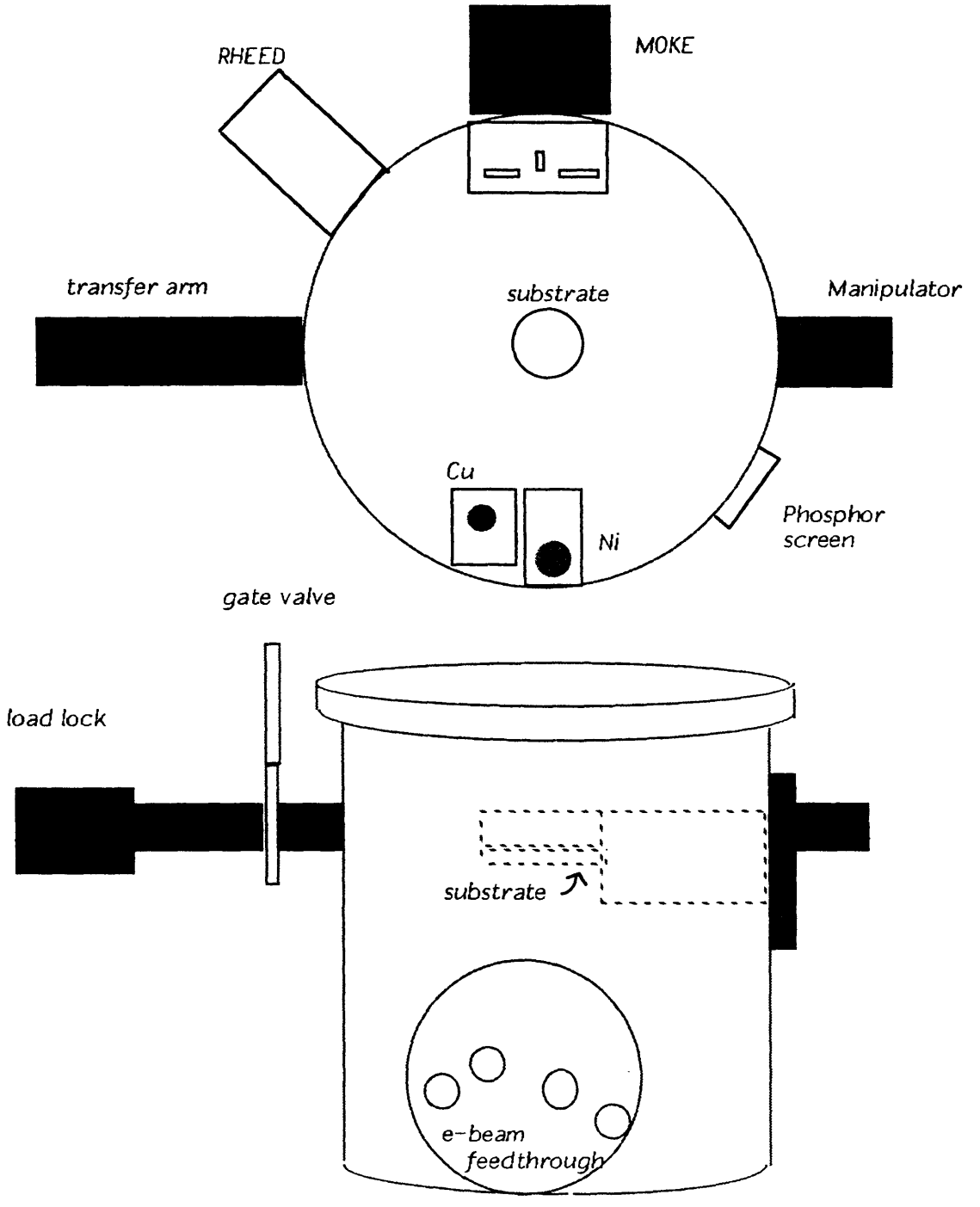

Figure 2.1 Schematic diagram of Perkin Elmer MBE chamber

heated during deposition, although radiative heating from the sources caused the substrates to heat to approximately 50°C during deposition. Any heating of the Si substrate above about 100°C was determined to result in formation of copper silicide rather than epitxial Cu. Pressure in the chamber rose to about 8 x 10^{-9} Torr during evaporation. Deposition rate and thickness was monitored using an Inficon photomultiplier rate monitor and deposition controller which was callibrated using a step profilometer. The computer interface for the rate monitor could also be used to control the power to the e-beams, thus maintaining a constant deposition rate. Cu and alloy films were generally deposited at a rate of 3 Å/s, and Ni epilayers were deposited at 0.5Å/s to 1 Å/s. Crystalline quality was determined immediately after deposition using RHEED.

2.3 GROWTH OF ALLOY FILMS

For some of this work, Ni-Cu alloy films were deposted. The purpose of depositing the alloy films on Cu was to look at the behavior of the system with varying degrees of misfit. By growing alloy films of various concentrations, it was possible to change the lattice constant of the film, thus changing the misfit between it and an adjacent film. The Ni-Cu system is ideal for this type of experiment since it exibits complete miscibility, and allows a relatively broad range of lattice constants. Ni-Cu alloys have been used as a substrate by other researchers when it was desirable to vary substrate lattice constant.[31] Also, Alkemade et al.[32] grew Ni-Cu alloys on Cu. They were able to achieve even mixing of the two elements within the alloy, and got the expected interfacial strain between the alloy and Cu substrate.

There has been some research indicating the presence of a miscibility gap in the Ni-Cu system.[33,34,35,36,37] This gap has its maximum at about 55 atomic % Ni.[37] The Cu/Ni phase diagram is shown in Figure 2.2. Since the temperature of the miscibility gap is so low (~350°C), the phase separation is extremely slow and is rarely observed in practice. This is certainly the case for this work, in which the alloy films are deposited

directly from the vapor phaseat temperatures no higher than 60°C. Additionally, it was shown from measurements of peak-to-peak separation in theta/two theta x-ray diffraction scans that the alloy layer had the lattice constant expected from the law of mixing.

The phase diagram also shows the dependence of the Curie temperature on atomic percent Ni. Ni concentrations were chosen for these films such that the film would be ferromagnetic at room temperature.

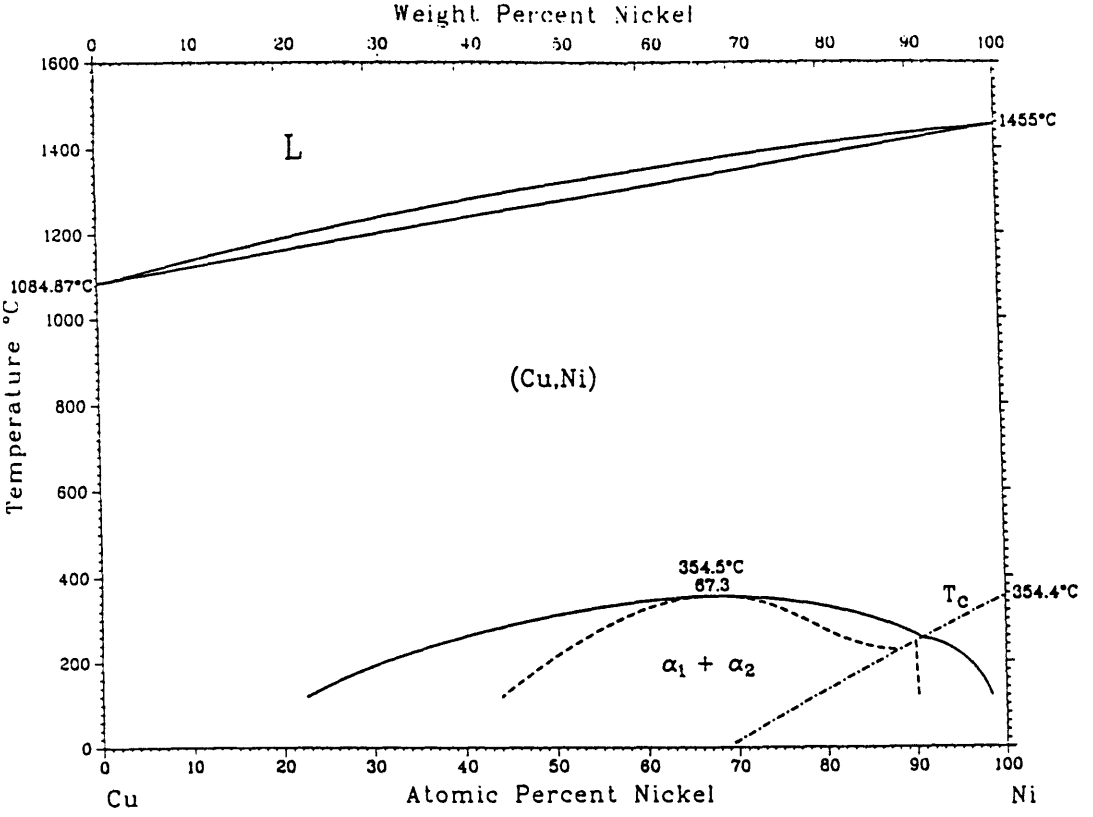

Figure 2.2 Cu-Ni phase diagram[38]

Interdiffusion is minimal at the low deposition temperature used for these materials, so a uniform co-deposition was necessary. The Inficon rate controllers discussed above facilitated such a deposition. The rate controller could be set such that the rate of one evaporator could be mantained to be a certain value relative to that of the other evaporator. This arrangement produces less variation in alloy composition than if the two evaporators are controlled independently.

2.4 Cu/Ni/Cu SANDWICHES

For some of the magnetic characterization, films were deposited with a 20Å Cu "capping layer". This was done in order to be able to fit the experimental data to the modified Neél model discussed in Chapter 1. As was discussed, the magnetic properties of a thin film are strongly influenced by the magnetic properties of the surface and interface layer. In the case of Ni/Cu, the free surface and interface are necessarily quite different and would thus exhibit different values for K^s and B^s, the surface magnetic constants. In the case of Cu/Ni/Cu, the two interfaces are magnetically very similar, and can be approximated as identical.

In order to combine measurements of the magnetic properties of the sandwiches with misfit and strain measurements made on Ni/Cu, it was first shown that the Ni/Cu films behaved qualitatively the same in terms of their magnetic properties, with quantitative differences that can be described through the use of different fitting parameters for surface and interface. These results will be discussed in detail in Chapter 5. Also, it was necessary to show that the presence of the Cu capping layer did not influence the state of strain in the Ni. It was shown using the type of strain measurements discussed in Chapter 4, that the presence of the capping layer did not exhert a measurable stress on the Si wafer. Further, the critical thickness of Cu on Ni has been measured by Chambers[11] to be 14Å. The capping layers used in this work were 20Å thick. Measurements of misfit dislocation spacing indicated that an increased number of misfit dislocations were observed as compared to films with no capping layer. The Cu is therefore relaxed and should have little influence on the strain in the Ni layer.

2.5 GENERAL CHARACTERIZATION

All films were characterized *in situ* using RHEED immediately after deposition to confirm that the films were epitaxial. *In situ* measurements were confirmed on some samples using *ex-situ* x-ray diffraction. RHEED patterns were spotty as shown in Figure 2.3, indicating a rough surface. Cross-sectional TEM was performed on some

(a)

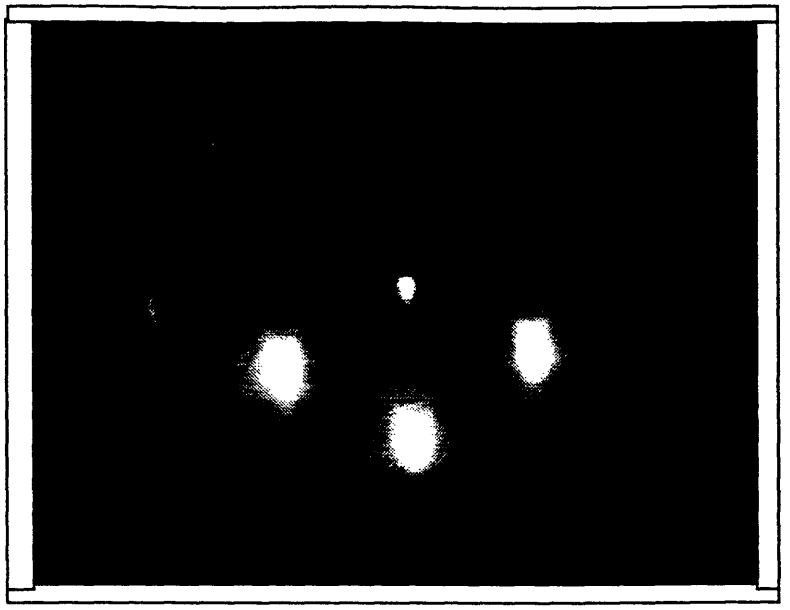

(b)

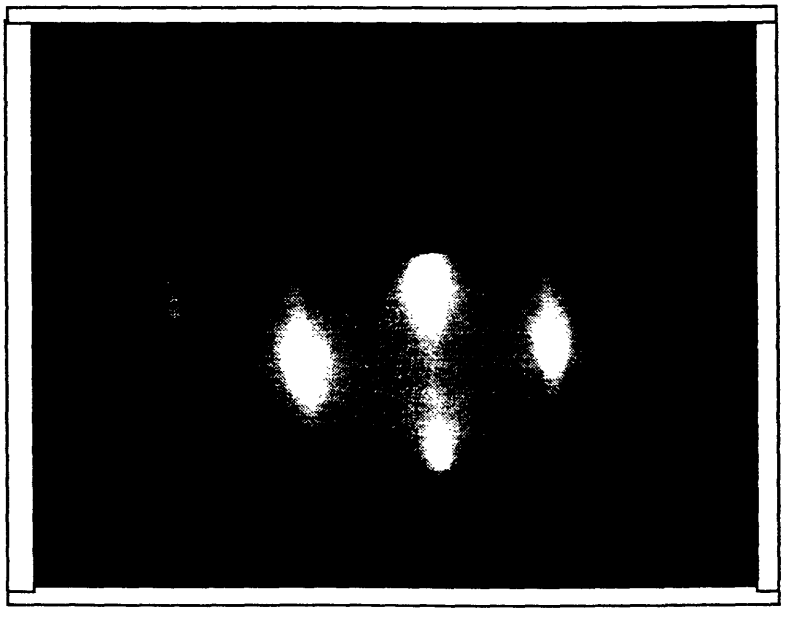

Figure 2.3 RHEED patterns in <110> direction of (a) Cu/Si (001), and (b) Ni/Cu/Si (001)

samples to estimate interface and surface roughness, as in the micrograph shown in Figure 2.4. The roughness was found to be approximately 20Å. This result was confirmed by atomic force microscopy (AFM), as seen in Figure 2.5.

Several samples were characterized using x-ray diffraction to determine crystalline quality. The samples were found to be epitaxial, as determined by x-ray pole figures, and free of measurable impurities.

The MBE system was equipped with an Auger electron spectrometer. This device was used to determine film purity as well as Ni film coverage. Auger showed that the films were extremely pure, as would be expected from the UHV environment. The coverage of the Cu by the Ni was determined to be complete at about 15Å thickness. The Auger, as well as the MOKE measurements required the use of a specially designed sample holder shown in Figure 2.5. This set-up will be discussed in more detail in Chapter 5.

Figure 2.4 Cross sectional TEM of Ni/Cu/Si (001) showing surface roughness. The Ni layer is 500Å thick.

In summary, the films were found to be epitaxial and of high purity. Both these qualities are necessary in order to describe thoroughly the behavior of the system. A major component of this work has been the modeling of the magnetic properties according to the Neél model described in Chapter 1. The Neél pair-interaction model

for magnetic anisotropy is based on an atomistic-level description of magnetic interaction. It is therefore easiest to model a pure, single crystal film so that the position and interaction of neighboring atoms can be predicted. The films used in this study meet these criteria.

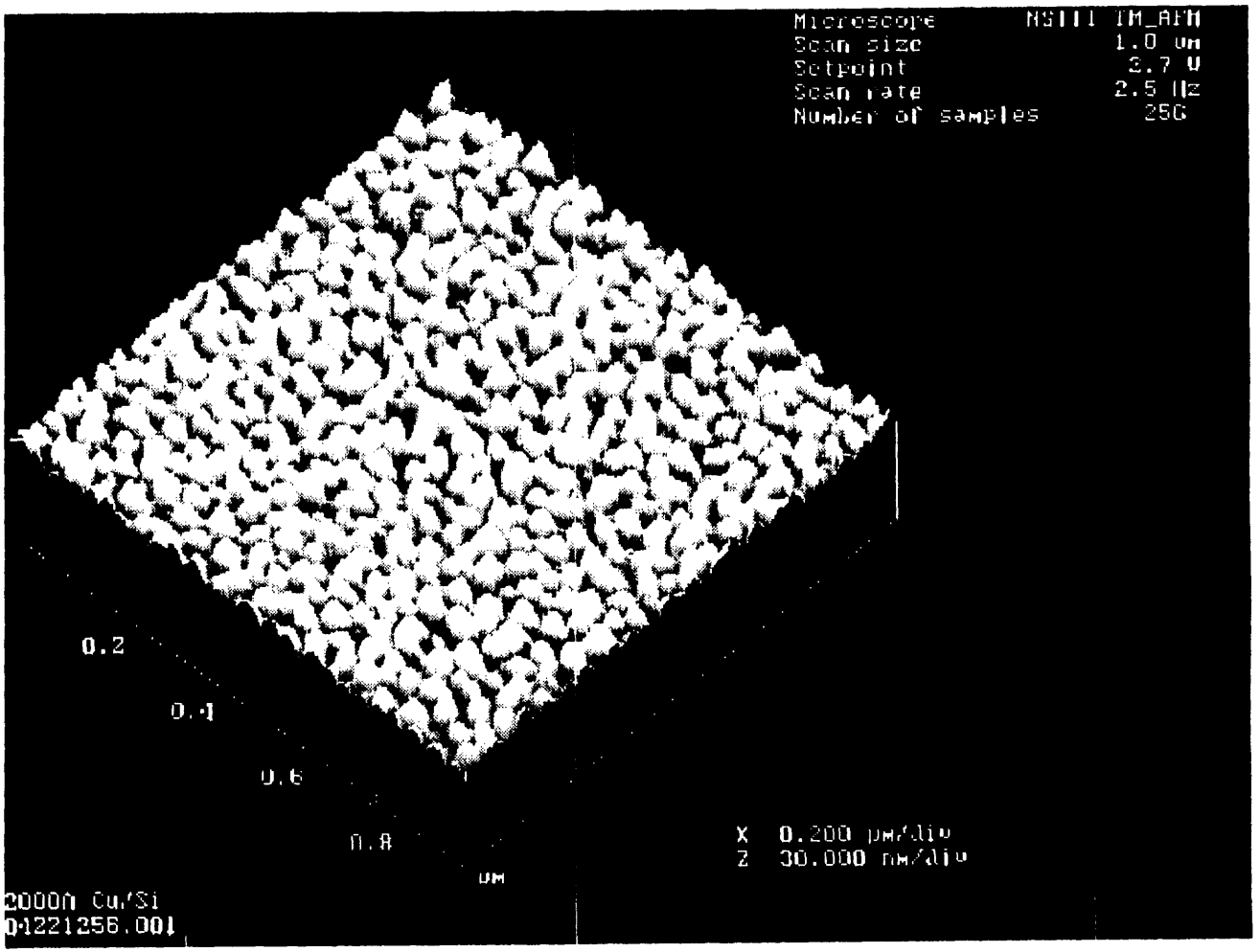

Figure 2.5 AFM of Ni/Cu surface. RMS roughness ~2 nm

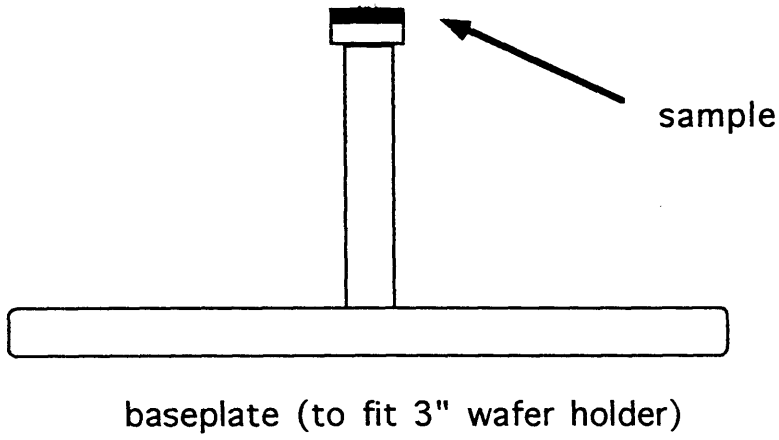

Figure 2.6 Sample holder used for MOKE and AES

3. CHAPTER 3: TEM

3.1 BACKGROUND

This chapter will describe the use of transmission electron microscopy to examine the structure of the Ni/Cu interface. As was described in Chapter 1, misfit dislocations are thought to be the primary mechanism for accommodation of epitaxial misfit strain. The main goal of the microscopy described here is then to characterize the dislocations at the interface. Possible mechanisms for the formation of the observed misfit dislocations will be discussed. Measurement of the average spacing between the dislocations will also be described. They will be compared to the thermodynamic model described in Chapter 1. These measurements will be analyzed in conjunction with the measurements of residual strain in Chapter 4 to determine the extent to which the misfit is actually being accommodated by dislocation generation.

3.1.1 Theory and g•b = 0 criterion for invisibility

Transmission electron microscopy has proven extremely useful in this research as a method of imaging the misfit dislocation networks in the samples. In general, TEM is a useful technique for imaging of dislocations in crystals. In order to understand the imaging of dislocations in the electron microscope, it is necessary to look at the results from both the dynamic and kinematic theory of electron diffraction. For a detailed discussion of the development of these theories see, for example, *Electron Microscopy of Thin Crystals* by Hirsch *et al.*[39]

The important factor to consider is the perturbation in the intensity of the diffracted electron beam in the form of $\mathbf{g} \bullet \mathbf{R}$ and $\mathbf{g} \bullet \frac{d\mathbf{R}}{dz}$, where **g** is the diffraction vector which forms the image and **R** is the displacement vector in the crystal. The displacement field surrounding the dislocation causes the intensity of the two beams to drop near the dislocation core, resulting in the dislocation appearing as a dark line in the TEM image.

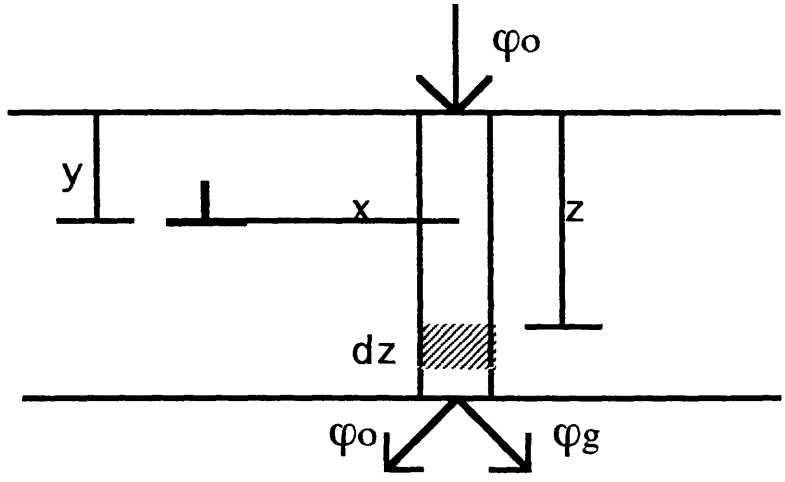

Figure 3.1 Dislocation embedded in a crystal

For a dislocation in a crystal as shown in Figure 3.1 at position (x,y,z), the displacement field around a dislocation is

$$\mathbf{R} = \frac{\mathbf{b}}{2\pi}\tan^{-1}\left(\frac{z-y}{x}\right) = \frac{\mathbf{b}}{2\pi}\alpha \tag{3.5}$$

for a screw dislocation and

$$\mathbf{R} = \frac{1}{2\pi}\left[\mathbf{b}\alpha + \mathbf{b}\frac{\sin 2\alpha}{4(1-\nu)} + (\mathbf{b}\times\mathbf{u})\left\{\frac{1-2\nu}{2(1-\nu)}\ln r + \frac{\cos 2\alpha}{4(1-\nu)}\right\}\right] \tag{3.6}$$

for an edge dislocation, where **b** is the Burgers vector, **u** is a unit vector along a dislocation, ν is Poisson's ratio, and r is the distance from the dislocation core. For a screw dislocation, the perturbation is therefore proportional to $\mathbf{g} \bullet \mathbf{b}$.

For the case where $\mathbf{g} \bullet \mathbf{b} = 0$ (the diffracting vector is normal to the Burgers vector), the perturbation is zero and there is no contrast corresponding to the dislocation. It is effectively invisible. This phenomenon can be useful in determining the direction of the Burgers vector of a given dislocation. By creating TEM images using many different two-beam conditions, it should be possible to unambiguously determine the direction of **b** by noting those two-beam conditions (values of **g**) for which the image of the dislocation disappears. These images can either be taken in bright field (image created by the transmitted beam) or in dark field (image created by the diffracted beam). The same criterion can be used for an edge dislocation where both $\mathbf{g} \bullet \mathbf{b}$ and $\mathbf{g} \bullet (\mathbf{b} \times \mathbf{u})$ must be equal to zero for invisiblity.

3.1.2 Microscopy techniques used in this work

In order to increase the contrast of a dislocation, a technique known as weak-beam imaging can be used. The intensity of the diffracted beam is low for $s >> 0$. When this beam passes through the region immediately surrounding the dislocation, it experiences a sharp increase in intensity due to the distorted region passing through the Bragg condition. This peak is much narrower than that caused by a dislocation in a bright field or strong ($s = 0$) dark field image. The possibility is therefore increased of resolving the images of two dislocations which are close together. Weak-beam images are more difficult to create, however, due to the fact that the overall intensity is very low, requiring long exposure times, during which the vibrational stability of the microscope becomes an issue. It is also necessary for this technique to have a large thin region of the sample for imaging.

The nature of the materials system created difficulties in the microscopy in this work. Due to the fact that the films were metallic, and therefore relatively elastic, considerable local bending occurred in response to the biaxial misfit strain. This bending

made it impossible to maintain a consistent two-beam condition over a large sample area. Dark field imaging was used therefore to make obvious those areas of the sample which were diffracting strongly and therefore had known **g**. In some cases, particularly for films with high misfit dislocation density, weak-beam imaging was used.

Additional complications resulted from the fact that the films were highly uniform with a high density of misfit dislocations, the misfit dislocation grid being the only distinguishable feature in most samples. For this reason, a detailed study determining the Burger's vector of a single dislocation using the $\mathbf{g} \cdot \mathbf{b}$ invisibility criterion described above is impractical. In order to perform such a study, it is necessary to switch from imaging to diffraction mode (in which the diffraction pattern, not the image of the crystal microstructure is visible to the microscopist) and tilt the sample such that a new set of crystallographic planes is at the Bragg angle (a new value of **g**), and then switch back to imaging mode. Keeping track of a single dislocation in a sea of many virtually identical dislocations is not likely during this operation. The solution to this problem has been to take many images at different **g**'s, and get a statistical average of the dislocations visible in a specific direction for each **g** in order to determine the Burgers vectors of the dislocations.

In addition to these techniques, measurement of moiré fringe spacing was used in some samples as a measurement of strain. The relationship between Ni strain and moiré fringe spacing can be deduced by comparing the system to a superposition of two optical gratings of different spacings, as shown in Figure 3.2. If d_1 and d_2 are the spacings of the first and second grating, the spacing of the fringes is

$$D = \frac{d_1 d_2}{|d_1 - d_2|} \tag{3.7}$$

The Ni/Cu crystal bilayer acts as a superposition of two gratings of different spacings. In the limiting case of the psuedomorphic film, there will be no fringes present ($D = \infty$). For a completely relaxed film, $D = \frac{d_{Cu}}{0.026}$ where d_{Cu} is the spacing of the lattice planes corresponding to the diffraction vector used to create the image. In general,

$$D = \frac{d_{Cu}}{\gamma} \tag{3.8}$$

where γ is the amount of relaxation.

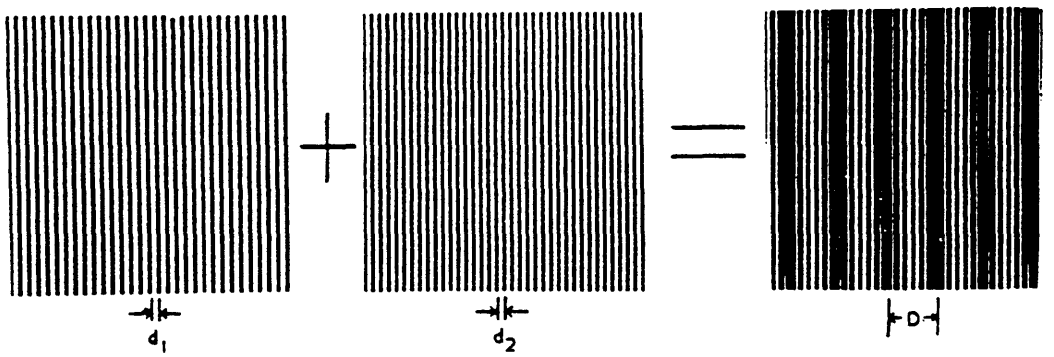

Figure 3.2 Illustration of fringes created by overlapping two gratings of different spacing.[40]

3.2 MISFIT DISLOCATIONS IN Ni/Cu (001)

3.2.1 Types of dislocations

In fcc metals, the most common dislocation is what is known as a 60° dislocation, with the Burgers vector making a 60° angle with the dislocation line. The dislocation line and Burgers vector both lie along ⟨110⟩ type directions. If we call the interface plane the (001) plane, a typical misfit dislocation observed has $\mathbf{u} = \frac{1}{\sqrt{2}}[\bar{1}\,10]$, and $\mathbf{b} = \frac{a}{2}[01\,\bar{1}]$. Notice that **u** lies in the interface and **b** is inclined to the interface. The component of **b** in the interface and normal to the dislocation line (the component that acts to relieve misfit) is b/2. The glide plane for this type of dislocation, the plane containing both **u** and **b**, is a {111} plane. Specifically, for the dislocation above, the glide plane is (111). There are four possible glide planes corresponding to the four

{111} planes which intersect the interface plane along $[\bar{1}10]$ and $[110]$ directions. Thus we expect to see, looking at the film in plan-view, an orthogonal grid of dislocations running along these lines of intersection, which is in fact what we observe, as is shown in Figure 3.3. It is presumed that these dislocations glide along their respective {111} planes toward the interface. The driving force for this glide is the excess stress described in Chapter 1.

Figure 3.3 Grid of misfit dislocations visible in plan-view TEM of Ni/Cu(001)

It was determined during the course of this investigation that two types of misfit dislocations are present in these films, 60° dislocations with **b** inclined to the plane of the interface and 90° dislocations with **b** lying in the plane of the interface. These two types of dislocation are illustrated in Figure 3.4. Both dislocation types lie along ⟨110⟩ directions, and thus form an orthogonal grid in the (001) plane. This result will be discussed in more detail later. It is relevant to the discussion of microscopy technique because, in order to accurately measure the average spacing between dislocations, it was necessary to choose **g** such that all misfit dislocations were visible. All such measurements were made on micrographs where **g** = (020) or **g** = (200). For this vector, $\mathbf{g}\cdot\mathbf{b} \neq 0$ for the 90° dislocations, and $\mathbf{g}\cdot\mathbf{b}\times\mathbf{u} \neq 0$ for the 60° dislocations. The criteria for invisibility for dislocations observed in these films in one of the orthogonal directions is

shown in Table 3.1. A similar one can be created for the dislocations in the other direction.

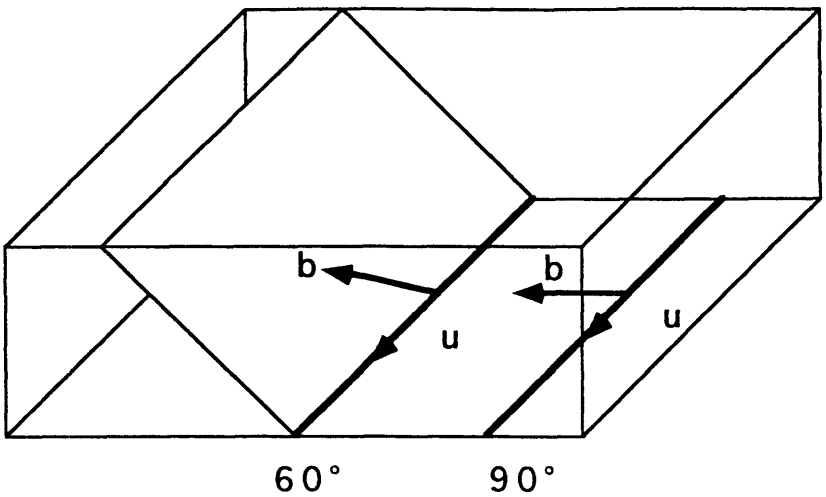

Figure 3.4 A 60° and a 90° dislocation lying parallel in the interface plane along the [110] direction the Burgers vector of the 90° dislocation lies in the (001) plane, whereas the Burgers vector of the 60° dislocation lies in a (111) plane. The component of **b** for the 60° dislocation which lies in the plane of the interface is b/2.

	g \ **b**	±a/2[220]	±a/2[202]	±a/2[$\bar{2}$02]	±a/2[022]	±a/2[0$\bar{2}$2]
g • b	(200)	1	1	1	0	0
	(220)	2	1	-1	1	-1
	(020)	1	0	0	1	-1
	($\bar{2}$20)	0	-1	1	1	-1
g • bxu	(200)	0	1	1	1	1
	(220)	0	2	2	0	2
	(020)	0	1	1	-1	1
	($\bar{2}$20)	0	0	0	-2	0

Table 3-1 g • b = 0 criterion for invisibility for dislocation in Ni/Cu (001) with u = $|1\bar{1}0|$

The magnitude of the Burgers vector of the 90° dislocations is the same as of the 60° dislocations and is equal to $\frac{a}{\sqrt{2}}$. Evidence of the presence of 90° dislocations is shown in Figures 3.5 and 3.6. The TEM micrographs shown in these Figures illustrate the fact that there are dislocations present for which there is no contrast when g is along the direction of the dislocation (the $g \cdot b = 0$ condition for an edge dislocation), and also dislocations which do not meet this criterion (60° dislocations). If all dislocations along [220] were edge type, they would all be invisible under the g = (220) condition. If they were all 60° dislocations, they would be visible under both diffraction conditions.

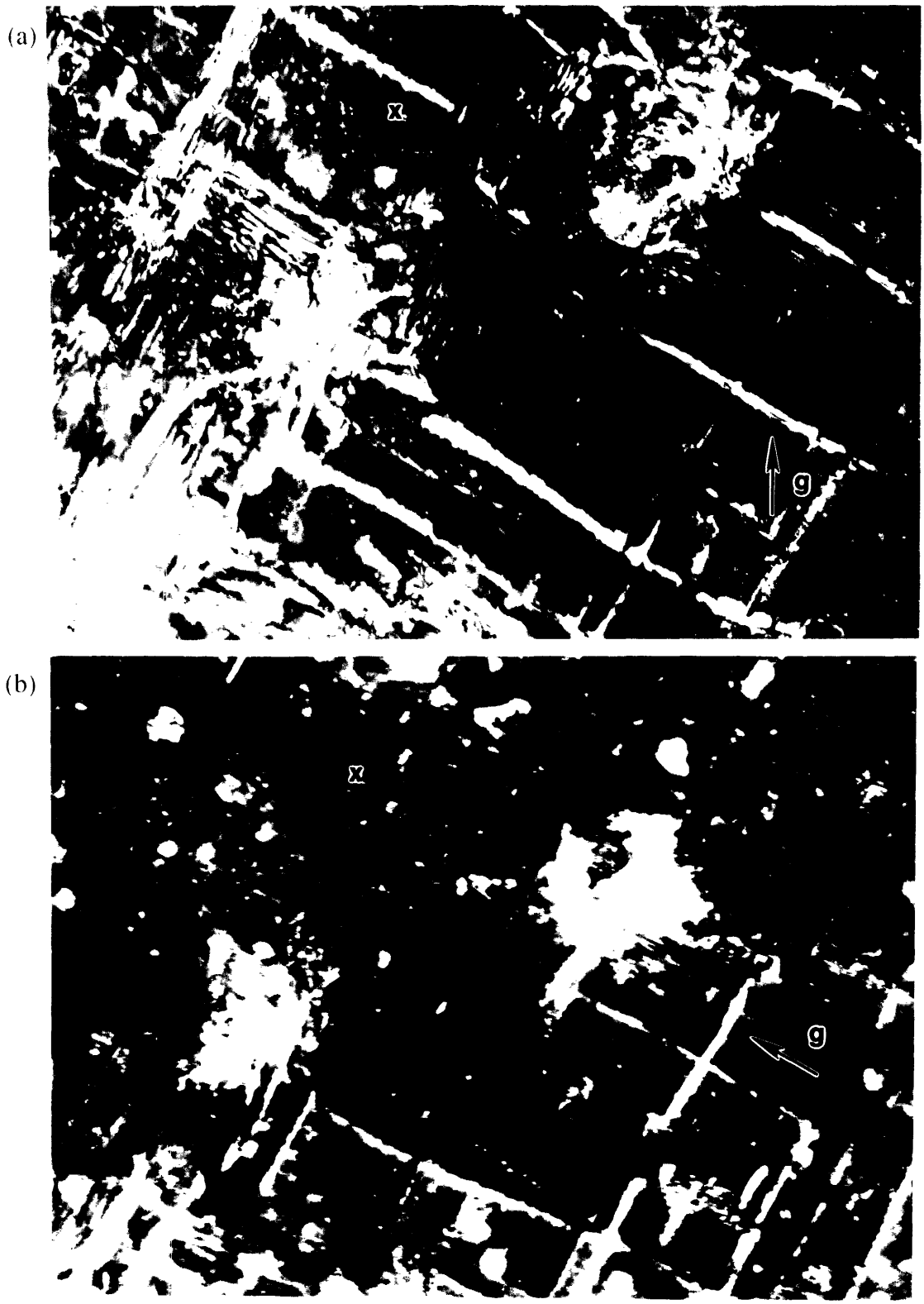

Figure 3.5 Plan-view TEM of Ni/Cu (001) (NaCl substrate). (a) **g** = (020), (b) **g** = (220). Edge dislocations, such as the one at position X, are at minimum contrast when **g** is parallel to **u**.

(a)

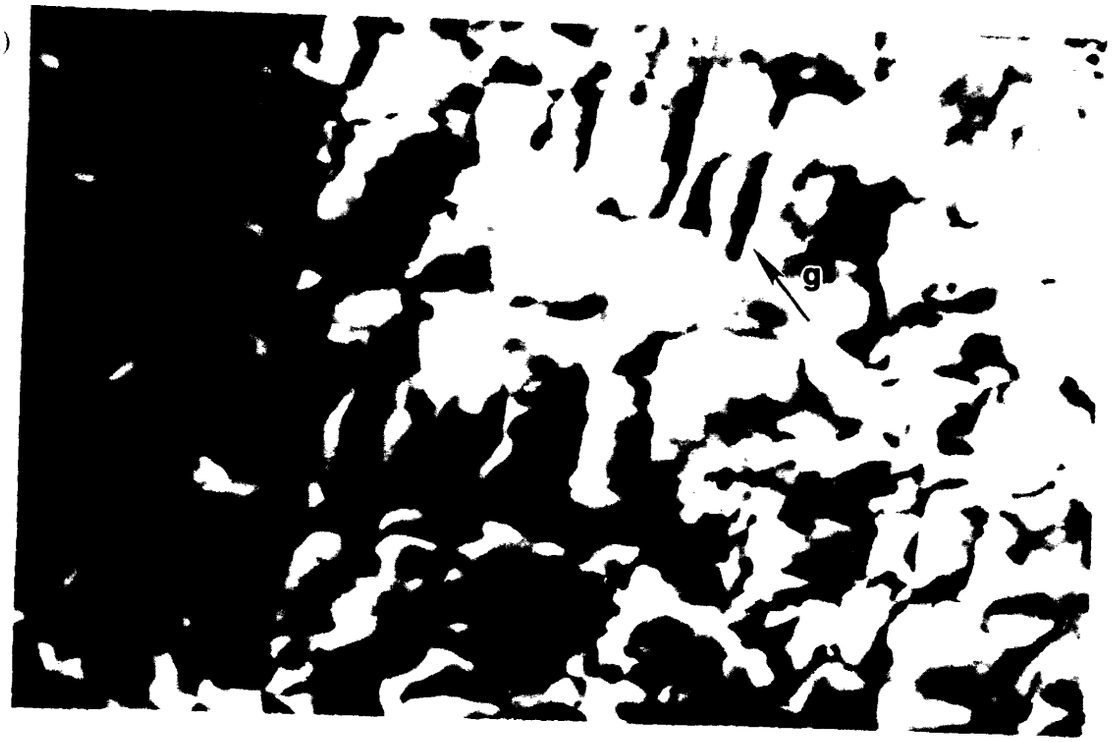

(b)

Figure 3.6 Plan-view TEM of Ni/Cu (001) (Si substrate). (a) is taken with $\mathbf{g} = (020)$ (all dislocations visible). (b) is taken with $\mathbf{g} = (220)$ (90° dislocations with $\mathbf{u} = \mathbf{g}$ are not visible).

3.2.2 Dislocation reactions

Recall from the analysis in Chapter 1 that an edge dislocation with **b** in the interface is the most efficient at relieving misfit strain. Thermodynamically, therefore, it's easy to see why this type of dislocation would be present in the film. The Burgers vector component acting to relieve misfit strain is simply b, or twice that of a 60° dislocation. Since the misfit relief contributed by one 90° dislocation is then equivalent to the misfit relief contributed by two 60° dislocations, the energy gained by having 90° dislocations is simply the difference in the self-energy of the dislocations,

$$2U_{60°} - U_{90°}. \tag{3.9}$$

or

$$\frac{\mu b^2}{4\pi(1-\nu)} \ln\left(\frac{R}{r_0}\right)\left(2\left(1-\nu\cos^2\beta\right)-1\right). \tag{3.10}$$

Kinetically, though, it is more difficult to understand the presence of the 90° dislocations. The 60° dislocations, since they lie in a close-packed plane, can glide easily, while 90° dislocations, since they lie in the (001) plane (the interface plane), cannot glide easily. The (001) plane in an fcc metal is not close-packed. This type of a dislocation is known as a Lomer lock, after the theorist who first postulated its existence, because of the fact that it is immobile and acts as a pinning site for dislocation motion.[41] Lomer locks have long been of interest to researchers studying work hardening for their role in limiting plastic deformation.

The issue for this work is, since these 90° dislocations cannot glide to the interface as the 60° dislocations can, they must get there via some other mechanism. Thompson and Lawless[15] were the first to observe these 90° dislocations in the interface plane of Ni/Cu (001). Recognizing that these dislocations could not have arrived at the interface via glide, they refered to them as "in-grown" dislocations. This description has to do with the growth mode of the films. It is known that metal films under high misfit will initially grow as islands on the substrate. The pseudomorphic regime is characterized by this type of microstructure. As the Ni is deposited, the islands grow

until at some thickness they coalesce. As they coalesce, edge dislocations will form at the borders between the islands. Therefore, there is no need for glide to occur for these edge dislocations to appear at the interface. In our films, however, there is evidence that the number of edge dislocations is increasing as the film gets thicker. Comparison of dislocation spacing with strain measurements discussed in Chapter 4 indicates that at h = 25Å, most of the dislocations are 60° type, while at h = 100Å, most are 90°. Therefore, the presence of only some of the edge dislocations can be explained through island coalescence.

In a similar study by Matthews and Crawford,[14] cross-slip was observed in dislocations at the Ni/Cu interface. Cross-slip refers to motion of a screw segment of a dislocation into a different glide plane. In order for this type of motion to occur, the observed dislocations had to be 60° dislocations. The threading segments of a 60° misfit dislocation which lead toward the free surfaces of the crystal are screw type. From this observation, the researchers concluded that all the observed dislocations were 60°.

It is useful to compare these results with those of semiconductor systems. Edge dislocations which are different from the ones described above have been found to occur in (Al)GaAs/$In_xGa_{1-x}As$/GaAs (001) by Bonar, et al.[42] They see dislocation lines in the interface along [010] and [100] directions with Burgers vectors along ⟨110⟩ directions normal to the dislocation line and inclined to the interface by 45°, in addition to 60° dislocations lying along ⟨110⟩ directions. The component of **b** relieving misfit in the 90° dislocations is then $\frac{b}{\sqrt{2}}$, and the dislocations lie in {110} planes. Some glide is known to occur along these planes under very high stresses, so unlike the 90° dislocations in the Ni/Cu system, they are not completely sessile. The 90° dislocations were only found in systems of high (>2%) misfit. In fact, glide has been observed of these dislocations along {110} planes.[42] They can therefore glide to the interface from a surface or internal nucleation site. A similar dislocation array was seen by Albrecht, et al. in $Ge_{0.85}Si_{0.15}$/Si (001) grown via liquid-phase epitaxy.[43] They, too, postulated the source of the dislocations to be glide along {110} planes.

Dislocations like the ones seen in Ni/Cu have also been observed in semiconductor systems, most notably, the Ge_xSi_{1-x}/Si (001) system.[44,45,46,47,48,49] It was

observed in this system, that above some critical value of heteroepitaxial misfit (about 2%), 90° dislocations lying along ⟨110⟩ directions with Burgers vectors in the interface plane are present.[46,48] Similar dislocations have also been observed in InGaAs/GaAs,[50,51] and GaAs/Si.[49]

Several explanations have been put forth for the existence of these dislocations, all of which involve the reaction of two dislocations to form a third. Such reactions are known to occur between dislocations when the energy of the system (the self-energy of the dislocations) is reduced by the reaction. Since the self-energy of a dislocation is approximately proportional to the square of the magnitude of the Burgers vector, the criterion for reaction of two dislocations to form a third is

$$b_1^2 + b_2^2 > b_3^2, \tag{3.11}$$

which is known as Frank's rule.[41] In this case, the Burgers vector reaction is

$$\mathbf{b}_1 + \mathbf{b}_2 = \mathbf{b}_3$$

or

$$\frac{a}{2}[01\bar{1}] + \frac{a}{2}[101] = \frac{a}{2}[110]. \tag{3.12}$$

All the dislocations in Equation (3.12) lie along the $[\bar{1}10]$ direction. Dislocations $\mathbf{b}_1$ and $\mathbf{b}_2$ are 60° dislocations, on intersecting {111} glide planes, with the line of intersection being $[\bar{1}10]$, the dislocation line. Dislocation $\mathbf{b}_3$ is a 90° dislocation in the (001) plane. This reaction produces a decrease in the energy of the system according to Equation (3.10).

Energetically, then, the reaction to form 90° dislocations is easily understood. The misfit relieved by $\mathbf{b}_3$ is equal to the misfit relieved by both $\mathbf{b}_1$ and $\mathbf{b}_2$. Consequently, the strain energy of the system is the same in both cases, and the total dislocation self-energy is lowered. Essentially, the reaction eliminates the Burgers vector components that do nothing to relieve misfit, the screw components and the

components normal to the interface. Also, glide toward the interface of the 60° dislocations is rapid. However, given a random array of 60° dislocations, it is extremely unlikely that the glide planes of two "complementary" dislocations (ones which can react with each other to become a 90° dislocation) will intersect precisely at the interface between the two materials. On the other hand, experimental evidence suggests that 90° dislocations do, in fact, form in these systems according to this reaction.[51,45] Solutions to this problem have been proposed based on two assumptions: (1) there is some climb involved, and (2) the process of forming 60° dislocations is not entirely random.

Climb is the motion of a dislocation out of its glide plane and requires the movement of vacancies toward or away from the dislocation core. It is limited by the rate of diffusion of vacancies in the material.[52] This process is highly temperature dependent. Since semiconductor films are deposited at several hundred degrees Centigrade, it is plausible that some climb can occur in these systems. Complementary 60° dislocations which react near the interface would be able to climb a short distance toward the interface. This type of reaction was proposed by Fitzgerald *et al.*[50] and is illustrated in Figure 3.7. It is assumed that the first dislocation is already at the interface due to initial misfit accommodation. The reaction is energetically much more likely to occur near the interface than near the surface, where image stresses on the dislocation would be high. The climb distance, therefore, is only a few atomic spacings. In the case of Ni/Cu, however, although climb is generally easier in films of metals than of semiconductors,[53] our films were deposited with no intentional substrate heating. The films reached a temperature of approximately 60°C during deposition due to radiative heating. Climb velocities at this temperature, even with the relatively strong driving force due to the misfit strain, are vanishingly small.[53] It is necessary, therefore to examine other possible mechanisms by which the dislocations can arrive at the interface.

Hull and Bean[46] note that in the Ge_xSi_{1-x}/Si system, the relative number of 90° dislocations increases with increasing degree of misfit (increasing x) as well as with increasing anneal temperature. This result has been interpreted to be indicative of the fact that at higher stress and higher temperature, nucleation of dislocations will be easier, and more nucleation sites will be active.[48] With an increasing density of nucleation sites it becomes more likely that two complementary 60° dislocations will meet at the

interface. Additionally, it has been suggested[45,48,49] that the presence of a 60° dislocation at the interface can influence the nucleation of other dislocations at the surface. In other words, the stress field surrounding the first dislocation can lead to the nucleation of a complementary dislocation, which will then glide toward the interface to react with the first dislocation to become a 90° dislocation.

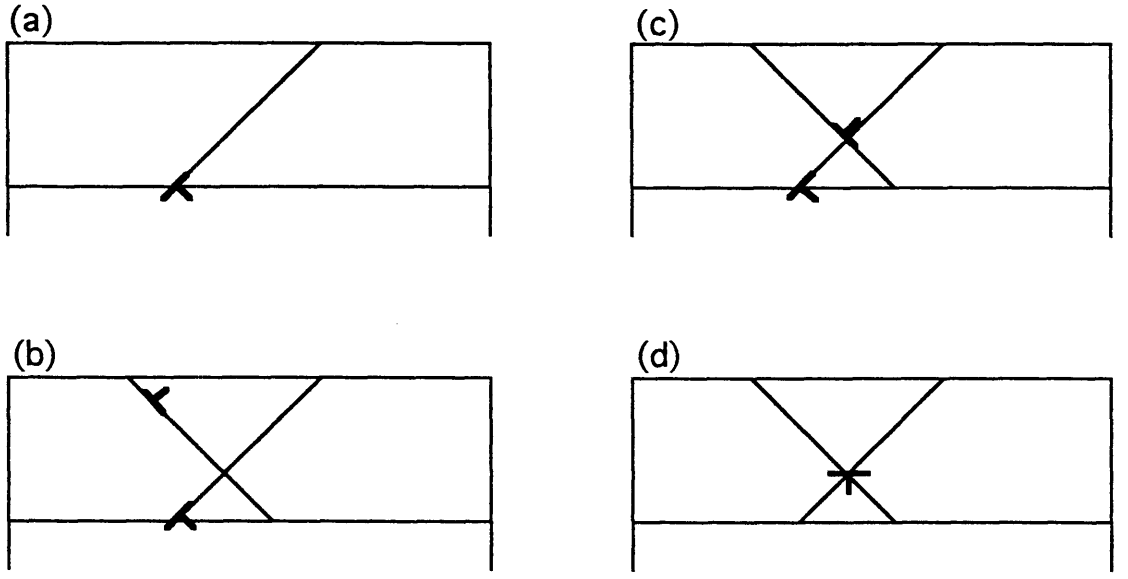

Figure 3.7 Two complimentary 60° dislocations react at the intersection of the glide planes (parallel to the dislocation lines) to form a 90° dislocation. This dislocation can then climb a short distance to the interface.

In their discussion of these reactions, Kvam *et al.*[45] refer to earlier work by Washburn *et al.*[54] which appears relevant to this discussion. They studied misfit due to high concentrations of Phosphorous in Si (001). The presence of the P in high concentrations causes expansion of the Si lattice. Misfit then exists between the doped and undoped regions. As the P diffuses into the Si, the "interface" between the doped and undoped regions moves deeper into the wafer. They observed through TEM a grid

of dislocations along ⟨110⟩ directions which were predominantly 90° type. The dislocations

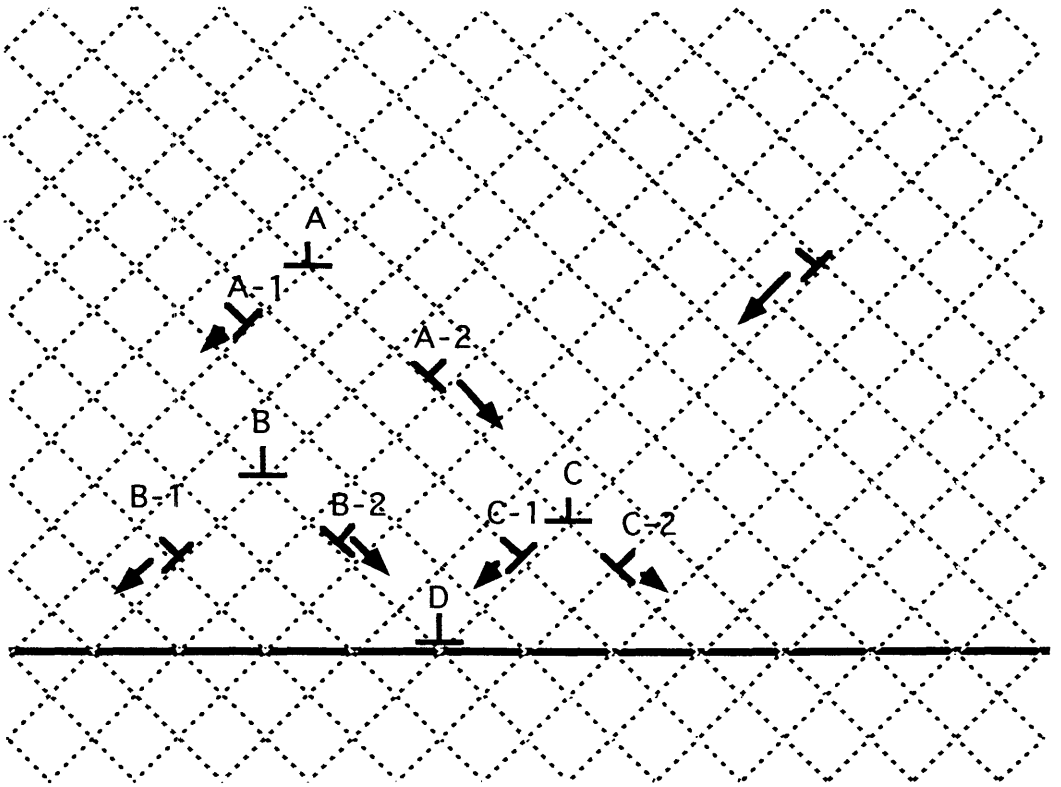

Figure 3.8 Proposed mechanism for migration of 90° dislocations toward the interface: The dashed lines represent the {111} glide planes. The solid line in the (001) interface. Edge dislocations above the interface will be unstable due to the misfit strain and will tend to break apart into mobile 60° dislocations. In the diagram above, dislocation A splits into complementary 60° dislocations A-1 and A-2.

were at different depths within the film, indicating that they had formed at different times during the doping process, and experimental evidence suggested that the dislocations were migrating toward the interface via a mechanism involving dissociation into 60° dislocations, glide toward the interface, and recombination into 90° dislocations.

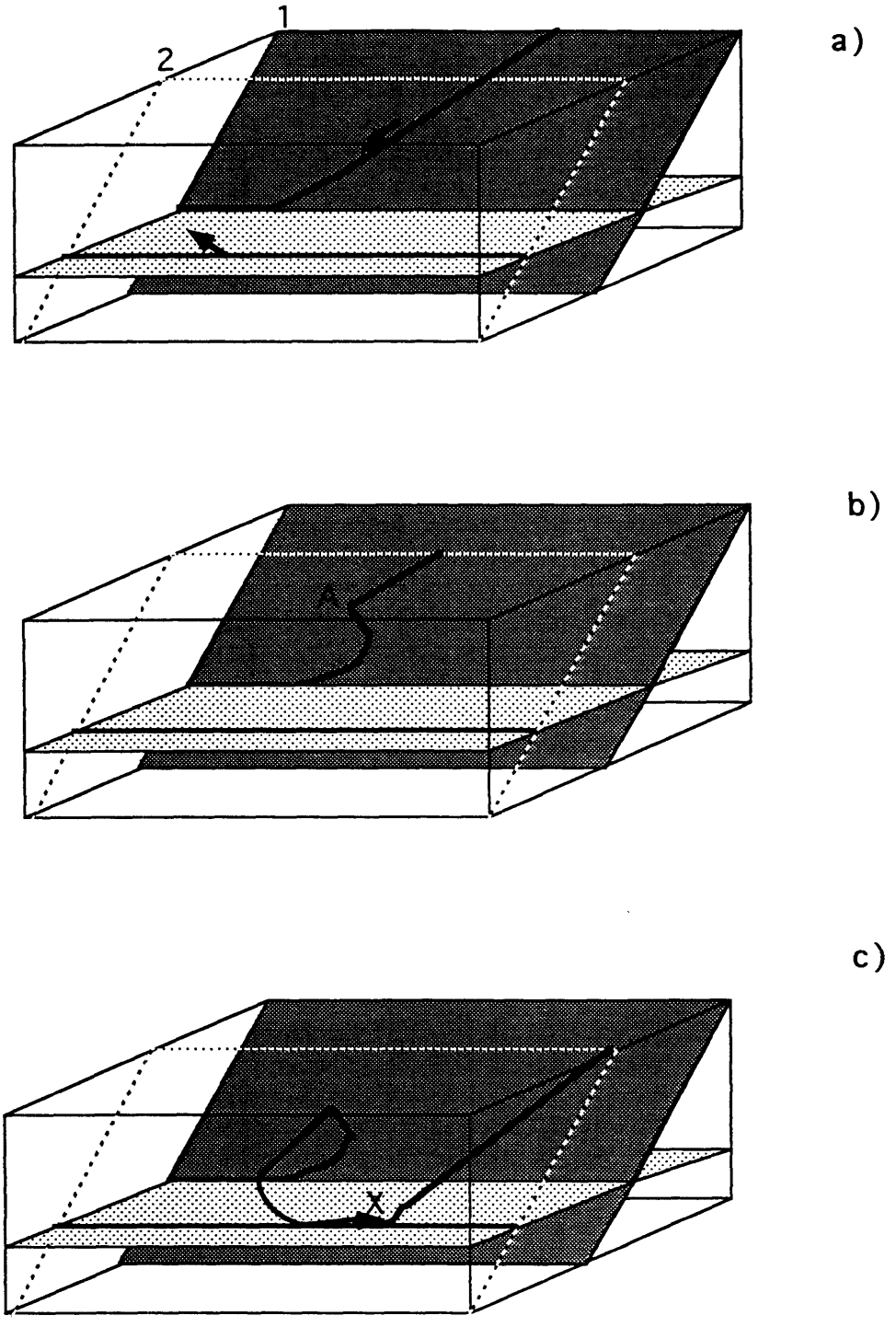

Figure 3.9 Cross-slip to aid dislocation reaction. (a) A 60° dislocation is in glide plane 1. A complementary 60° dislocation lies at the intersection of glide plane 2 with the interface. (b) The screw segment of the threading dislocation cross-slips to glide plane 2. (c) The dislocation bends toward the interface in glide plane 2 and reacts with the complementary dislocation to form a 90° dislocation segment.

This process is illustrated in Figure 3.8. The driving force for this type of motion is the excess stress. If there is sufficient driving force to generate a new dislocation, there is sufficient driving force to split an existing edge dislocation that is above the interface into two 60° dislocations that can travel toward the interface. For this type of mechanism to be active in the Ni/Cu system, an internal source, such as a Frank-Read source must exist for 90° dislocations.

Another possible mechanism is that the complementary 60° dislocations combine at the interface, rather than at the line of intersection of the two glide planes. This idea is illustrated in Figure 3.9. Assume one 60° dislocation is already lying in the interface. If a complementary dislocation glides toward the interface, the trailing threading dislocation is screw-type. This threading segment can cross-slip so that it can then glide to form a 60° misfit dislocation coincident with the first 60° dislocation, and the two can react to form a 90° dislocation segment. Additionally, cross-slip can promote defect formation which will lead to an increase in climb rate.

3.3 DISLOCATION SPACING

The spacing between misfit dislocations was measured using plan-view TEM images of the samples. Between 10 and 20 images were taken for each Ni thickness, and 150 individual spacings measured. It was determined through statistical analysis that, with 150 individual dislocation spacing measurements per sample, the measured mean was within 5% of the true mean of the distribution.

3.3.1 Work on NaCl substrates

3.3.1.1 Sample preparation for TEM

The biggest advantage of working with NaCl as a substrate material was the fact that plan-view TEM samples were easy to prepare. In order to view the films in plan-view in a transmission electron microscope, the substrate material must be removed so that the sample is electron transparent. After deposition, the samples were simply

cleaved into roughly 3mm square pieces. The samples were then placed in deionized water with the film side up. As the NaCl dissolved, the film (Ni/Cu) would float off on the surface of the water. It was then scooped up using a Cu TEM grid. The Ni/Cu bilayer was sufficiently thin to be electron transparent.

This preparation technique could be done quickly, as compared to traditional methods of TEM sample preparation, and ensured minimal damage between deposition and introduction to the microscope. The resulting TEM samples were of uniform thickness. In other words, there was a working sample area of about 9 mm^2, extremely large by TEM standards.

3.3.1.2 Dislocation spacing vs. thickness

The average spacing between dislocations was measured for a range of Ni thicknesses from 25Å to 200Å.[55] It was assumed during this preliminary investigation, however, based in part on the results of Matthews and Crawford,[14] that all dislocations were 60° dislocations. Since all choices of **g** in the (001) plane would show contrast for a 60° dislocation, the diffraction vector chosen to create the plan-view images was arbitrary. The spacing measured was therefore greater than the actual dislocation spacing in the films. Misfit dislocation grids were observed for all thicknesses. A typical micrograph is shown in Figure 3.4. The results of the spacing measurements are shown in Figure 3.10. The curves represent the predicted equilibrium spacing from the Matthews-Blakeslee model assuming either all 60° or all 90° dislocations. Since both types are present in the films, the true equilibrium prediction lies between these two curves. It can be seen that the spacing decreases as expected from equilibrium theory, but not to the extent that Matthews-Blakeslee would predict. This result is consistent with the work of other researchers in which dislocation spacings were actually measured directly in this way (see for example Nix[56]).

3.3.1.3 Moiré fringe spacing measurement

As stated above, the spacing between moiré fringes gives a measure of the amount of strain relief, and therefore the residual strain in the Ni film. The strain was measured as a function of Ni thickness for films grown on NaCl. The results of these measurements are shown in Figure 3.11. The relatively large error in the measurement arises from the fact that the presence of the dislocations themselves distorts the fringes, as can be seen in Figure 3.4. Once again, however, we see behavior that is expected from the Matthews-Blakeslee model. The strain decreases as the thickness increases and more misfit dislocations are formed. The residual strain as a function of Ni thickness will be discussed in more detail in Chapter 4, where the strain measurements of the samples grown on Si wafers are discussed.

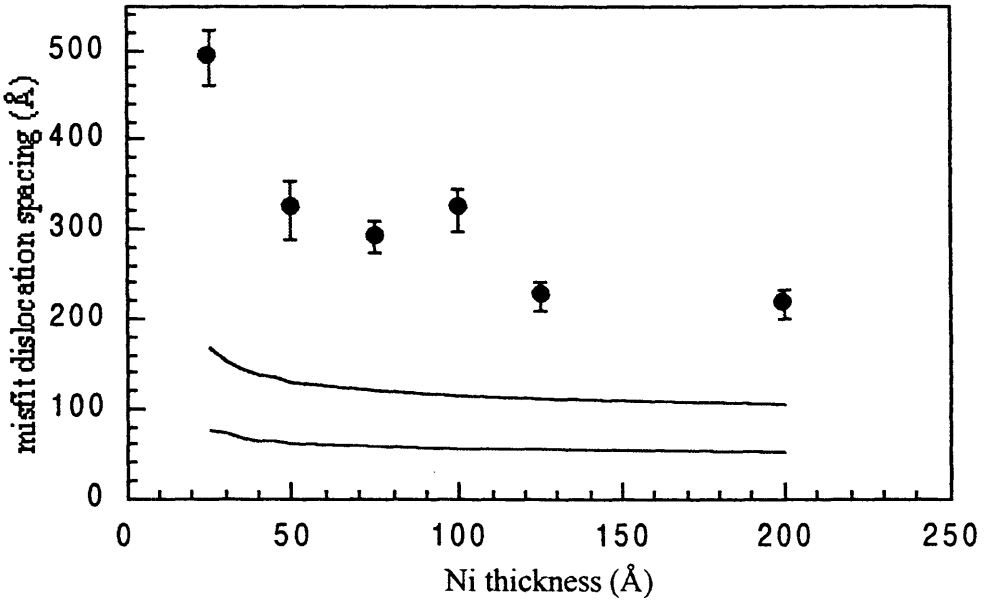

Figure 3.10 Misfit dislocation spacing measurements vs. Ni thickness for samples of Ni/Cu/NaCl (001). The curves represent the dislocation spacing expected from the Matthews-Blakeslee analysis if all dislocations are 90° (upper curve) or all are 60° (lower curve).[55]

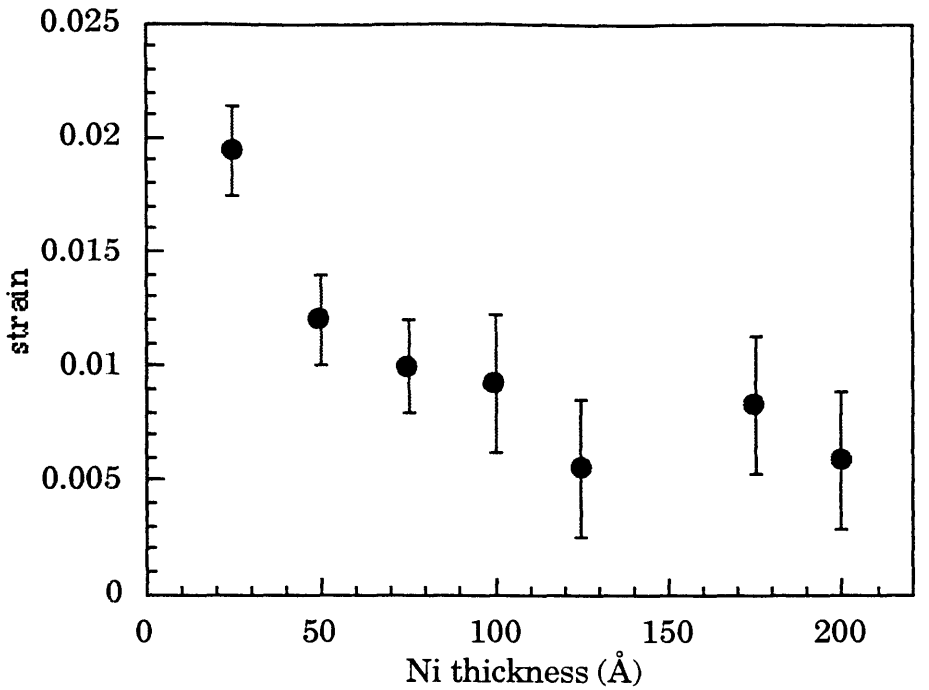

Figure 3.11 Residual strain vs. Ni thickness as measured by moiré fringe spacing[55]

3.3.2 Work on Si substrates

3.3.2.1 Sample preparation for TEM

As was described earlier, it was determined early in this investigation that Si would be a better substrate that NaCl for optical Kerr effect measurements due to its optically flat surface. Preparation of films deposited on Si for TEM was considerably more difficult than for those on NaCl. Since no chemical etch is available that would remove Si without also damaging the Ni/Cu film, the Si wafer had to be removed mechanically. The proceedure used was mechanical polishing and dimpling followed by ion milling. This procedure produced a large enough thinned area to image the misfit dislocation grids. The sample temperature was maintained at or below room temperature during this process in order to avoid further relaxation of the film and the formation of silicide at the Cu/Si interface (see Appendix). The Si was completely removed during this process so that all misfit dislocations observed could be assumed to be at the Ni/Cu interface.

3.3.2.2 Dislocation spacing vs. thickness

Misfit dislocation grids were observed in Ni/Cu (001) deposited on Si for samples with Ni thicknesses 20Å or greater. No misfit dislocations were observed in films of 15Å Ni or less. This result indicated that the critical thickness for misfit dislocation generation is between 15 and 20Å. This value is in agreement with h_c for Ni/Cu (001) measured by other researchers. Matthews and Crawford[14] measured the Ni/Cu critical thickness using TEM to be 14.6Å. Gidley[10] measured h_c = 9Å using positron tunneling on samples that had been annealed at 200°C. The Matthews-Blakeslee model predicts h_c = 19Å. A possible reason for the discrepency between measured values for h_c and that predicted thermodynamically is the coalescence of the islands during growth as discussed above. If coalescence occurs at a thickness below the critical thickness, dislocations may still be introduced where the islands meet.

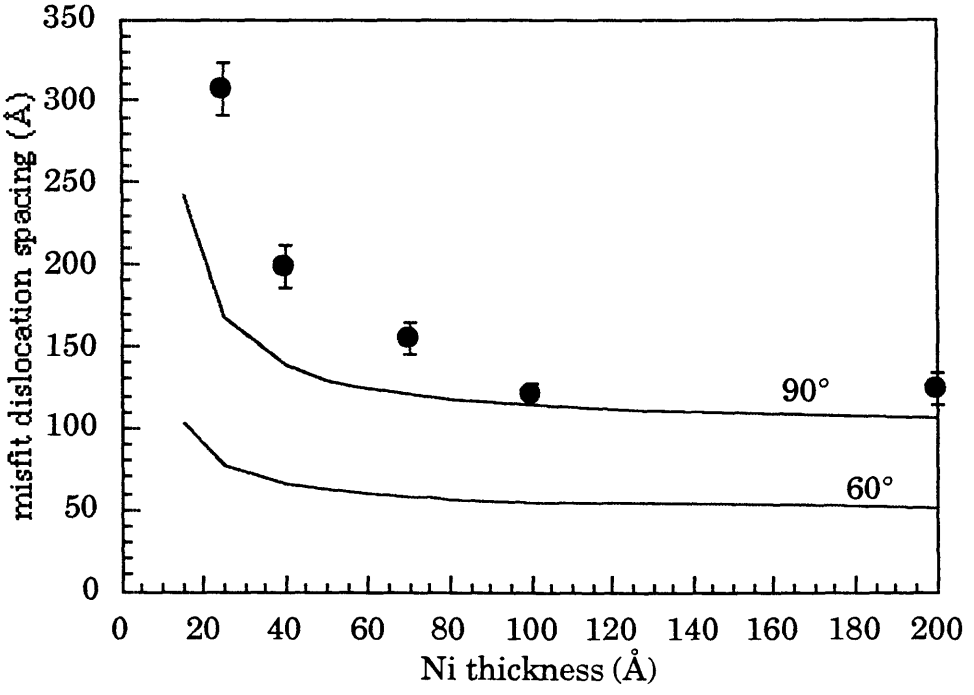

Figure 3.12 Misfit dislocation spacing vs. Ni thickness for Ni/Cu (001) (Si substrate). Curves represent spacing predicted by Matthews-Blakeslee model assuming strain relief via 90° dislocations or via 60° dislocations

The average spacing bewteen misfit dislocations was measured. The results are shown in Figure 3.12. The measured spacings are smaller than those reported for NaCl substrates, illustrating the error introduced when 90° dislocations are ignored. The measured spacing approaches the predicted spacing at large thicknesses. This result is consistent with the idea that the misfit accommodation is kinetically limited. As the driving force gets higher, the activation barrier is overcome and dislocations form. Gronet[57] described similar behavior in Ge/Si.

3.4 Summary

To conclude, the work discussed in this chapter has shown that misfit dislocations which act to relieve strain are present at the Ni/Cu interface. The spacing between dislocations decreases as the thickness increases, indicating that the Ni layer gets closer to complete relaxation. The consequences of this result will be discussed in later chapters as they relate to the magnetic properties which have been measured in these films. Knowledge of the strain state of the system and of the microstructure will allow a thorough understanding of the magnetic properties, and allow the development of magnetic anisotropy measurements as a tool for strain analysis.

4. CHAPTER 4: SUBSTRATE CURVATURE

In Chapter 3, we examined misfit dislocation formation as a mechanism for misfit strain relief in Ni/Cu (001). It is the residual strain in the film, and not necessarily the dislocation content that affects the magnetic properties according to the modified Neél model. Therefore, we want to measure residual (elastic) strain as a function of Ni thickness in conjunction with measurements of magnetic anisotropy energy so as to obtain a fit to the model which will give values of the surface anisotropy constants. The measurements of moiré fringe spacing discussed in the previous chapter gave us a measurement of strain in the films grown on NaCl. However, the magnetic characterization, which will be discussed in Chapter 5, was all performed on samples grown on Si substrates. Consequently, it is necessary to determine the Ni strain in those samples. In addition, the moiré fringe measurements are not highly accurate due to the fact that there is considerable distortion of the fringes due to the localized strain fields associated with the dislocations themselves. The screw components of the dislocations in particular cause a rotation of the Ni lattice which distorts the fringes.

The curvature of the Si wafers, in addition to providing a good surface for optical Kerr effect measurements, provides a useful way of measuring the strain in the Ni film. The strain in the Ni induces a slight, but measurable, bending of the Si wafer as a whole. This bending can be measured using optical techniques as discussed below. Strain measurements made in this way are quite accurate, and can be made quite easily. The technique does not require extensive sample preparation as TEM does, and is non-destructive.

4.1 RELATIONSHIP BETWEEN SUBSTRATE CURVATURE AND FILM STRESS/STRAIN

The most convenient way to measure thin film stress is through measurement of substrate curvature. Any intrinsic (or thermal) stress in a film will cause bending of the substrate.[58] To illustrate this effect, consider the film and substrate shown in Figure 4.1. If the film and substrate were separated, the film would shrink to its equilibrium size. The film is therefore in tension when attached to the substrate. This tension puts a stress on the substrate, and the substrate bends in response. This effect was first measured by Stoney in 1909.[58] The following description follows the analysis given by Ohring.[59] Substrate bending has since become a useful way of determining stress in a thin film. Determining the film stress from substrate curvature is fairly straightforward. For a free-standing film/substrate sandwich as shown in Figure 4.1-a, the total force and total moment are zero:

$$F = \int \sigma dA = 0, \tag{4.1}$$

and

$$M = \int \sigma z dA = 0, \tag{4.2}$$

where σ is the stress, A is the surface area, and z is the distance in the direction of the film normal. Figure 4.1-b shows a film-substrate combination of total thickness h and width w. The interfacial forces can be replaced by a force acting on the entire cross section of the film (or substrate) and a corresponding moment as shown in Figure 4.1. The bending of the sample results from the moments M_f and M_b of the film and substrate respectively. Since, as stated above, the total moment in the system must be zero, the sum of the counterclockwise moments M_f and M_b must be equal to the clockwise moment acting on the entire system:

$$\frac{\left(h_f + h_s\right)}{2} F_f = M_f + M_b \tag{4.3}$$

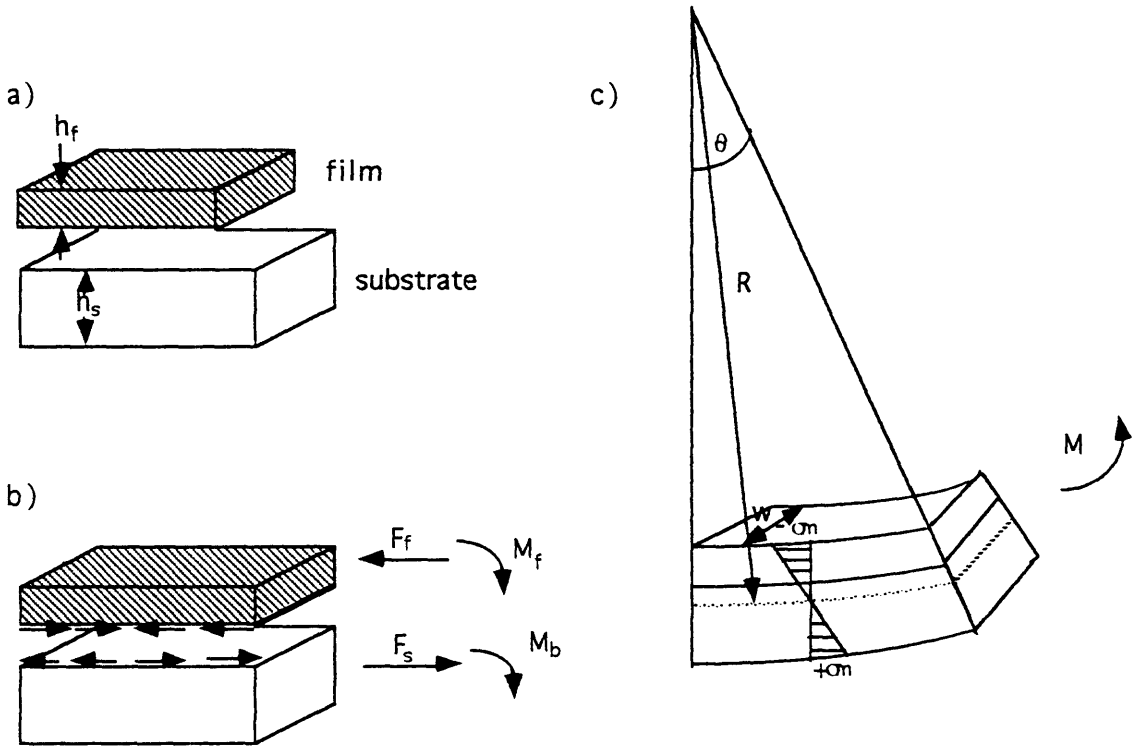

Figure 4.1 Illustration of the relationship between film stress and substrate curvature

As seen in Figure 4.1-c, the film-substrate system has a radius of curvature R which terminates at $\frac{\left(h_f + h_s\right)}{2}$. The lattice distortion will vary linearly from zero at this point to a maximum on either face of the piece where it is equal to

$$\frac{\left(R \pm \frac{h}{2}\right)\theta - R\theta}{R\theta} = \pm \frac{h}{2R}, \tag{4.4}$$

where θ is the angle subtended. The maximum stress is therefore equal to

$$\sigma_m = \pm \frac{Eh}{2R}, \tag{4.5}$$

where E is Young's modulus. From this stress distribution, we can calculate the moment across the sample:

$$M = 2\int_0^{h/2} w\left(\frac{\sigma_m}{h/2}\right) y \bullet y dy = \frac{\sigma_m h^2 w}{6} = \frac{Eh^3 w}{12R}. \tag{4.6}$$

By analogy,

$$M_f = \frac{E_f h_f^3 w}{12R} \text{ and } M_s = \frac{E_s h_s^3 w}{12R}. \tag{4.7}$$

Substituting these into equation (4.3) gives

$$\frac{\left(h_f + h_s\right)}{2} F_f = \frac{w}{12R}\left(E_f h_f^3 + E_s h_s^3\right). \tag{4.8}$$

Since $d_S >> d_f$, the film stress is given by

$$\sigma_f = \frac{F_f}{h_f w} = \frac{E_s h_s^2}{6Rh_f}. \tag{4.9}$$

In order to account for the biaxial nature of the stress, we must use the biaxial modulus and the result becomes

$$\sigma_f = \frac{E_s h_s^2}{6(1-\nu_s)Rh_f}. \tag{4.10}$$

This equation is known as Stoney's equation and has been used in this work to determine the film stress from substrate bending. The strain in the film can then be determined using Hooke's law.

It is important to note from the above analysis that the strain value calculated from a measurement of substrate curvature represents an average strain across the film. It should be apparent from the discussion in Chapter 1 that the strain in the film is quite high at the (dislocated) interface, and drops off sharply with increasing distance from the interface. It has been assumed throughout this work that the highly strained region is small relative to the thickness of the film, a reasonable assumption given that the radius of the dislocation core is of the order of the nearest-neighbor distance of the lattice.

4.2 EXPERIMENT

There are, in general, three ways of measuring the substrate curvature experimentally. They are optical interference mapping, optical reflection, and x-ray topography. The method that has been primarily used in these experiments is optical interference mapping. Measurements of a few samples were made using x-ray topography in order to verify the interference measurements.

4.2.1 Optical interference

Optical interference mapping was the primary technique used for room temperature strain measurement. In this technique, a laser is reflected off the sample while simultaneously reflecting off a reference flat. The phase difference between these two reflected beams produces an interference pattern like that shown in Figure 4.2. By making a series of shifts in optical path length, the path length difference beween the two samples can be computed for all points on the sample surface, giving the shape of the sample surface. A software routine then fits this shape to a sphere, thus giving the sample curvature.

These measurements were performed using a commercial system produced by WYKO corp. It is designed conveniently for three inch wafers. Measurements can be

made within seconds. Error, as measured by measuring a single wafer repeatedly over several days, is about 5%. Measurements are made in air. In order to determine the change in curvature due to the presence of the deposit, the wafer was measured before and after deposition.

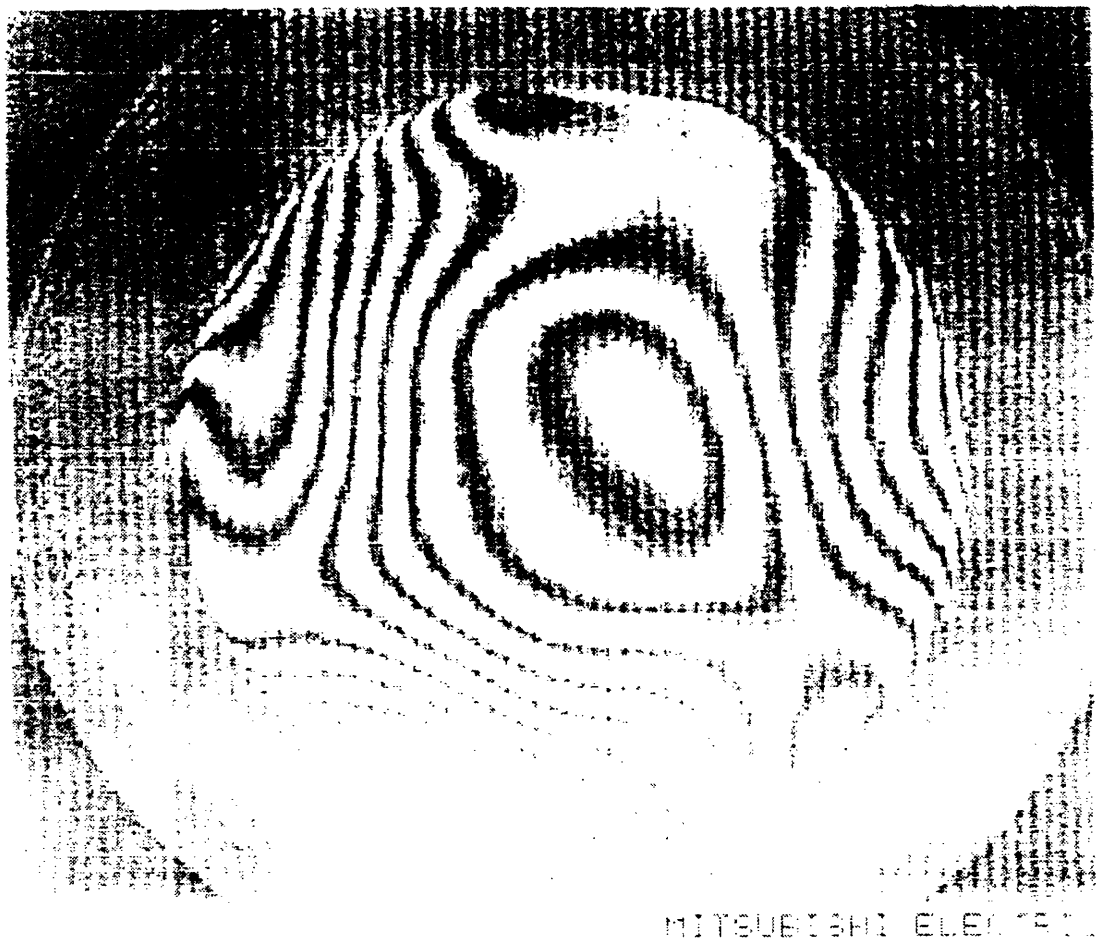

Figure 4.2 Interference fringes from WYKO interferometer

Ideally, in order to measure directly the residual misfit strain after accommodation through misfit dislocations, one would want to measure the change in curvature due to Ni deposition alone. Such a measurement is not possible however, due to the fact that the sample cannot be exposed to air between deposition of Cu and deposition of Ni. At first it was assumed that the change in curvature due to Cu alone

could be measured on one wafer, and that value merely subtracted from the curvature change measured on the Ni/Cu samples. However, there is evidence, which will be discussed in more detail in the Appendix, that the presence of the Ni layer affects the stress in the Cu. For this reason, a simple substraction of the two measured values would not be an accurate measure of the curvature change due to Ni. Additionally, some change in curvature would be expected due to the formation of a NiO layer on top of the Ni film when the sample is exposed to air. Matthews and Crawford[14] estimated the thickness of this oxide layer to be about 10Å. The oxide will be under compression. It can be assumed that the oxide will not alter the dislocation structure of the film, since it induces a relatively small strain and will itself impede the motion of dislocations.[14] We therefore wish to subtract any curvature change due to the oxide in the same way as curvature change due to the strain at the Cu/Si interface. To get an estimate of the curvature change due to the Cu and the oxide, the curvature change for a 15Å Ni/Cu film was measured. Since films of this thickness were determined to be free of misfit dislocations, as discussed in Chapter 3, the residual strain for this film was assumed to be equal to 2.6%, the misfit strain. Given the thickness of the Si wafer, the expected curvature change due to this amount of strain was calculated. This value was then subtracted from the actual measured curvature change. This difference was then subtracted from all other measurements to get a value for the curvature change due to Ni alone. The stress in the Ni film was calculated using Stoney's equation and the residual elastic strain determined from Hooke's law.

4.2.2 X-ray Topography

As stated above, the results of measurements made using optical interference were confirmed using x-ray topography. The x-ray topography measurements were performed for us by Laraba Parfitt, using a measurement system described by Tao.[60] This technique is based on the fact that only the portion of the crystal lattice that is at the Bragg condition will diffract x-rays. The image of the diffraction from a curved wafer captured on x-ray photographic film will be a topographic map of the wafer. Table 4-1 shows measurements of the curvature change for films using both x-ray

topography and optical interferometry. Agreement between the two types of measurements indicates that surface roughness and refraction do not have an effect on curvature measurements via optical interference.

	WYKO	x-ray
Cu/Si	3.14×10^{-3}	2.83×10^{-3}
24 Å Ni/Cu/Si	4.34×10^{-3}	5.17×10^{-3}
200 Å Ni/Cu/Si	8.32×10^{-3}	7.93×10^{-3}

Table 4-1 Measurements of change in wafer curvature after film deposition as measured by optical interferometry and x-ray topography

4.3 Results

4.3.1 Strain vs. Ni thickness

The strain in the Ni film was determined for films of varying Ni thickness. The results of these measurements are shown in Figure 4.3, where residual elastic strain is plotted as a function of Ni thickness. It can be seen that the strain decreases with increasing Ni thickness as expected. Shown is a fit to the data which will later be used to describe the strain behavior as a function of Ni thickness when fitting our data to the modified Neél model. These measurements are in fairly close agreement with the strain expected as a result of the measured misfit dislocation spacing. In Figure 4.4, the strain is plotted against the residual strain expected after strain relief due to dislocations, assuming all the dislocations are 60° or all are 90°. In reality, some dislocations of each type are present as discussed in Chapter 3. The measured strain value is closer to the strain expected assuming all misfit dislocations are edge dislocations, indicating that the

dislocations are predominantly edge-type, particularly at higher thicknesses. The consequences of this result have been discussed in detail in Chapter 3.

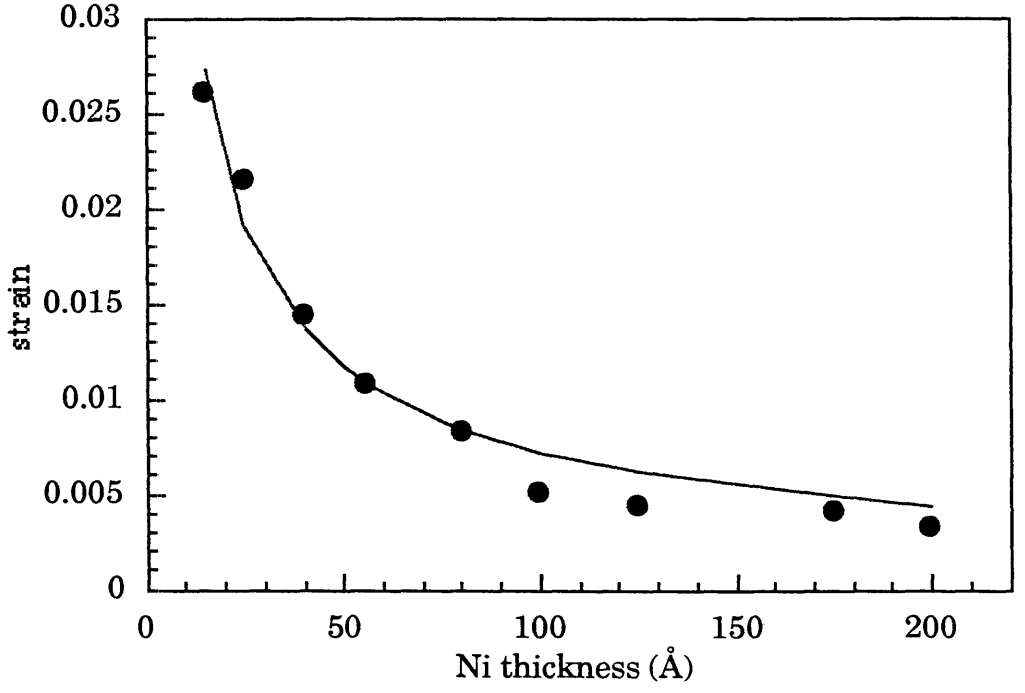

Figure 4.3 Ni strain vs. Ni thickness for Ni/Cu/Si (001) as measured by WYKO. The curve represents a fit to the data

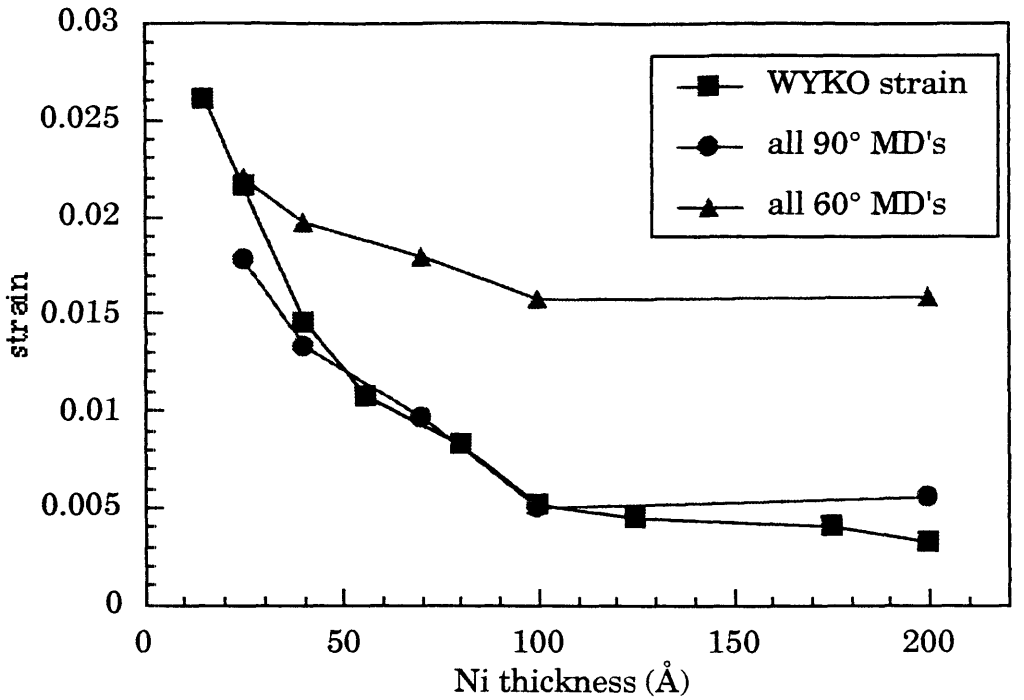

Figure 4.4 Comparison between strain measured by WYKO and strain after relieve from measured dislocation spacing assuming all 60° dislocations and assuming all 90° dislocations

Figure 4.5 shows the strain measured using WYKO™ optical interferometry as compared to that measured by moiré fringe spacing measurement on NaCl samples. There is good agreement between the two measurements. This result is not surprising since the dislocation spacing measurements were also in fairly good agreement. Also shown in Figure 4.5 are the results of strain measurement by moiré fringe spacing made by Matthews and Crawford.[14] Their results show a lower residual strain than those measured in our films. This discrepency can be explained by the fact that their films were deposited at a slightly higher temperature (80°C) than ours. This result emphasizes the amount of variation in misfit accommodation that can result from small changes in deposition conditions. If we had merely compared our measurements of magnetic anisotropy to strain measurements of other researchers in order to calculate the surface anisotropy constants, our results would have been inaccurate. It also emphasizes the fact that these films are metastable, that the misfit accommodation is kinetically limited, and that heating the films can lead to increased misfit accommodation.

From these measurements, we have information about the strain in the Ni film as a function of film thickness. If the strain behavior was that predicted by the Matthews-Blakeslee model, the strain would vary approximately as $\frac{1}{h}$ (see Chapter 1). The measurements show, however, that the strain is higher (the film is less relaxed) than the Matthews-Blakeslee prediction. The fit to our data gives a dependence of strain on thickness of approximately $\frac{1}{h^{0.7}}$. Specifically, the fit gives[3]

$$\varepsilon \approx \frac{0.1815}{h^{0.70}}. \tag{4.11}$$

4.3.2 Strain vs. alloy concentration

Strain measurements were made using optical interferometry on samples of 25Å Ni_xCu_{1-x}/Cu/Si. The results are shown in Figure 4.6. Increased Ni concentration in the alloy layer gives an increased misfit between the epilayer and substrate with a maximum misfit of 0.026 for pure Ni on Cu. It was determined using TEM that all of these samples had misfit dislocations, as discussed in the previous chapter. In other words, the critical thickness for the alloy/Cu system was exceeded. It is interesting to note that the residual strain depends on alloy concentration. The Matthews-Blakeslee model, in fact, predicts no dependence of residual strain on initial misfit beyond the critical thickness. Recall from Chapter 1 that the strain dependence on thickness is given by

$$\varepsilon = \frac{b}{8\pi \cos\lambda} \frac{\left(1 - \nu \cos^2\beta\right)}{(1+\nu)} \ln\left(\frac{4h}{b}\right). \tag{4.12}$$

Equation (4.12) is shown graphically in Figure 4.7. The dependence of residual strain on initial misfit is therefore further evidence that the thermodynamic limit is not being achieved and that the misfit accommodation is kinetically limited. A similar dependence of residual strain on misfit was found by Westwood and Woolf in $In_xGa_{1-x}As$/GaAs (100) films.[61]

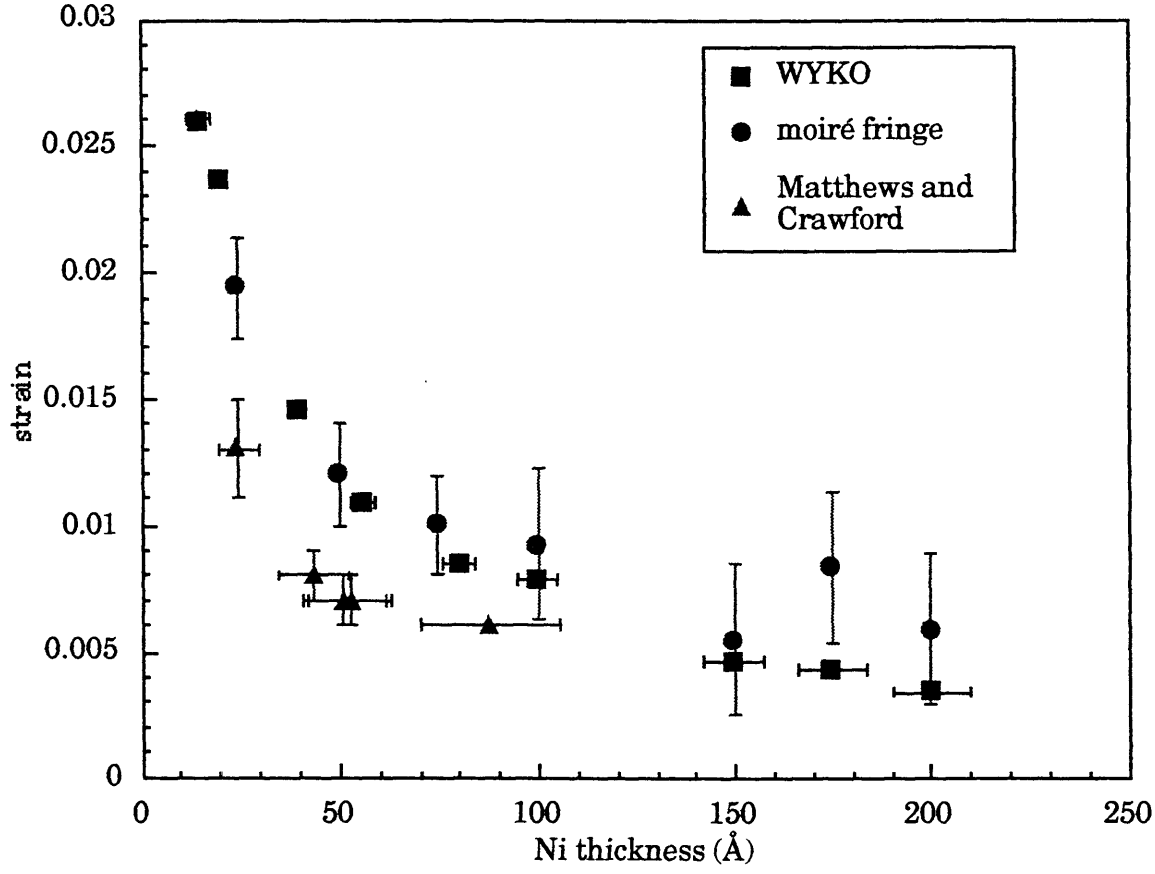

Figure 4.5 Results of Ni strain measurement in Ni/Cu (001) films, using moiré fringe contrast as discussed in Chapter 3, using subtrate curvature (WYKO) measurements, and measurements made by Matthews and Crawford[14] using moiré fringes.

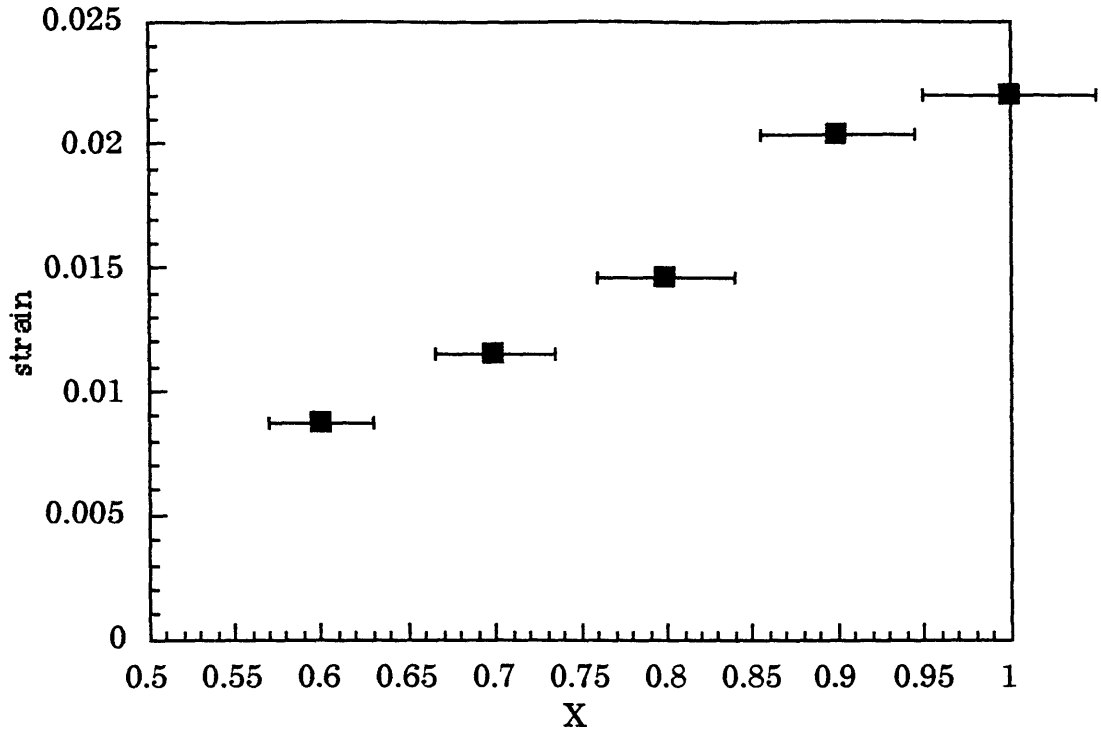

Figure 4.6 Strain in Ni_xCu_{1-x}/Cu/Si as measured by WYKO. Alloy layer thickness is 25Å

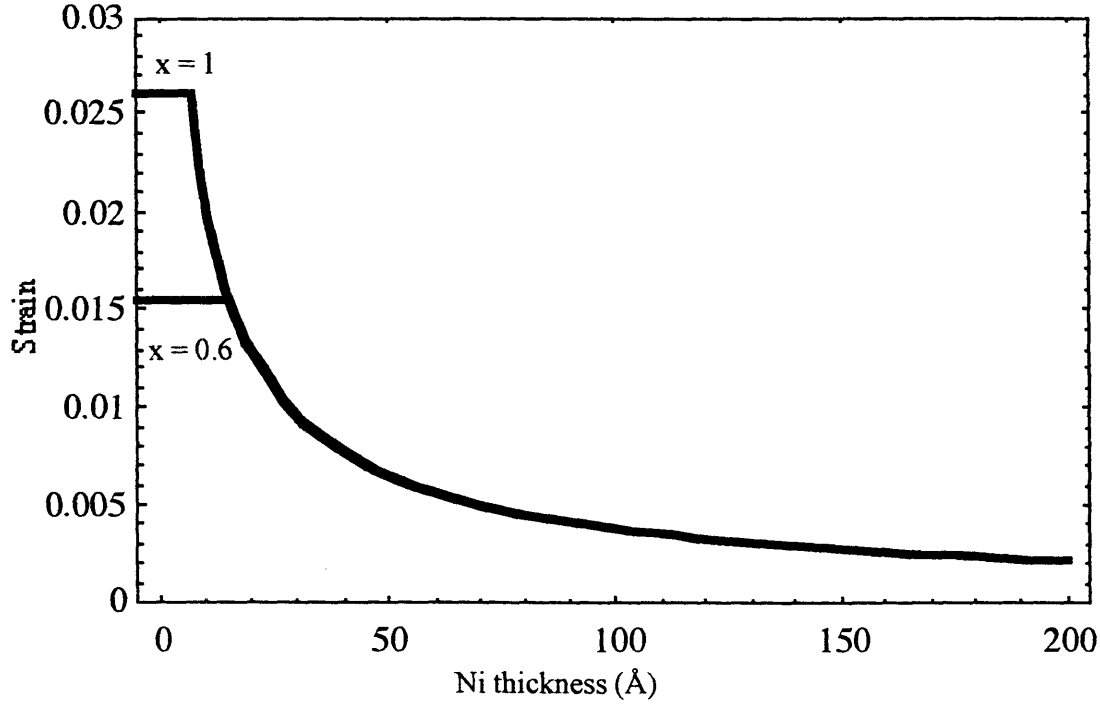

Figure 4.7 Strain vs. film thickness as predicted by the Matthews-Blakeslee model for Ni_xCu_{1-x}/Cu films

4.4 DISCUSSION

The results of these measurements give a description of the strain in the Ni/Cu (001) interface as a function of Ni thickness. Chapter 5 describes how Equation (4.11) can be used in combination with measurements of magnetic anisotropy to determine the dependence of anisotropy on strain in these films. Once this dependence is established, measurements of magnetic anisotropy can be used to determine strain in these films.

5. CHAPTER 5: MAGNETIC CHARACTERIZATION

In Chapter 1 a model was described relating strain to magnetic anisotropy. Results were presented in the previous chapter which describe the state of strain in the Ni film as a function of film thickness. The current chapter will describe measurements of magnetic anisotropy energy of Ni films over the same thickness range deposited under the same conditions. It will then be shown how the data from these two types of measurements were fit to the model to obtain a complete description of the anisotropy behavior as a function of strain in these films.[3]

As stated in Chapter 1, the goal of this project has been to develop magnetic anisotropy measurements, specifically measurements of the magneto-optic Kerr effect (MOKE), as an *in situ* tool for measuring strain. We have, as described in Chapter 2, an apparatus for measuring MOKE in the MBE deposition chamber. Unfortunately, the magnetic field that can be generated with this set-up is not sufficient to saturate the magnetization in these films. Measurements made using the *in situ* MOKE apparatus therefore give only qualitative information about the magnetic properties of the films. In order to obtain a quantitative measure of the magnetic anisotropy energy of our films, *ex situ* analysis was necessary. This was provided through vibrating sample magnetometry (VSM). This system is capable of generating a magnetic field of 10,0000 Oe, which is more than sufficient for saturation of these films. It is possible to design an *in situ* MOKE system which could provide sufficient field. The results presented in this chapter therefore show that this type of *in situ* measurement of anisotropy energy is, in fact, possible.

Experimentally, the anisotropy energy is defined by:

$$K^{eff} = \int_0^{M_s} H_{//} dM - \int_0^{M_s} H_{\perp} dM \ , \qquad (5.1)$$

where $\mathbf{H}_{//}$ and $\mathbf{H}_{\perp}$ are the applied field parallel and perpendicular to the plane of the film, respectively. For this convention, $K^{eff} > 0$ corresponds to magnetization perpendicular to the plane of the film. The area corresponding to one of these integrals is shown in Figure 5.1. In order to determine K^{eff}, it is necessary to measure this area for two orientations: with the applied field parallel to the film and with the field perpendicular to the film.

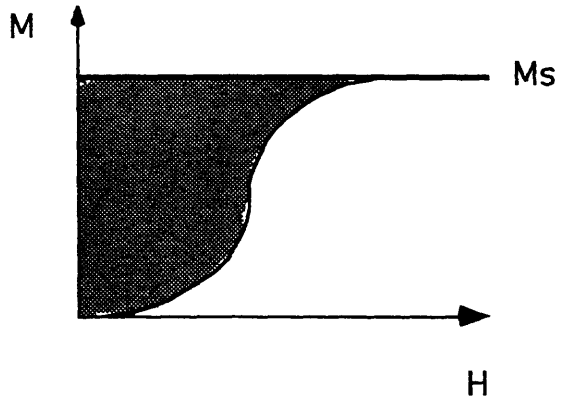

Figure 5.1 Shaded region is anisotropy energy K

5.1 MOKE

5.1.1 The Kerr effect

The Kerr effect refers to the phenomenon that occurs when polarized light is reflected off a magnetized surface.[62] The plane of polarization of the light is rotated by an amount proportional to the magnetization of the sample,

$$\theta = K_r \mathbf{M}. \tag{5.2}$$

The angle of this rotation is dependent on the magnitude and direction of **M**. Specifically, the angle of rotation is dependent on the component of the magnetization in the surface parallel to the direction of propogation of the light. Two types of Kerr effect, depending on the relative orientation of the magnitization with respect to the surface plane and the plane of incidence of the light beam, were measured in the course of this investigation. The first, the polar Kerr effect illustrated in Figure 5.2(a), was used to measure the component of **M** perpendicular to the plane of the surface. This is the configuration in which the angle of the rotation is largest.[62] Figure 5.2(b) illustrates the configuration for the longitudinal Kerr effect. In this case, the component of **M** in the plane of the film and in the plane of incidence is measured. The angle of the rotation in this case is much smaller.

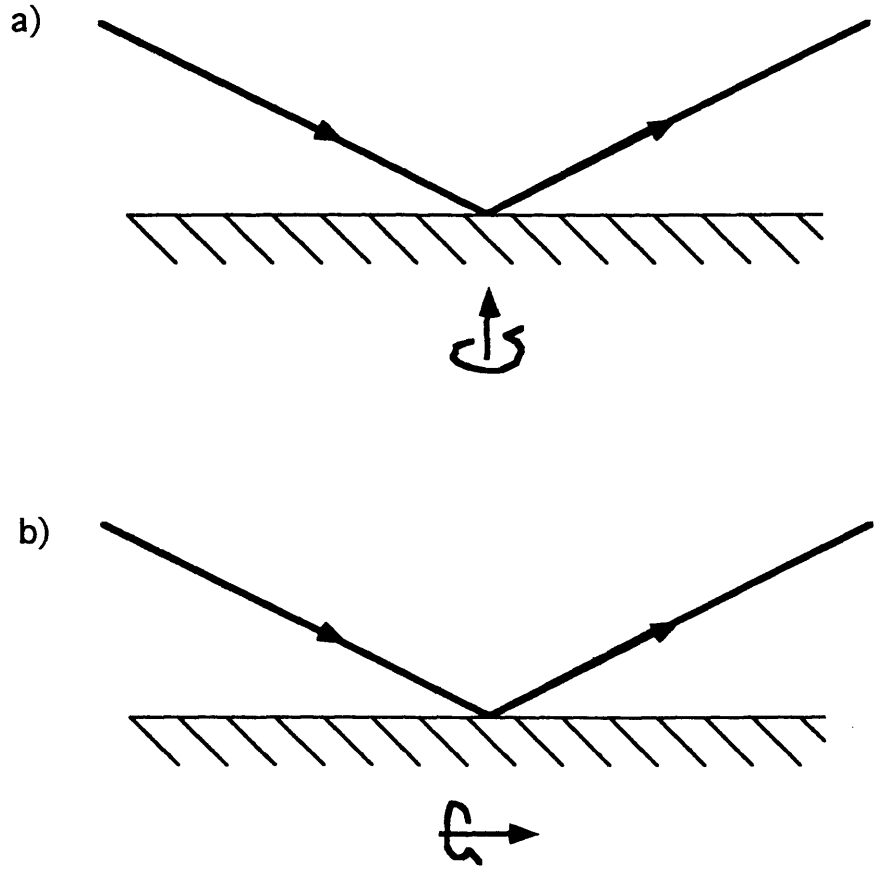

Figure 5.2 Configurations for polar (a) and longitudinal (b) Kerr effects

In practice, it is the intensity of the light transmitted through a polarizer and detected by a photodiode that is measured. This changing component of the intensity is referred to as the Kerr intensity I_K. By monitoring the change in I_K while cycling the applied magnetic field, it is possible to measure a magnetic hysteresis curve for the sample. This is the method by which hysteresis curves were measured *in situ* for these experiments.

5.1.2 MOKE apparatus description

The apparatus that was constructed for this research by Craig Ballentine, a post-doctoral fellow, is shown in Figure 5.3. Light from a He/Ne laser is polarized and sent through a chopper wheel which is connected to a lock-in amplifier. The light then enters the chamber through a viewport, and is incident on the sample at approximately 45°. The reflected light then leaves the chamber through a second viewport. A second polarizer blocks the light that is polarized in the same direction as the incident light, so that the intensity of the light passing through is the signal which is picked up by the photodetector and fed to an IBM XT computer. The computer in turn controls the cycling of the applied field and records I_K as a function of **H**. The field can be applied either parallel to or perpendicular to the plane of the film for measurement of both polar and longitudinal Kerr effect, up to a field strength of about 1000 Oe.

5.1.3 Results

The results of the MOKE measurements have been reported by Bochi *et al.*[63] Figure 5.4 shows hysteresis loops measured on samples of Ni/Cu/Si (001) for a range of Ni thicknesses. Both polar and longitudinal loops were measured. If the applied field is in the prefered direction of magnetization (low anisotropy energy), the loop will be square shaped, indicating a high remanence. Conversely, if the applied field is normal to the prefered direction (high anisotropy energy), the remanence will be close to zero and the loop will be almost linear. Figure 5.4 illustrates a transition from a preferred perpendicular direction of magnetization for thin Ni films to a preferred direction in the plane of the film for thicker films, with a transition thickness h_{Ni} of about 75Å. This

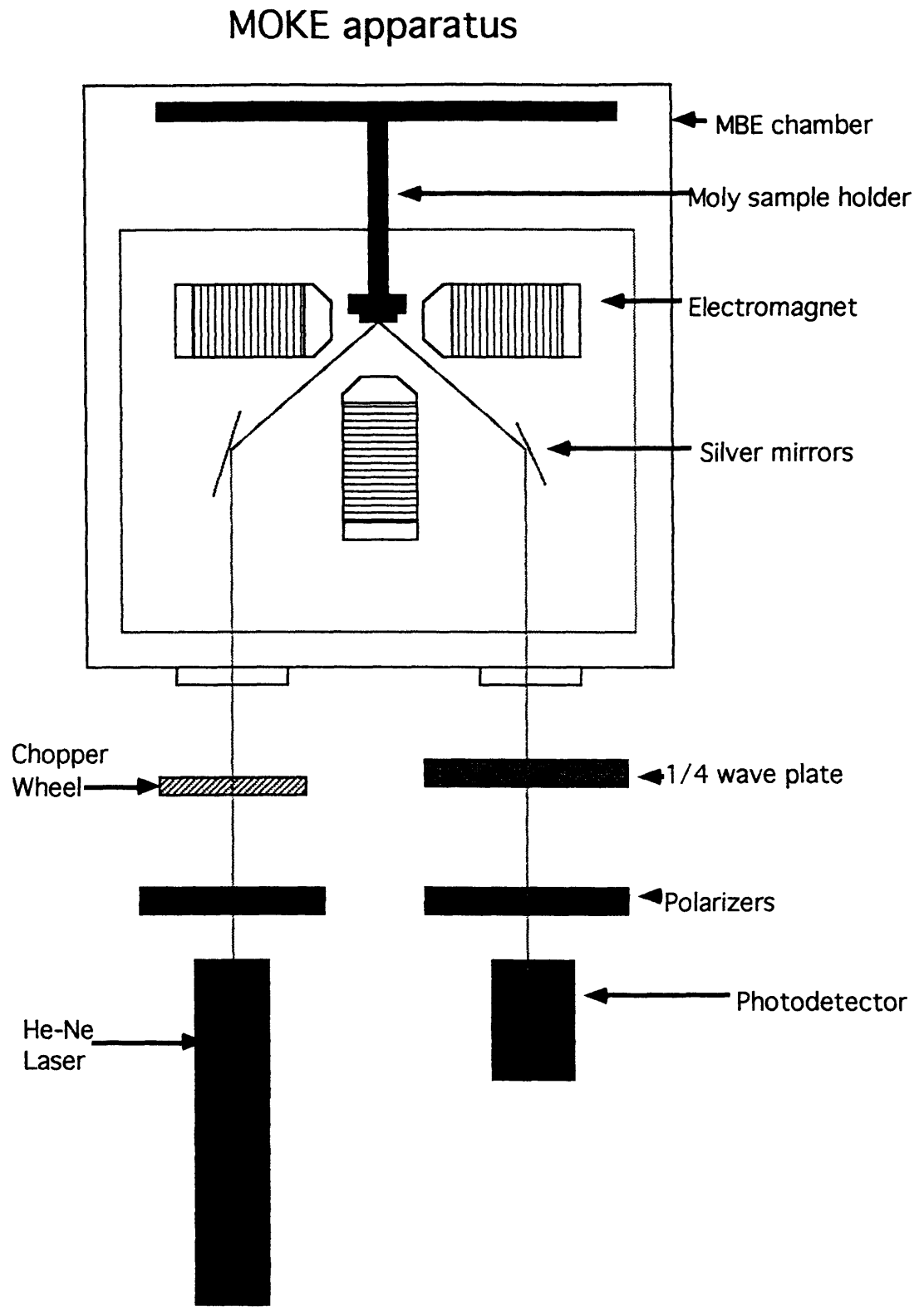

Figure 5.3 Schematic diagram of MOKE apparatus used in this work

h_{Ni} = 100Å

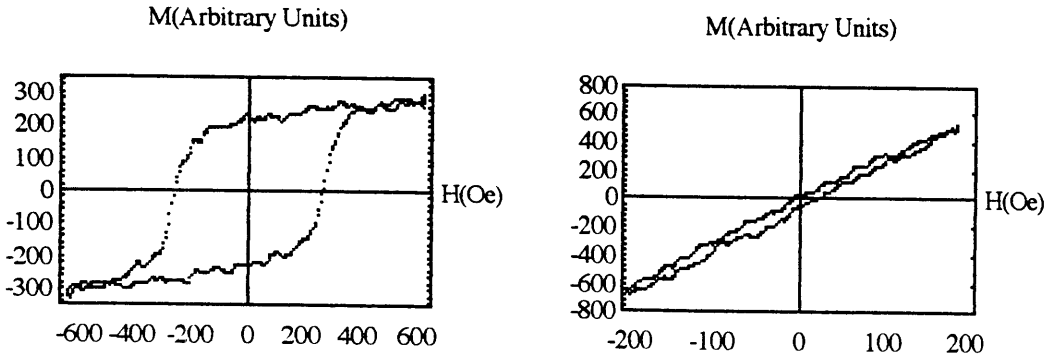

h_{Ni} = 50Å

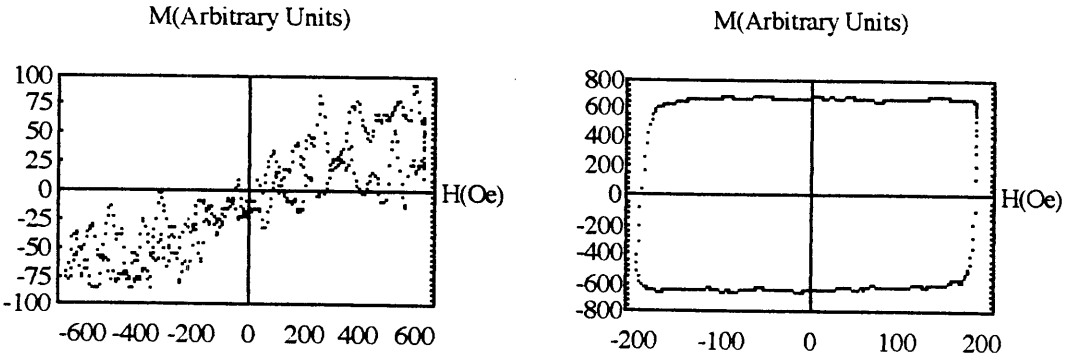

h_{Ni} = 15Å

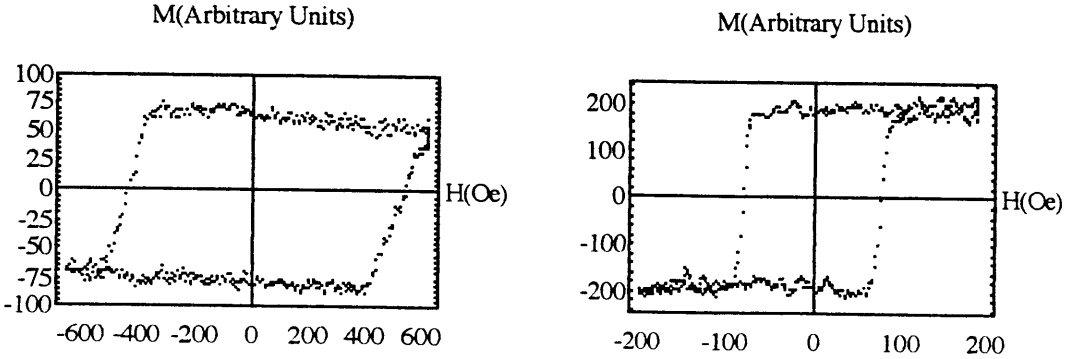

Figure 5.4 Longitudinal and polar MOKE loops of Ni/Cu/Si (001)[63]

result is illustrated in Figure 5.5, where the remanence relative to the saturation of the polar Kerr effect is plotted as a function of Ni thickness. The value of M_r/M_s is close to one for a square (low anisotropy energy) loop, and close to zero for a linear (high anisotropy energy) loop. Once again, it can be seen that the preferred orientation of **M** is perpendicular to the film plane for $h_{Ni} < 75$Å.

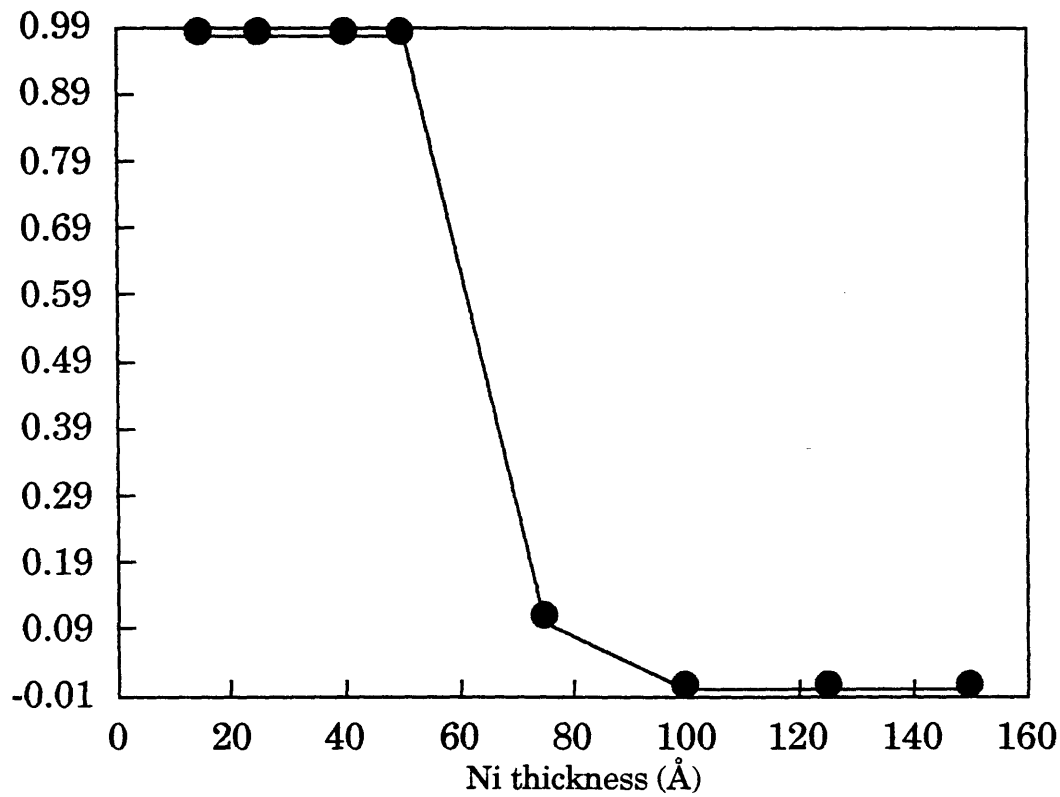

Figure 5.5 Mr/Ms (approximate)for polar MOKE loops of Ni/Cu/Si (001)[63]

5.1.4 Discussion

This result can be analyzed qualitatively using the model described in Chapter 1. Recall the thickness dependence of the magnetic anisotropy energy K^{eff}:

$$K^{eff} = -2\pi M_s^2 + 2B_1\varepsilon + 2\frac{K^s + B^s\varepsilon}{h} \qquad (5.3)$$

At large thicknesses, the surface terms become insignificant, and due to the fact that the misfit strain is low at large thickness (see Chapter 4), the magnetostatic term ($-2\pi M_s^2$) dominates and the preferred magnetization direction is in the plane of the film. At smaller thicknesses, the surface and magnetoelastic terms become significant and the magnetization is perpedicular to the film plane. Notice, also, that at very small thickness ($h_{Ni} \sim 15$Å), the magnetization direction appears to be changing toward the in-plane direction. This result is consistent with that of Ballentine.[64] This result can be explained if the surface magnetoelastic coefficient, B^s is negative. At very low thicknesses, the misfit strain is very high ($\varepsilon = \eta = 0.026$). Therefore a negative B^s can explain why the magnetization direction is in the plane of the film at very low thicknesses. This analysis gives an explanation for the fact that the thickness for the transition to perpendicular magnetic anisotropy corresponds to the critical thickness for misfit dislocation formation (see Chapter 3), since there is a dramatic decrease in strain in the film corresponding to the onset of dislocation formation. The in-plane to out-of-plane transition is not, therefore, related to the influence of the dislocations themselves, as was originally postulated,[64] but rather to the drastic strain change which accompanies the onset of misfit accommodation.

5.2 VSM

As stated earlier, a quantitative measurement of anisotropy energy was not possible with the MOKE apparatus due to the limited applied field achievable. Magnetic hysteresis loops were therefore also measured *ex situ* using Vibrating Sample Magnetometry (VSM). The principle behind VSM measurement is the measurement of magnetic induction.[62] The sample is vibrated near an induction coil such that the coil can measure the flux with and without the sample present. The change in the induction **B** between the two positions, is proportional to the magnetization of the sample **M**.

5.2.1 Experimental technique

The VSM used in these measurements allowed measurement of hysteresis loops through oscillation of the applied magnetic field. It also allowed measurement of the anisotropy energy as described above by allowing demagnetization of the sample. The output of the VSM is electromotive force (e.m.f.) vs. applied field, **H**. The data from the magnetometer can also be used to calculate the area corresponding to the integral

$$\int_0^{V_{max}} HdV, \tag{5.4}$$

where V is the e.m.f. **M** is equal to the volume of the sample times the e.m.f. It was assumed for these measurements that the saturation was equal to the saturation for bulk Ni. From the maximum e.m.f., therefore, it was possible to calculate the effective volume of the sample, and therefore convert the integral given by the VSM (Equation (5.4)), to K^{eff} (Equation (5.1)).

5.2.2 Results for Ni/Cu/Si (001)

VSM measurements were performed on the Ni/Cu/Si (001) samples for a range of Ni thicknesses from 15Å to 200Å.[63] Figure 5.6 shows the remanence divided by the saturation for a perpendicular applied field as in Figure 5.5. The results are similar to the MOKE measurements in that there is a transition from a perpendicular preferred magnetization direction to in-plane. The thickness for the transition is higher, though--about 125Å. This difference is the result of the Ni films being exposed to air for the *ex situ* VSM measurement. It was found that, if a sample was returned to the MBE after being exposed to air that it would exhibit the same magnetic properties when measured using MOKE as was seen using VSM. In other words, the change in the transition thickness is irreversible. The difference, therefore, was a result of the oxidation of the Ni film. This is not surprising given that the model predicts a strong effect of surface properties on the anisotropy of a film. In the case of the *in situ* MOKE measurements, the surface of the film can be described as a vacuum/Ni interface, whereas, in the case of the *ex situ* VSM measurements, it is a NiO/Ni interface. It is reasonable to assume that

these two types of interfaces will be magnetically different, i.e. that K^s and B^s would take on different values. The difference in strain between an unoxidized and an oxidized film could also contribute. This result will be discussed further in Chapter 6.

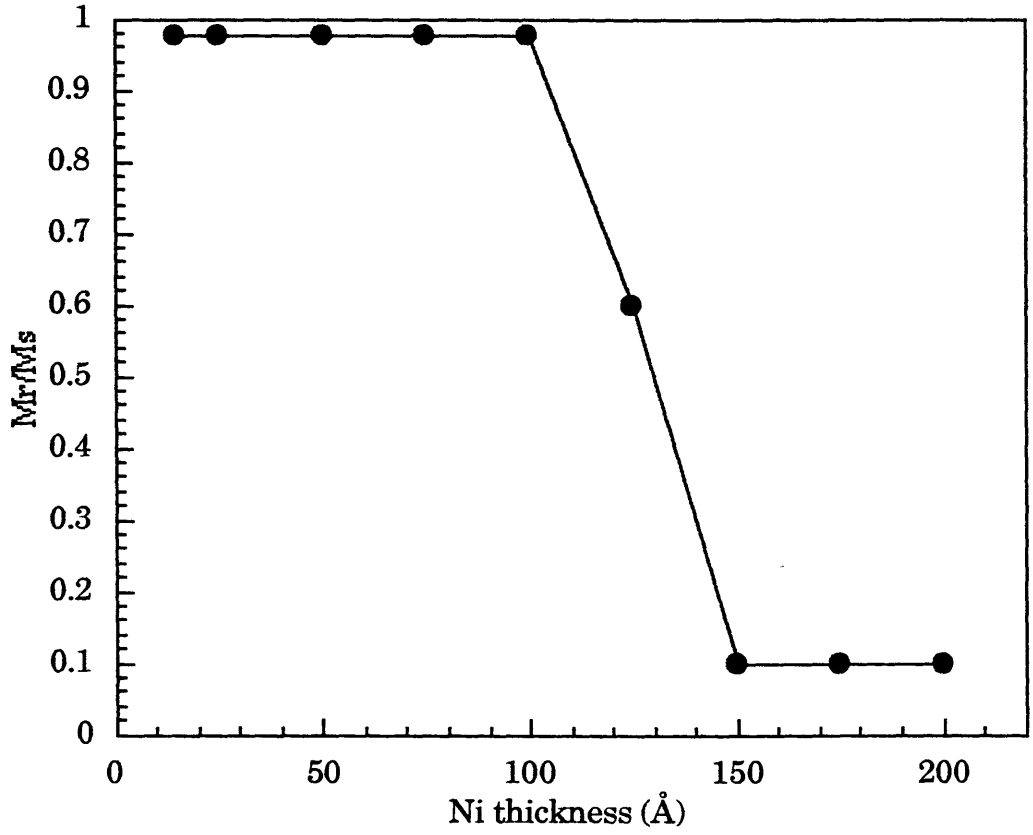

Figure 5.6 Mr/Ms of hysteresis loops measured by VSM with **H** perpendicular to the plane of the film for films of Ni/Cu/Si (001)[63]

5.2.3 Results for Cu/Ni/Cu/Si sandwiches

In an attempt to avoid the complication of oxidation of the Ni surface upon removal from the MBE, a series of films was deposited with a thin (20Å) Cu capping layer. The fabrication of these samples was discussed in detail in Chapter 2. In addition to preventing Ni oxidation, the capped samples had the added advantage that the two interfaces were both Ni/Cu and could be assumed to be magnetically identical. This fact is important for the fitting of the experimental data to the modified Neél model.

The results of these measurements are shown in Figure 5.7 and Figure 5.8. Figure 5.7 shows hysteresis loops for samples with various Ni thicknesses. Once again, a transition from perpendicular to in-plane prefered direction for magnetization is seen. The transition thickness is approximately 130Å. The effective anisotropy energy, K^{eff}, as measured using the technique described above, is shown as a function of Ni thickness in Figure 5.8. $K^{eff} < 0$ indicates in-plane anisotropy.

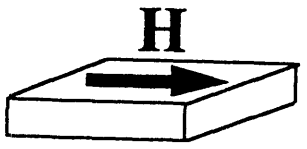

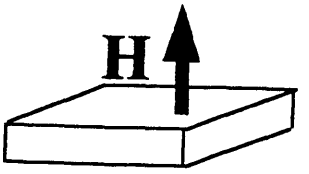

h_{Ni} = 150Å

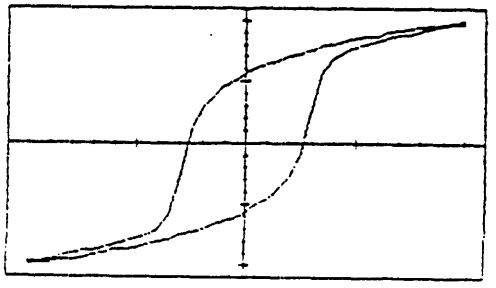

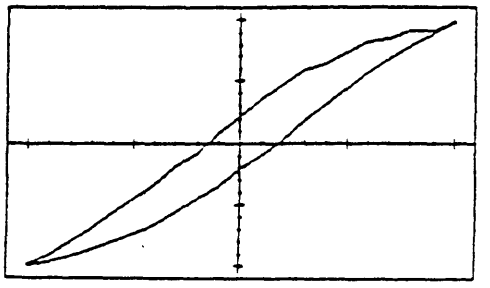

h_{Ni} = 125Å

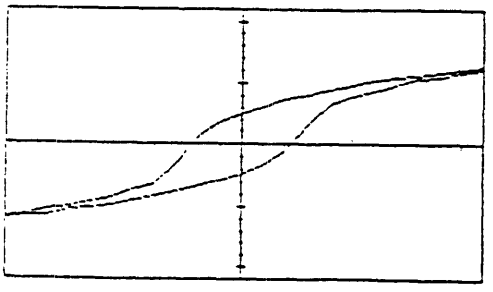

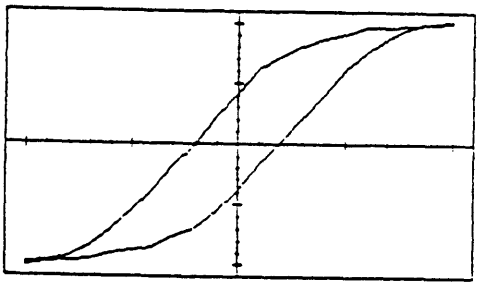

h_{Ni} = 100Å

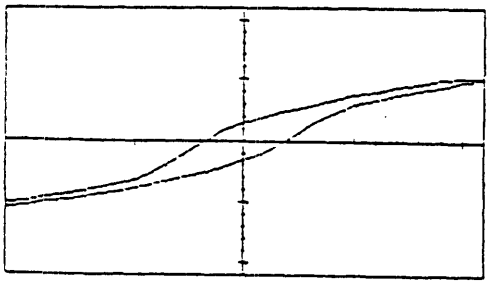

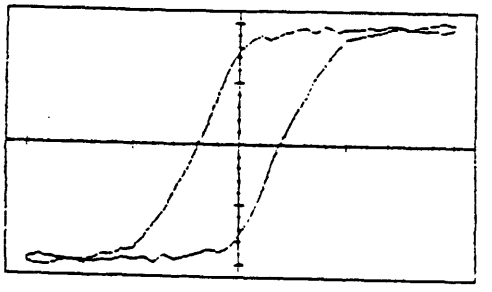

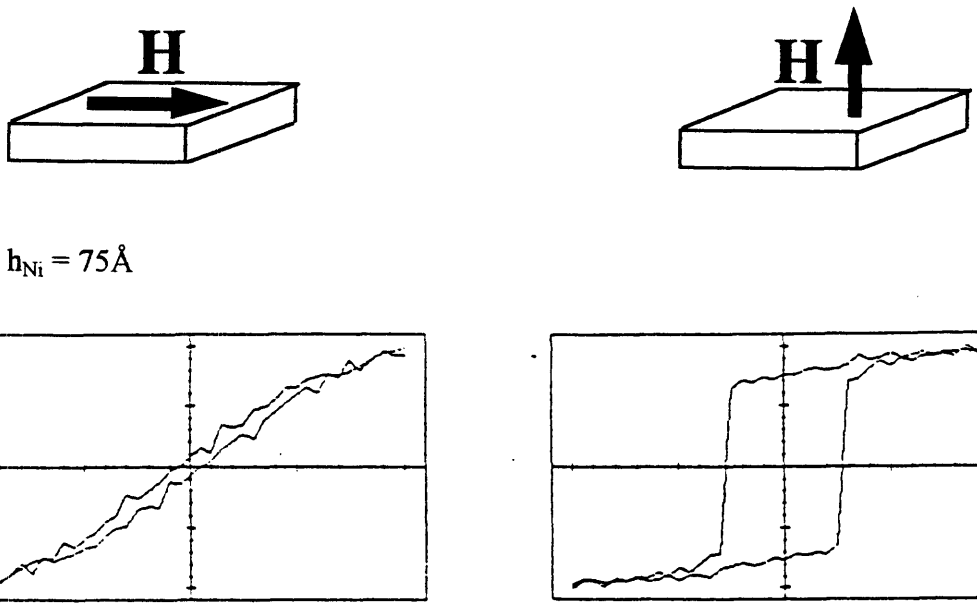

Figure 5.7 VSM loops of Cu/Ni/Cu sandwiches[3]

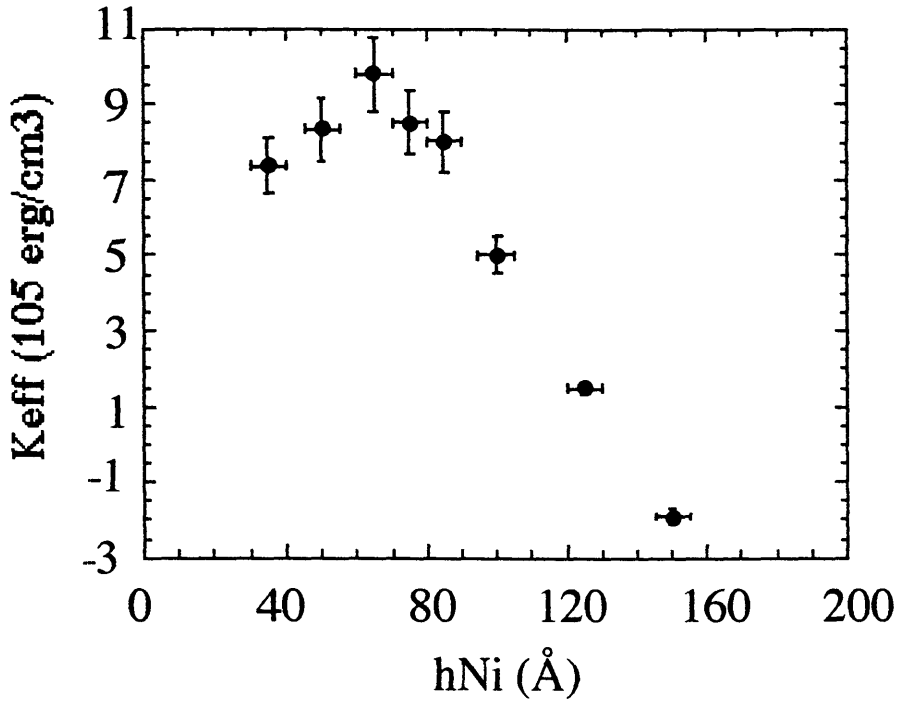

Figure 5.8 K^{eff} vs Ni thickness of Cu/Ni/Cu sandwiches as measured by VSM[3]

5.2.4 Fit to phenomelogical model

With the quanititative information gained from the Cu/Ni/Cu sandwich measurements, and the strain measurements described in Chapter 4, it is possible to obtain a fit to the modified Neél model described in Chapter 1. Recall that the strain can be described by

$$\varepsilon \approx \frac{0.1815}{h^{0.70}}, \tag{5.5}$$

as a fit to experimental data. Figure 5.9 shows $\left[K^{eff} + 2\pi M_s^2 - 2B_1\varepsilon\right]\cdot h$ vs. h. Once plotted in this way, the data can be fit to the functional form $C + \frac{D}{h^{0.7}}$. The dashed and solid lines represent fits to the data. The dashed line is a fit ignoring the surface

magnetoelastic term, B^s (D = 0). The solid line is a fit including this term. The experimental results are well represented by the model when this term is included, indicating that the surface magnetoelastic term is essential in understanding the magnetic behavior of these films. The values of the surface constants that result from this analysis are: $K^s = 0.89$ erg/cm^2, and $B^s = -52$ erg/cm^2. Recall from Chapter 1 that B^s is expected to be opposite in sign to K^s and greater by a factor of 6:

$$K^s = \frac{1}{2} L^{f-s}(r_0) \tag{5.6}$$

and

$$B^s = 3L^{f-s}(r_0). \tag{5.7}$$

Our results show that B^s is opposite in sign to K^s, but it is greater by approximately a factor of 60. It has been postulated by Bochi[3] that this discrepency is due to the fact that the pair interaction model ignores the effect of second-nearest neighbors.

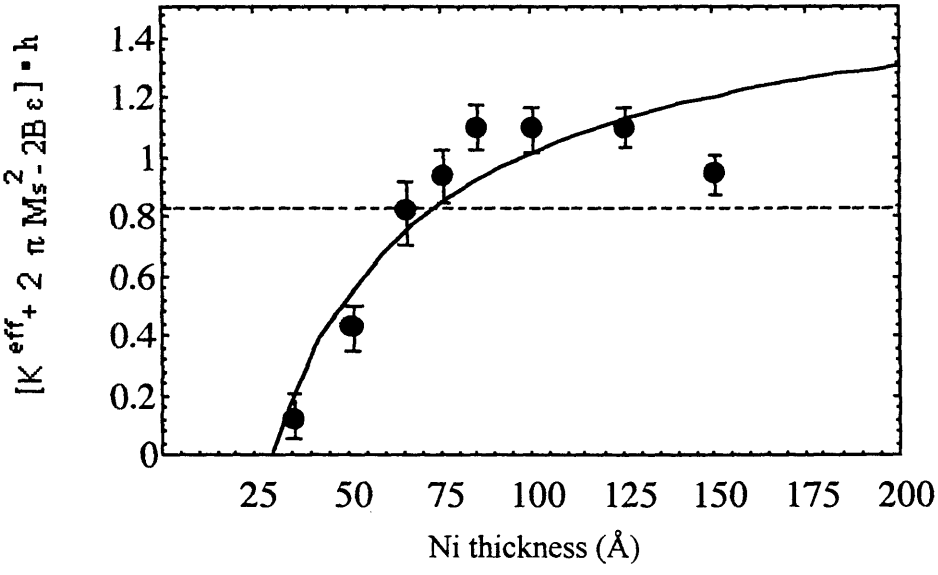

Figure 5.9 Fit to data shown in **Figure 5.8** using modified Neél model

5.3 Discussion

The information presented in this chapter, together with the strain data presented in Chapter 4, gives a complete picture of the relationship between strain and magnetic anisotropy. Using the experimentally determined residual strain and anisotropy energy in Ni/Cu (001) films, together with the modified Neél model, we have a description of the behavior of the anisotropy energy as a function of the thickness and the residual strain. All of the terms in Equation 5.3 are significant for thin films. The magnetostatic term is negative and so acts to pull the magnetization into the plane of the film. It is a constant and therefore becomes more significant at larger thicknesses. The bulk magnetoelastic term is positive and so increases the tendency toward perpendicular magnetization, as does the surface magnetostatic term. Both these terms will be large at small thickesses. The surface magnetoelastic term is negative, however, and will dominate for extremely thin films due in part to the 1/h dependence, and also to the linear dependence on strain, which is large for films smaller than the critical thickness.

In practice, the thickness of a film is generally known. Therefore residual strain can be determined from measurement of the magnetic anisotropy. For a given thickness, K^{eff} will be linearly dependent on the film strain. The constant of proportionality can be described as the effective magnetoelastic coupling coefficient

$$B^{eff} = B_1 + \frac{B^s}{h} . \tag{5.8}$$

The dependence of B^{eff} on Ni thickness is shown in Figure 5.10. The measurement of K^{eff} can be performed *in situ* using MOKE, provided that sufficient magnetic field can be achieved. The original goal of developing MOKE as a tool for measurement of strain has been achieved. The next chapter outlines experiments designed to test this tool.

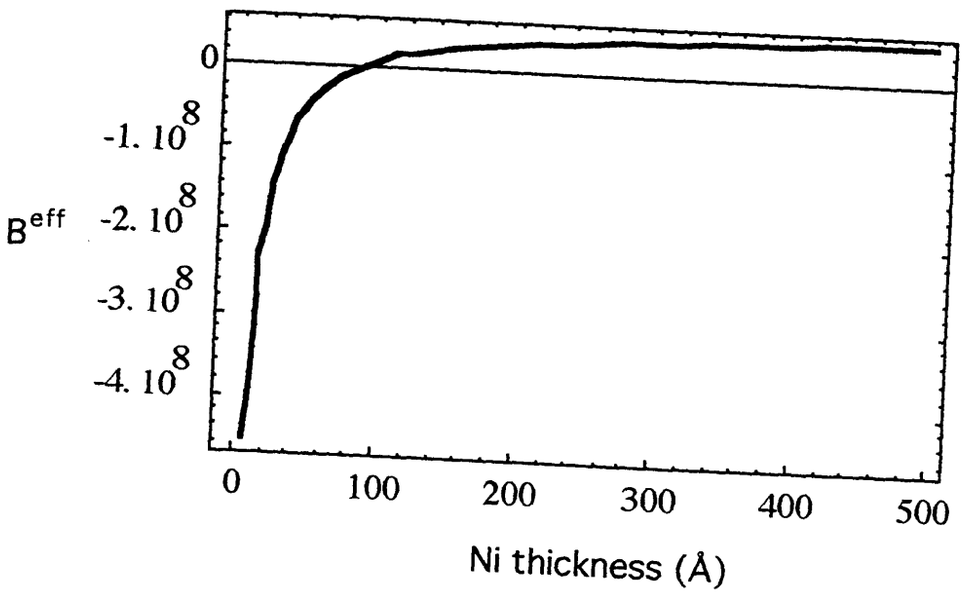

Figure 5.10 Effective magnetoelastic coupling coefficient for Ni (001)

6. CHAPTER 6: ANNEALED SAMPLES

The combined results from Chapters 4 and 5 have been used to describe the magnetic anisotropy of the Ni/Cu (001) films as a function of strain in the films using the modified Neél model. The experiments described in this Chapter were designed to test whether or not this model holds for other variables in addition to thickness. They focus on changing the strain state in films of moderate Ni thickness by annealing the wafers *ex situ*. By measuring the strain state and the magnetic anisotropy energy before and after the anneal, a comparison can be made to determine the efficacy of the model. The results are analysed using the effective anisotropy modified according to the Neél model:

$$K^{eff} = -2\pi M_s^2 + 2\frac{K^s}{h} + 2\left(B_1 + \frac{B^s}{h}\right)\varepsilon, \qquad (6.1)$$

with the numerical values of the fitting parameters as described in Chapter 5.

Previous experiments indicate that changing the state of strain in the films will have a significant effect on the anisotropy energy. Results reported by Bochi[3] show that in films of Ni/$Cu_{0.6}Ni_{0.4}$/Cu/Si, the thickness region of perpendicular magnetization is narrower than for that of the Ni/Cu/Si. The misfit is lower for Ni films grown on alloy substrates and, as shown in Chapter 4, the residual strain is lower. A lower strain means that the bulk magnetoelastic term in the model, which favors perpendicular magnetization, is weaker. With less tendency for perpendicular magnetic anisotropy, the magnetization will fall in-plane (the low energy state for thick films) at a lower

thickness. These results indicate, therefore, that the Ni films behave as the model predicts. Furthermore, the results of magnetic anisotropy measurement on Ni/Cu/Si films (without a Cu capping layer) discussed in Chapter 5 support this claim as well. Recall that the magnetic behavior of these films changes upon removal from the MBE. Specifically, the region of perpendicular magnetization extends to greater thickness after exposure to air. Oxidation of the Ni film will undoubtedly have an effect on the magnetic properties of the surface layer. More importantly, however, the mismatch between NiO and (relaxed) Ni is about 19%. The lattice constant of NiO, predicted from ionic radii, is 4.18Å. NiO has the rocksalt structure.[65] The presence of the oxide will therefore induce a large tensile strain on the Ni film. In this case, therefore, the magnetoelastic term is larger, giving a greater tendency for perpendicular magnetization.

To make a quantitative analysis of this result, it would be necessary to measure the strain in these films using another technique. The technique of wafer curvature measurement discussed in Chapter 4 depends on the ability to isolate the effect of the Ni epilayer on the curvature of the wafer from the effect of the Cu layer. In the case of the alloy films, this effect is dependent on alloy concentration, and therefore not easy to isolate. Likewise, strain induced in the Ni film due to oxide growth is not easily measureable using the wafer curvature method of strain measurement. As described in Chapter 4, wafer curvature gives a measurement of the strain at the film/substrate interface. The way that the Ni strain was calculated using curvature measurements assumed that the curvature change due to the Cu/Si strain and due to oxide growth was constant over all Ni film thicknesses. Consequently, the strain described in Chapter 4 is the strain due to Ni/Cu misfit.

The work described in this Chapter deals with modifying the Ni strain at a constant thickness. In this case, the strain is changed through annealing of the sample. From a simplistic view, heating the sample would lead to further relaxation of the misfit strain toward the equilibrium state. Some mechanisms for this type of relaxation were discussed in Chapter 1. The strain behavior of these films at elevated temperatures (in the range of 100 - 150°C) is fairly complex, partially because it is a multilayered system, rather than just a bilayer and because there are reactions occuring at some interfaces rather than simply structural relaxation.

As the sample is heated, there is a strain due to differential thermal expansion between the Cu and Si. The thermal expansion coefficients for Cu and Si in the temperature range of these experiments are 17×10^{-6} and 7.6×10^{-6} respectively. As the sample is held at the annealing temperature, relaxation of this strain will occur at the Cu/Si interface. Further, as is discussed in detail in the Appendix, the Cu has a tendency to react with Si to form Cu_3Si. This silicide layer will be strained relative to the Si wafer, leading to a change in the curvature of the wafer. Another complication is that , although these experiments were performed in inert ambients, some additional oxidation may occur. The essential difficulty is that, although the primary interest for this work is relaxation of epitaxial misfit, many other forms of relaxation are occuring in these films.

6.1 EXPERIMENT

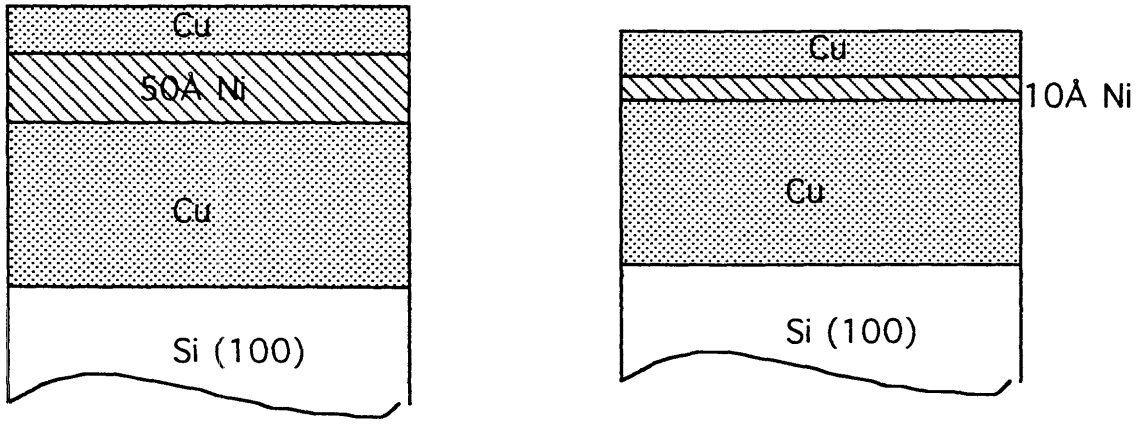

Figure 6.1 Schematic cross-section of samples used in annealing study

Two different thicknesses of films were deposited for these measurements using the techniques described in Chapter 2: one with a 10Å Ni film, and one with a 50Å Ni film. Schematic cross-sections are shown in Figure 6.1. The 50Å thickness was chosen because it is above the critical thickness for misfit relief through misfit dislocation formation, but not so thick that the misfit is completely relieved. As is apparent from the data described in Chapter 4, the residual strain in a 50Å film, as deposited, is significantly higher than the residual strain predicted at equilibrium by the Matthews-

Blakeslee model. It is therefore reasonable to suspect that heating of the film will lead to increased misift accommodation, since it will increase dislocation mobility. Since the 10Å film is below the critical thickness, it is unlikely that any misfit accommodation at the Ni/Cu interface will occur. Comparison between these two films, annealed under the same conditions, should give an indication of the misfit relief occuring at the Ni/Cu interface due to the anneal.

The experiment consisted of measuring the strain in the films using both wafer curvature measurements and magnetic anisotropy measurements before and after the films were annealed under various conditions. The two types of measurements were used to check for consistency. The curvature of the wafers was measured using a Tencor commercial wafer measurement system. This device is based on the optical reflection method of wafer curvature measurement. The principle behind this type of measurement is illustrated in Figure 6.2. A laser beam is reflected off a wafer and the position of the reflected beam recorded. The position of the reflected beam will depend on the radius of curvature. As the beam is scanned across the curved surface of the wafer, the position of the reflected beam as a function of the position of the incident beam is recorded. In the case of a perfectly spherical wafer, this function is a straight line. The slope of the line is equal to 2/R, where R is the radius of curvature of the wafer, as illustrated in the Figure. The Tencor system is equipped with a hot stage so that wafers could be annealed in a gas ambient and the curvature monitored during the anneal.

VSM was performed on the 50Å samples after annealing. The strain was then calculated from the anisotropy energy using Equation (6.1), with the values for the surface anisotropy constants calculated by Bochi[3] and discussed in Chapter 5.

Two sets of measurements like this were performed. In the first, the behavior of the films as a function of annealing temperature was examined. Wafers with both Ni thicknesses were annealed at 100, 125, and 150°C for one hour using the Tencor hot stage in a flowing Ar environment. The wafer curvature was monitored during the anneal. The pre- and post-deposition wafer curvatures were compared to determine the strain upon annealing. The 50Å wafers were then analyzed using VSM, and the strain in the Ni film was calculated using Equation (6.1).

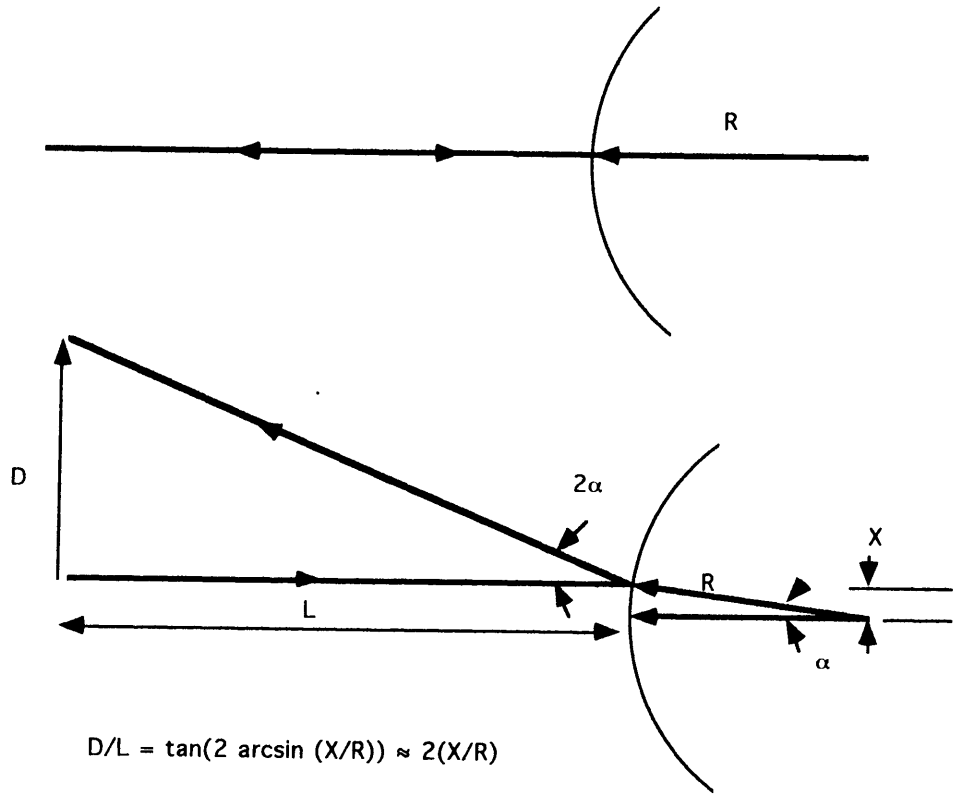

Figure 6.2 Schematic diagram illustrating the measurement of curvature via laser reflection

The second set of measurements was an attempt to measure the effect of annealing time on the strain state of the films. In this case, in an effort to save time and ensure that the 10Å and 50Å films were annealed under precisely the same conditions, the films were annealed simulataneously in a furnace separate from the Tencor measurement system (which can only be used to anneal one wafer at a time) with a flowing N_2 ambient for 5, 9, and 14 hours at 100°C. The curvature of both wafers was measured before and after the anneal to determine the change in curvature as a result of the anneal. The pairs of wafers (one 10Å and one 50Å) were annealed simultaneously in the same quartz boat, equidistant from the center of the boat. The 50Å films were then characterized with VSM and the results compared to the Tencor wafer curvature measurements.

6.2 STRAIN VS. TEMPERATURE RESULTS

6.2.1 VSM measurements

The measurements of magnetic anisotropy on samples annealed at various temperatures showed an increase in anisotropy energy with increasing annealing temperature. Note that the effective magnetoelastic constant,

$$B^{eff} = B_1 + \frac{B^s}{h} \tag{6.2}$$

is negative for a 50Å Ni film ($B_1 = 6.2 \times 10^7$ erg/cm^3 and $B^s = -52$ erg/cm^2). Examination of Equation (6.1) shows that a change in strain is proportional to a change in anisotropy, where the constant of proportionality is the effective magnetoelastic constant. Therefore, for a negative B^{eff}, an increase in K^{eff} is indicative of a decrease in strain. The strain in the films as calculated using Equation (6.1) is shown in Figure 6.3. A significant relaxation is seen upon annealing.

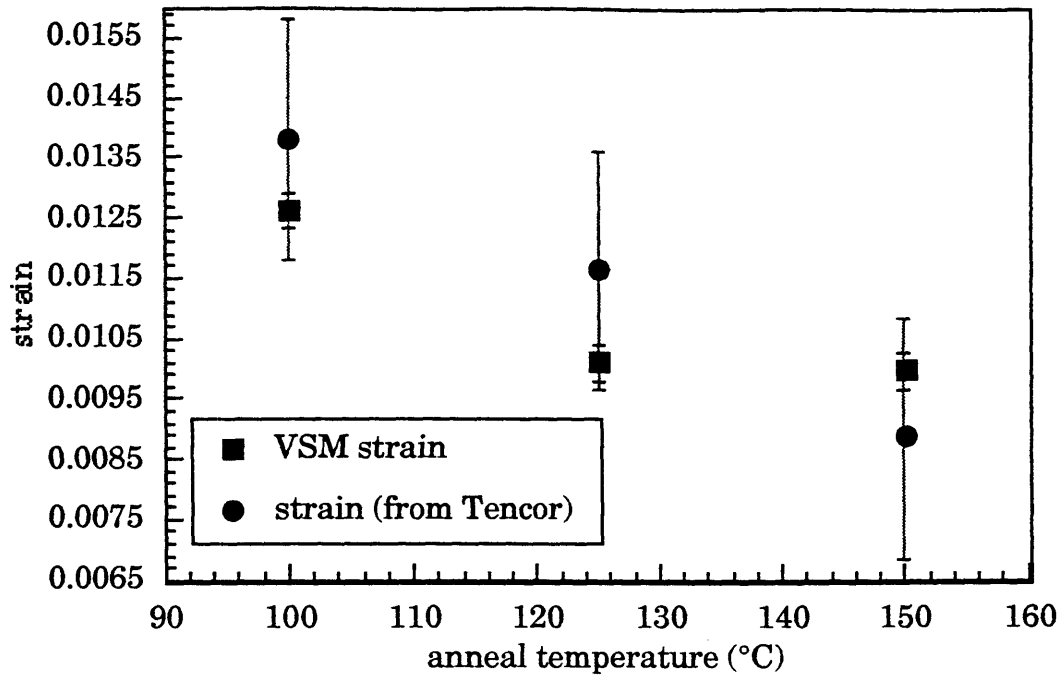

Figure 6.3 Strain in Ni films measured by magnetic anisotropy and Tencor curvature measurements. Ni thickness was 50Å. Films were annealed for 1 hour.

6.2.2 Tencor measurements

The change in curvature due to the anneal was measured in both sets of samples. The curvature change for both 10Å and 50Å films is positive at low annealing temperatures, indicating an increased tensile strain in the film. In order to understand this result, we must examine the behavior at the Cu/Si interface during the anneal. The strain behavior of the Cu/Si interface during a typical anneal is illustrated schematically in Figure 6.4. Without annealing, the Cu is under tension due to lattice mismatch between the Cu and Si. Most of this strain will be relieved through dislocation formation during the course of the anneal. The small residual strain (about 10^{-4}) results in a significant change in the curvature of the Si wafer due to the fact that the Cu is 2000Å thick. The Stoney equation (Equation (4.10)) shows that the curvature due to strain is proportional to the thickness of the film. As the film is heated, the Cu lattice expands to a significantly greater extent than does the Si due to the difference in their

coefficients of thermal expansion (α_{Cu} = 17 x 10^{-6} and α_{Si} = 7.6 x 10^{-6}), such that the Cu is actually under compression during the anneal. Again, although this strain is small relative to the strain in the Ni film, it results in a significant curvature change due to the thickness of the Cu layer. As the sample is held at the annealing temperature, this compressive strain begins to relax, as shown in section 2 of Figure 6.4. The sample is then cooled (section 3), resulting in a strain change equal and opposite to that of section 1. The resulting strain is then higher (more tensile) than the original strain.

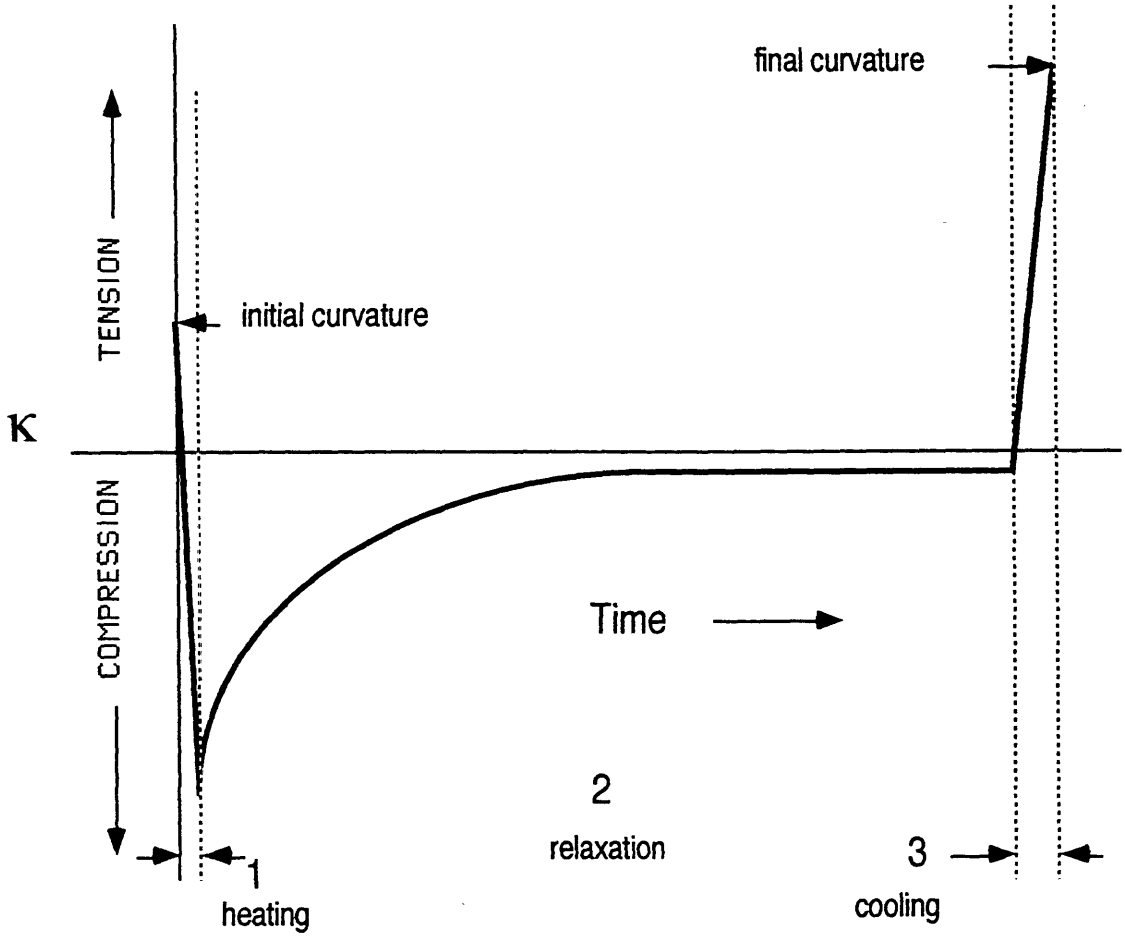

Figure 6.4 Predicted curvature change during anneal due to thermal mismatch at Cu/Si interface. The horizontal line represents the curvature of the Si wafer before deposition.

If we assume that the difference between the measured values for 10Å and 50Å films is due to the strain change in the Ni, the strain values are those shown in Figure 6.3. In doing this the assumptions are made that there is no strain change in the 10Å film, and that the strain change in the Cu layer is the same for both samples. Since 10Å is below the critical thickness for misfit accommodation, it is reasonable to assume no strain change in the film upon annealing. The results discussed in the Appendix show that the presence of the Ni does, in fact, affect the strain state at the Cu/Si interface, but the effect does not appear to be dependent on the thickness of the Ni. As is shown, the strain values measured using both techniques agree reasonably well. This result indicates that the magnetic anisotropy measurements give a good quantitative measure of strain for these films.

6.3 STRAIN VS. TIME RESULTS

For the second set of measurements, as stated earlier, the samples were annealed at 100°C for 5, 9, and 14 hours. The samples were annealed in a nitrogen furnace rather than in the Tencor measurement system itself.

6.3.1 VSM measurements

The strain was calculated from measurements of anisotropy as before. The results are shown in Figure 6.5. It was expected, that the misfit strain would relax over time at 100°C due to dislocation motion. The strain would therefore be lower for longer annealing times. This is in fact the trend observed between samples annealed at 5, 9, and 14 hours in Figure 6.5. These are the samples that were annealed in the N_2 furnace. If we compare these values to the strain measured in the unannealed sample and the sample annealed for 1 hour (in Ar) however, we see that the strain is significantly higher. It is reasonable to suppose that there is something different happening in the samples that were annealed in the N_2 ambient. One possibility is that there some oxidation of these samples. The presence of NiO will induce a tensile strain in the film, as discussed before, which is what is observed. In order for the Ni film to oxidize, the oxygen must

reach the Ni film through the 20Å Cu capping layer. The mechanism by which this transport can occur is diffusion of Cu through Cu_2O. This diffusion coefficient is vanishingly small at room temperature, but becomes appreciable at 100°C, which was the annealing temperature used in the study.[65]

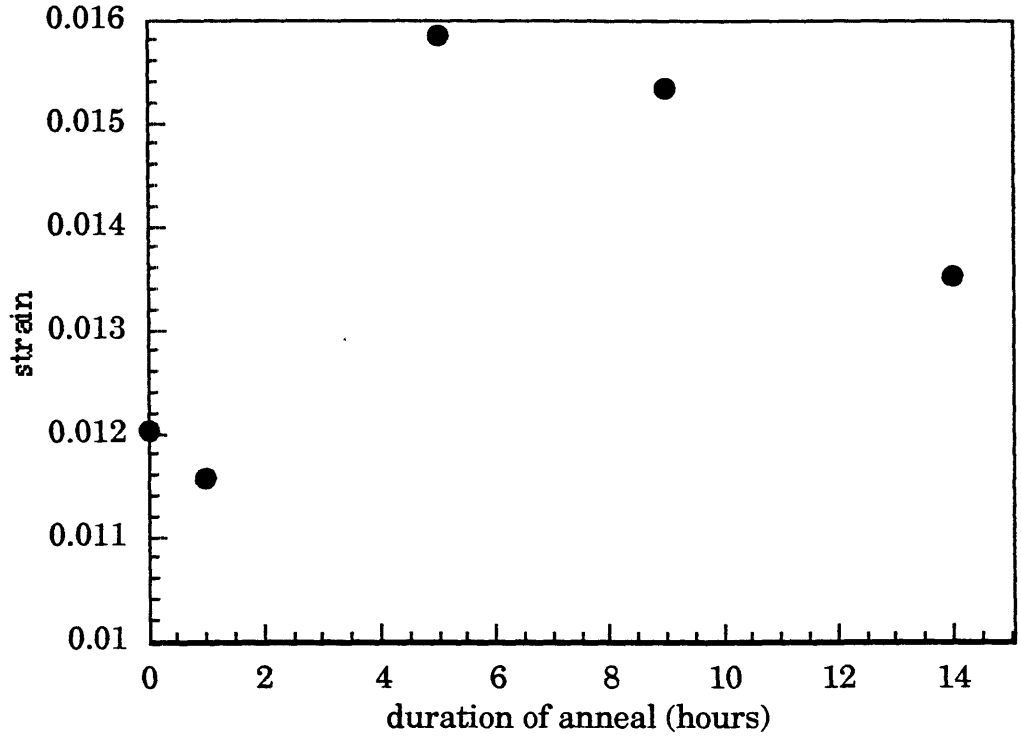

Figure 6.5 Strain in Ni calculated from magnetic anisotropy measurements of Cu/50Å Ni/Cu/Si. Anneal temperature = 100°C. One hour sample was annealed in Ar. Samples annealed for 5, 9 and 14 hours were annealed in N_2.

Additional evidence that the unusual behavior of these films is due to the annealing process is from the measurement of magnetic anisotropy energy in films annealed in the VSM. Preliminary measurements were done in which films were annealed in a small furnace with flowing Ar gas which is attached to the VSM. The curvature of these samples could not be measured, due to the fact that the samples must be small in order to fit between the pole pieces of the magnet, and not whole 3 inch

wafers. The results of these measurements are shown in Figure 6.6. As is shown, the strain in the Ni films decreases with increasing anneal time. This is the behavior that is expected from relaxation of the misfit strain.

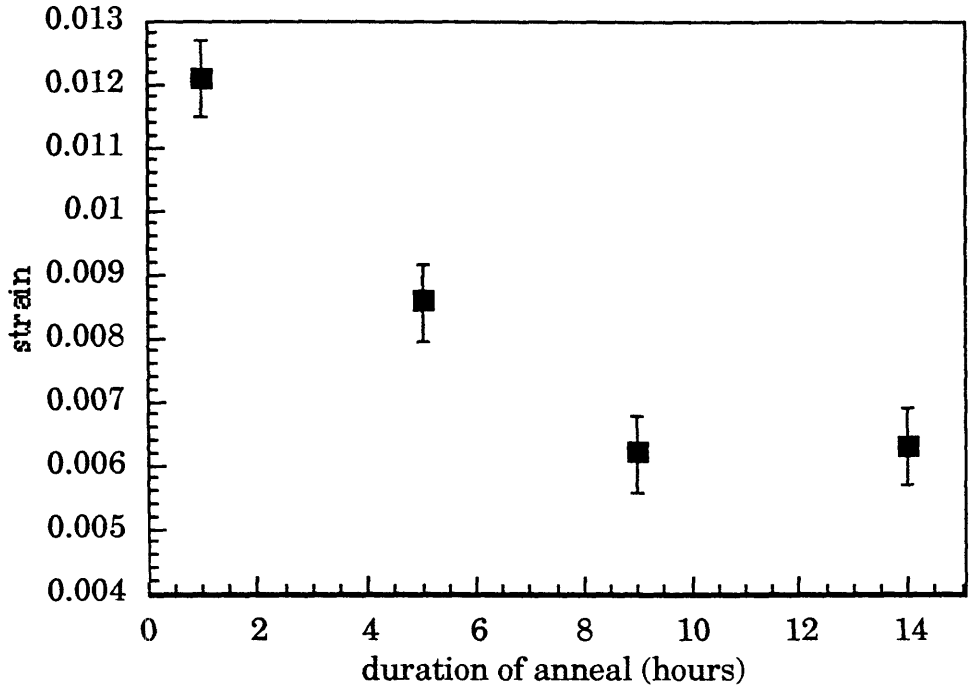

Figure 6.6 Strain calculated from anisotropy measurements for samples annealed in Ar at 100°C in VSM furnace.

6.3.2 Tencor measurements

Although the films were not annealed in the Tencor system, the wafer curvature was measured before and after annealing with this system. The results are unusual, as it was expected from the behavior of the magnetic anisotropy. Figure 6.7 shows the curvature change of the 10Å and of the 50Å samples, in which no misfit relaxation is expected. If the only mechanism acting on these films were relaxation at the Cu interface as illustrated in Figure 6.4, the curvature (which is directly proportional to the strain according to Stoney's equation) would increase with longer annealing time. This is the behavior expected in the 10Å films, where no misfit relaxation is expected to occur. In

fact, the opposite is seen. The result can be explained if we assume oxidation of the film. An oxide film would be under compression, as discussed above, and thus result in a negative curvature change in the wafer. Additionally, since the oxide will put the film under a large tension, there will be some relaxation at the film/oxide interface, and the degree of this relaxation may increase as the sample is annealed. The resulting curvature change is then

$$\Delta\kappa = +\Delta\kappa_{Cu/Si} - \Delta\kappa_{Ox} + \Delta\kappa_{Ox}^{R} - \Delta\kappa_{Ni/Cu}\,, \tag{6.3}$$

where $\Delta\kappa_{Cu/Si}$ is the change in curvature due to relaxation of the thermal mismatch illustrated in Figure 6.4, $\Delta\kappa_{Ox}$ is the curvature change due to the growth of the oxide layer, $\Delta\kappa_{Ox}{}^{R}$ is the curvature change due to relaxation at the oxide/film interface, and $\Delta\kappa_{Ni/Cu}$ is the curvature change due to relaxation of the misfit strain. It is assumed that there is no relaxation of misfit strain in the 10Å Ni films as discussed above. According to the Matthews-Blakeslee model, the magnitude of $\Delta\kappa_{Ox}{}^{R}$ will be different for the two different films since it is a function of the film thickness.

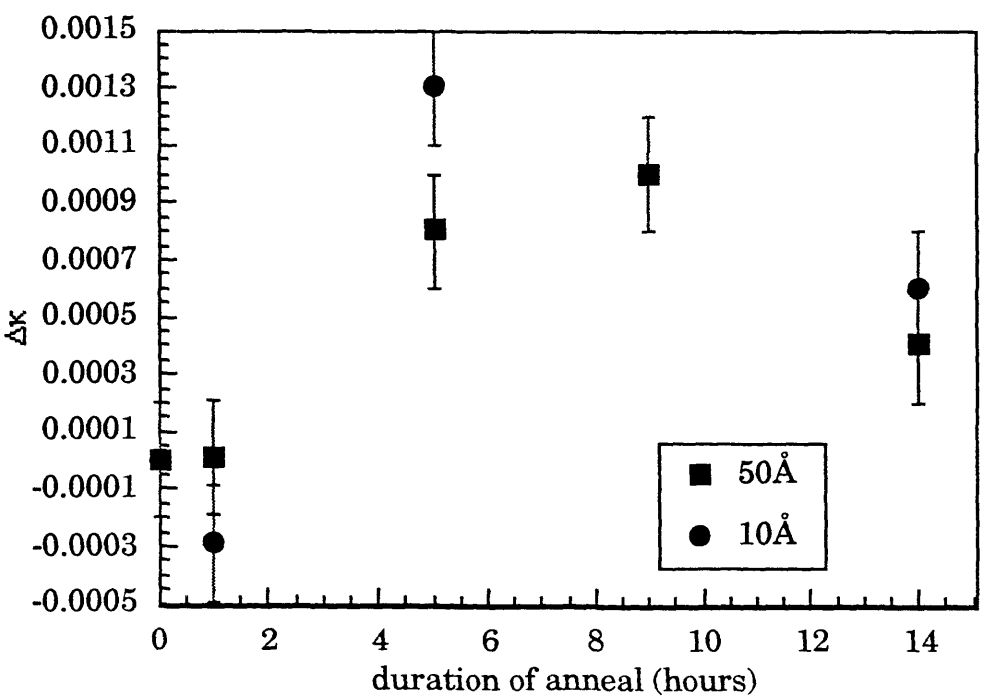

Figure 6.7 Measurements of radius of curvature change due to anneal in unpure N_2

The mechanism by which the oxide grows is first diffusion of Cu through Cu_2O in the capping layer, and then diffusion of Ni through NiO. The NiO layer becomes metastable at a thickness of approximately 10Å.[66] As the oxide grows through the thickness of the Cu capping layer, the curvature becomes more negative. The relaxation at the Cu/Si interface will cause an increase in the curvature of the wafer. Relaxation at the film/oxide interface will also cause the curvature to increase. Misfit relaxation will cause a decrease.

Since the strain in the Ni cannot be isolated from the information within the curvature measurements due to the presence of the oxide film, it is not possible to determine quantitatively the strain in the Ni film from the curvature measurements. Although the first two terms of Equation (6.3) will be close to equal for the two Ni thicknesses, the second two will not. Also, since the relaxation at the two interfaces will cause curvature changes in opposite directions, the film strain cannot be deduced from the sum of the quantities. Qualitatively, however, the results are consistent with the strain calculated from VSM measurements.

6.4 DISCUSSION

The results presented in this Chapter provide further evidence that the relationship between magnetic anisotropy energy and Ni film strain is as described by the modified Neél model. Additionally, these experiments are an illustration of the way in which magnetic anisotropy measurement can be used to measure strain in these films. The change in magnetic behavior due to changing the strain state of the Ni film of the same thickness is well described by the modified Neél model.

The dependence of K^{eff} on film thickness is complex, as shown by the experimental observations outlined in Chapter 5, and can be seen from examination of Equation (6.1). The work described in this Chapter has been an attempt to examine the relationship between magnetic anisotropy and strain more directly. It is not clear, however, to what extent it is possible to change the strain state of the film without changing some other property which would affect its magnetic behavior. Since very thin

films have been studied for this work, any change in K^s or B^s will have a strong effect on K^{eff}. Oxidation, interdiffusion, and surface roughening can all change the values of K^s and B^s. By performing the experiments *in situ*, oxidation can be eliminated as one source of error. Interdiffusion, as stated earlier, is minimal in the Ni/Cu system. The effect of surface roughening is unknown. It has been determined by Chuang[30] that the regular array of surface steps found in viscinal surfaces will influence the direction of magnetization in the plane of the film. Specifically, the magnetization will tend to allign parallel to the steps at small thicknesses. It is unknown what effect a random surface roughening will have on the surface coefficients. RHEED patterns indicated small, random variations in surface roughness from sample to sample that were independent of thickness. This observation indicates that small variations in surface roughness do not have a significant effect on the magnetic anisotropy in these films. Strain is therefore the variable which will have the largest effect on anisotropy energy in Ni/Cu.

7. CHAPTER 7: SUMMARY AND FUTURE WORK

7.1 SUMMARY

The work discussed in this thesis has utilized a variety of analytical techniques. Through the use of these techniques, the description of the strain behavior of Ni/Cu (001) has been quite thorough. The films deposited for this study were Ni/Cu/NaCl (001), Ni/Cu/Si (001), Ni_xCu_{1-x}/Cu/Si (001), Ni/Ni_xCu_{1-x}/Cu/Si (001) and Cu/Ni/Cu/Si (001). The first part of the study consisted of measuring the strain and magnetic properties of the films as a function of Ni thickness. The data from these two measurements was fit to a phenomelogical model based on the Neél pair interaction model of magnetic anisotropy. The second part consisted of measuring strain and magnetic properties as a function of annealing conditions. Important information has been gained from this work. The following is a summary of the results:

• Ni/Cu was deposited epitaxially on NaCl and on Si substrates. These samples were found to be best for preparation of TEM specimens and gave the cleanest misfit dilsocation images.

• Cu does not grow epitaxially on the native oxide of Si (001). Cu was found to deposit epitaxially on HF-etched and deionized water rinsed Si (001) wafers which gives a hydrogen-terminated Si (001) surface. The ideal deposition temperature was determined to be room temperature (no intentional substrate heating). RHEED patterns indicated that an epitaxial film with considerable surface roughness was produced.

• Cu/Si epitaxy is such that the [100] axis of Cu is parallel to the [110] axis of Si.

• A Cu_3Si layer grows at the Cu/Si (001) interface at room temperature over the course of several weeks, or at elevated (> 200°C) temperature over hours. The maximum silicide thickness observed was on the order of 100Å. The growth of this layer does not affect the epitaxial quality of the top surface of the Cu film.

• Oxygen was found to be present at the Cu_3Si/Si interface in samples annealed with no Ni overlayer present as determined by RBS. The presence of a Ni epilayer prevented this process.

•X-ray diffraction measurement indicated that the Cu layer was fully relaxed at thicknesses of 1000Å and greater. The lattice constant of the Cu (001) surface was equal to the bulk value of 3.615Å for $h_{Cu} \geq 1000$Å.

• The Cu surface is rough. Cross-sectional TEM and AFM showed a RMS roughness of about 20Å.

• Ni was found to grow pseudomorphically on Cu/Si (001) with a misfit of 2.6% up to 15Å thickness, at which point misfit dislocations formed at the Ni/Cu interface to relieve this misfit. The dislocations lie along $[110]$ and $[\bar{1}10]$ directions, forming a rectangular grid in the plane of the interface. It was determined that the dominant mechanism for relief of misfit strain is the formation of interfacial misfit dislocations.

• Two types of misfit dislocation were found at the Ni/Cu interface, 60° dislocations, the most common in fcc metals, and 90° dislocations, the most efficient at relieving misfit strain. It was discovered that the number of 90° dislocations increases with increasing Ni thickness. Some possible mechanisms were proposed for creation of the sessile 90° dislocations in order to explain their presence at the interface. Observation

of this increase in the number of 90° dislocations with thickness has never been reported for the Ni/Cu (001) interface.

• Measurements of the average spacing between the misfit dislocations were made and the results compared with the Matthews-Blakeslee thermodynamic model for misfit accommodation through dislocation formation. The spacing between dislocations was found to decrease as expected with increasing Ni thickness, but not to the extent that the model predicts. The most likely cause for the descrepency is kinetic limitations to dislocation nucleation and motion. This discovery emphasizes the need for further research into the kinetics of misfit accommodation.

• Strain was measured in Ni/Cu (001) as a function of Ni thickness using substrate curvature measurements. It was found that the strain measurements agreed well with the measurements of dislocation spacing, indicating that misfit dislocation formation is the primary misfit strain relief mechanism in these films. The strain in the film was found to decrease as Ni thickness increased. These measurements were fit to the functional form

$$\varepsilon = \frac{X}{h^{Y}}, \tag{7.1}$$

where h is the Ni film thickness in Å. The fit to the data gave X = 0.1815 and Y = 0.7. The strain was assumed to follow this functional form when interpreting magnetic anisotropy measurements. The Matthews-Blakeslee equilibrium model predicts a 1/h dependence of the strain. The higher measured strain is indicative of the fact that strain relief is kinetically limited.

• Magnetic hysteresis loops were measured *in situ* using MOKE and *ex situ* using VSM for Ni thicknesses ranging from 15Å to 200Å. The Ni/Cu/Si (001) films were found to have a tendency toward perpendicular magnetization for Ni thickness between 15Å and

60Å when measured *in situ* and between 25Å and 100Å when measured *ex situ*. The discrepency between these two types of measurements was found to be the result of the exposure of the films to air. These results were analyzed using a phenomenological model.

• Quantitative measurements of magnetic anisotropy energy K^{eff} were made on Cu/Ni/Cu/Si (001) sandwiches with VSM. The films were found to exhibit the same qualitative behavior as the Ni/Cu/Si films. The data was analyzed quantitatively in combination with the measured strain behavior of the Ni films as a function of thickness using a modified version of the Neél model, in which the effective anisotropy energy is given by

$$K^{eff} = -2\pi M_s^2 + 2B_1\varepsilon + 2\frac{\left(K^s + B^s\varepsilon\right)}{h}. \qquad (7.2)$$

The parameters of this equation are defined and chosen as follows:

$2\pi M_s^2$ (magnetostatic energy)	1.47×10^6 erg/cm^3
B_1 (bulk magnetoelastic coupling coefficient)	6.2×10^7 erg/cm^3
K^s (surface magnetocrystalline anisotropy energy)	0.88 erg/cm^2
B^s (strain dependent surface anisotropy energy)	-52 erg/cm^2

Table 7-1 Bulk and surface magnetic terms for Ni/Cu (001)

The saturation magnetization and bulk magnetoelastic coupling coefficient are assumed to be the same as for bulk. The surface terms were calculated from a fit to experimental data. It is the determination of these terms which gives a quantitative prediction of K^{eff} from a given strain.

• The addition of a 20Å Cu capping layer approximately doubles the Ni thickness range over which perpendicular magnetization is observed compared to uncapped films. This observation is consistent with the analytical results in Table 7-1 which show K^s of the Cu/Ni interface to be the strongest positive effect.

• A series of measurements was performed in which samples of 20Å Cu/50Å Ni/Cu/Si were annealed for from 1 hour to 14 hours at temperatures of between 100°C and 150°C. The results indicated good agreement with our fit to the Neél model.

7.2 SUMMMARY DISCUSSION

The goal of this work has been to develop MOKE as an experimental analysis tool for measuring strain *in situ* for magnetic thin films. An accurate, easily implemented method of *in situ* strain measurement is extremely useful in the study of misfit accommodation. Most of the strain relief associated with misfit accommodation occurs during growth, and therefore must be studied *in situ*. To this end, we have measured the surface magnetocrystalline anisotropy constant and the surface magnetoelastic coupling coefficient for Ni (001). The Neél model predicts that the anisotropy energy in a thin film can be described by

$$E = K^{eff} \sin^2\theta \ , \tag{7.3}$$

where

$$K^{eff} = -2\pi M_s^2 + 2B_1\varepsilon + 2\frac{K^s}{h} + 2\frac{B^s\varepsilon}{h} + K_1 \ . \tag{7.4}$$

For Ni (001) films, the bulk magnetocrystalline term, K_1, is small relative to the others and can be ignored in this analysis. It was determined in this research that the surface magnetoelastic term, $2\frac{B^s\varepsilon}{h}$, is significant, particularly at low Ni thicknesses and cannot be ignored in the analysis.

With the surface terms defined experimentally, Equation (7.4) gives the relationship between strain and effective anisotropy energy for a Ni (001) thin film of a given thickness. One can therefore measure K^{eff} to determine the strain. The surface constants measured in this work are unique to the Ni (001) system. In order to use magnetic anisotropy to measure strain in other orientations in materials systems these surface constants must be experimentally determined.

Recall from Chapter 5 that the relationship between anisotropy and strain for a given thickness depends on the effective magnetoelastic coupling coefficient, B^{eff}, where

$$B^{eff} = B_1 + \frac{B^s}{h} . \tag{7.5}$$

Figure 5.10 shows that B^{eff} is strongly negative at low Ni thickesses, where the surface term dominates. As the thickness increases, B^{eff} becomes positive and approaches the bulk value.

Figure 7.1 shows the dependence of anisotropy energy on Ni thickness for different strains using Equation (7.4) and the surface constants calculated in this work. For all deposition and annealing conditions the strain will decrease with increasing thickness. Figure 7.1 illustrates the behavior of the effective anisotropy if the strain is higher or lower than the measured value across all thicknesses. This curve has important predictive value if the range of perpendicular magnetization is to be engineered for a particular application by changing misfit strain. For an increase in strain over the measured value, the anisotropy energy is lower at low Ni thickesses, and higher for thicknesses above 84Å. The point of intersection of the curves is the point where $B^{eff} = 0$.

The usefulness of the technique of measuring strain in thin films using magnetic anisotropy measurements depends on how precisely the strain in the film can be determined. Examination of Figure 7.1 indicates dependence of the resolution of the technique on Ni thickness. The magnitude of B^{eff} determines the magnitude of the dependence of effective anisotropy energy on strain. For very thin films, up to about 50Å, B^{eff} is large and negative, giving good strain resolution. The resolution goes to zero

at h = 84Å. It is therefore not possible to determine the strain from K^{eff} measurements for Ni films with h ≈ 84Å. At higher thicknesses, B^{eff} approaches the bulk value, and the resolution is not strongly thickness dependent.

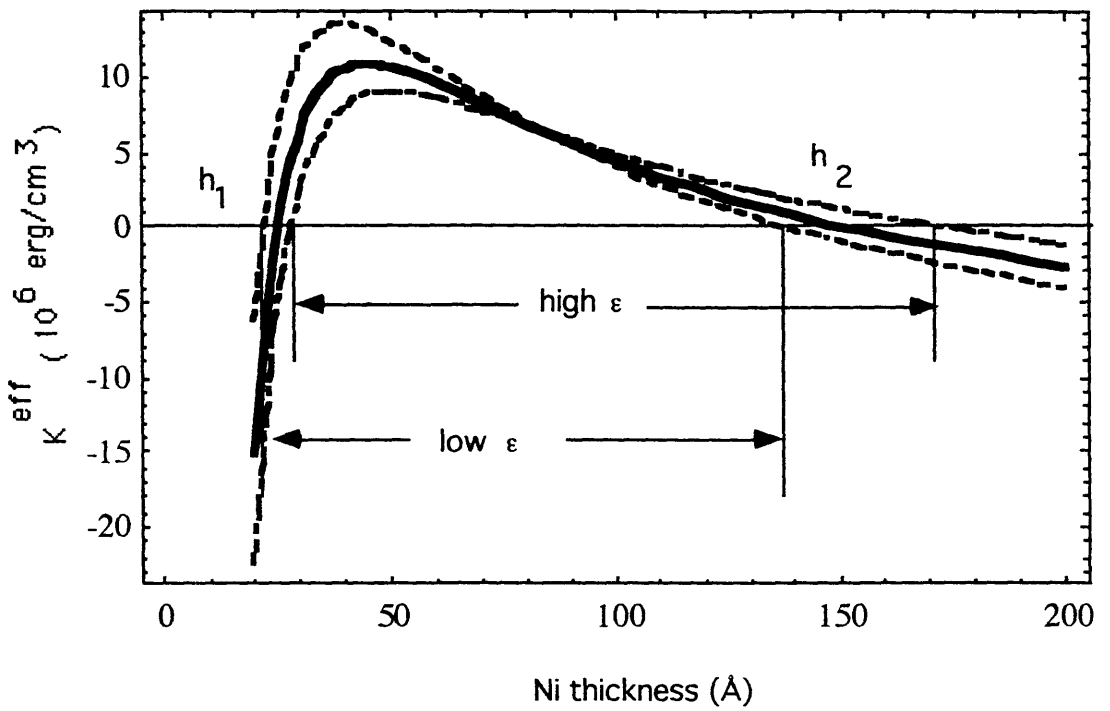

Figure 7.1 Dependence of K^{eff} on Ni thickness calculated from Equation (7.4) for different strains (± 0.2%). The solid line represents K^{eff} for the measured strain (the fit to the experimental data). The intersection of the curves is the thickness were $B^{eff} = 0$ (84Å). h_1 and h_2 are the critical thicknesses for the transition to perpendicular and in-plane magnetization, respectively.

Other *in situ* strain measurement techniques which have been used in the past, i.e. RHEED[2] and STM[3], are suited for semiconductor thin film with atomically smooth surfaces. For measuring strain in epitaxial magnetic thin films, MOKE is ideal. It does not depend on a smooth surface within limits. STM measurements measure misfit dislocation content via measurement of step density. Extrapolating these measurements to strain values depends on the assumptions that all surface steps are associated with misfit dislocations and that all strain relief is via dislocation formation. RHEED measurements only measure strain in the surface layer. Any relaxation or reconstruction at the surface may be incorrectly interpreted. MOKE can be performed in a variety of

deposition environments. Although this work was performed in a UHV environment, MOKE could just as easily be performed in a sputtering system. A MOKE apparatus has been built by Hashim, et al.[67] in which the magnet is outside a narrow vacuum chamber. This type of design eliminates exposure of any of the MOKE equipment to the deposition environment. From an experimental perspective, therefore, MOKE has been shown to be quite useful.

It is the strong effect of strain on magnetic anisotropy in thin films which has prompted our investigation into the usefulness of the technique for *in situ* strain measurement. An important contribution of this work has been toward the development of the modified Neél model for describing anisotropy in thin films. The effect of strain on anisotropy clearly cannot be determined without the inclusion of a surface magnetoelastic coupling coefficient. The development of this model has therefore been an essential component of the progress toward the utilization of magnetic anisotropy measurement, and specifically of MOKE, for measuring strain in epitaxial thin films.

7.3 FUTURE WORK

The obvious next step in this work is the construction of a MOKE system capable of generating a sufficient magnetic field for saturation of the magnetic moment. The analysis of quanititative data taken *in situ* is more accurate, since oxidation and other impurities do not contribute to the strain state and/or the magnetic state of the film. Additionally, such measurements are more useful in terms of learning about misfit accommodation. Most misfit accommodation occurs during growth, particularly when a film is deposited while heating the substrate. Therefore, any serious exploration into the kinetics of misfit accommodation must be performed *in situ*, and ideally, during growth. A system could be designed such that the MOKE signal could be monitored during growth. There would need to be a sufficiently low deposition rate, such that scattering of the laser beam due to the vapor phase is minimized. Additionally, the influence of the magnetic field on the deposition process itself needs to be taken into account.

Generally, though, the information that could be gained would be extremely valuable and applicable to epitaxial systems other than magnetic materials.

As a result of this work, measurement of strain in Ni (001) using this technique involves simply the measurement of the magnetic response both parallel to the plane of the film and perpendicular to it to determine K^{eff}. The strain is then calculated using Equation (7.4). For other materials systems, or other orientations of Ni, one must first determine the values of the surface magnetic constants. In order to make this calculation, K^{eff} and strain must be measured independently over a range of film thicknesses and the data fit to the phenomelogical model. The dependence of strain on thickness, ε(h), must be determined. This operation allows the prediction of strain values from subsequent measurements of anisotropy. The fact that the constants must be determined experimentally for each system to be studied is a drawback of the technique.

Specifically, measurement of magnetic anisotropy could be used to experimentally measure misfit accommodation of Ni/Cu (001) during growth. As the film is deposited, the thickness is changing at a constant rate. With a slow deposition rate and a rapid enough anisotropy measurement, the anisotropy can be measured for a particular thickness during the deposition. Measurement of K^{eff} in this way several times during the deposition gives strain as a function of time. Recall the Dodson-Tsao model for kinetics of misfit accommodation:

$$\frac{d\gamma}{dt} = \frac{\sigma_{exc}^2(\gamma)}{\mu^2}\left(\Gamma_s e^{-Q_s/kT} + \Gamma_c e^{-Q_c/kT}\right)(\gamma + \gamma_0). \qquad (7.5)$$

A fit to this model gives the strain in a film as a function of substrate temperature and deposition rate. Additionally, the rate limiting step in the misfit accommodation process can be determined.

The study of strain relaxation during anneal is proposed. As the temperature approaches the Curie point, the magnitude of the magnetostatic energy, $2\pi M_s^2$, will decrease. Thermal expansion will result in a change in strain in the film as a function of

temperature. Both these factors are easily predicted quantitatively and can be accounted for in the analysis. Measurements of K^{eff} over time at the annealing temperature can be directly related to strain relaxation over time. Again, this type of measurement is best described by an equation such as Equation (7.5).

We propose a series MOKE measurements on samples of Cu/Ni/Cu/NaCl (001). A sufficiently smooth NaCl surface (free of cleavage steps), is necessary. Such a surface could be achieved with polishing of NaCl (001). A comparison with of these results with measurements made on Cu/Ni/Cu/Si (001) should prove useful. Comparison between moiré fringe measurements of strain made on NaCl substrate samples and curvature measurements of strain made on Si substrate samples shows good agreement (see Chapter 4). Comparison of anisotropy data would therefore be an indication of the effect of surface roughness on these measurements, as this appears somewhat different for the two deposition conditions.

Additional experiments are necessary to determine the accuracy of MOKE as a method of strain measurement. Unfortunately, the very reason for developing the technique is a hindrance to making this assessment. A highly accurate method of *in situ* strain measurement for epitaxial magnetic thin films is not readily available. One of the most conclusive methods of measuring strain in epitaxial thin films is measurement of the lattice spacing of the film using x-ray diffraction. Unfortunately the thickness regime of interest in misfit accommodation is generally very small. Sufficient intensity for lattice spacing measurement is often not achievable with a conventional rotating anode x-ray source. Often a synchrotron source is necessary. Design of an experiment in which lattice spacing could be determined using synchrotron radiation and MOKE measured, both *in situ* is a formidable task. *Ex situ* experiments could be done, but error is introduced any time oxidation takes place due to the fact that the presence of the oxide will affect the surface magnetic properties of the film as well as affecting the strain.

One way that synchrotron radiation could be used for this work is using a technique called grazing incidence x-ray spectroscopy (GIXS). Using this technique, a depth profile of the strain in the film can be measured. Since the strain in the film is high near the dislocated interface as compared to the free surface, this type of analysis would

be a more complete picture of the strain state of the film than measures of an average strain across the film thickness. GIXS measurement could be used in conjunction with imaging of the magnetic domains in these films to determine the effect on the magnetic anisotropy of the local strain fields surrounding the dislocations.

In summary, use of MOKE can be useful as an *in situ* strain measurement. The ability to measure strain accurately during growth and during *in situ* anneal has many advantages. A major goal of the use of this technique is the advancement of the understanding of the kinetic limitations of misfit accommodation. With this information, it becomes possible to fabricate thin films with controlled strain levels and misfit dislocation distributions, and therefore with desired magnetic properties.

8. APPENDIX: THE Cu/Si INTERFACE

8.1 Cu/Si EPITAXY

Although the focus of this work has been the study of the Ni/Cu interface, it was necessary to study the Cu/Si interface in order to determine what effects its properties were having on the strain state through the thickness of the layers. Specifically, the issues which prompted an extensive investigation of the interface were discussed in Chapters 4 and 5. In Chapter 4, the strain in the Ni film was calculated from the change in curvature due to film deposition. In order to make this calculation, it was necessary to isolate the change in curvature due to the Ni alone. It was determined that the curvature change due to a Cu film alone was not the same as the curvature change due to a Cu film when covered by a Ni film. In Chapter 6, annealing of deposited samples was performed. In order to understand the curvature response of the wafer during the anneal, it was necessary to understand the strain behavior of the Cu films and of the Cu/Si interface during the anneal. Cu/Si turns out to be a fairly complex system due to its tendency to form a silicide at the interface. The formation of this silicide and subsequent silicon oxide formation has been studied in conjunction with this work.

The reason for depositing the Cu on a Si substrate was discussed in Chapter 2. A readily attainable, single crystal (001) substrate was needed for deposition of a high quality (001) Cu film. Cu is known to grow epitaxially on Si.[68] Therefore Si was a reasonable choice for a substrate material. Also, since Si is generally polished so that it is optically flat, it provides an ideal material for the optical Kerr effect measurements.

It has been shown by several researchers, most notably Chang,[68] that Cu can be deposited epitaxially on Si at room temperature. Since (001) Si is readily available,

reasonably affordable, and optically flat, it was the most likely candidate as a substrate material. It is not immediately obvious that Cu (001) would grow epitaxially on Si since there is a large difference in lattice constants of the two materials. The lattice constants of Cu and Si are 3.615Å and 5.430Å, respectively, giving a misfit of 50%. To reduce the energy of the system and create an epitaxial film, the Cu atoms will have a tendency to line up with the Si (001) surface such that the Cu lattice is rotated by 45° with respect to the Si in the plane of the film. In other words, the Cu is alligned such that the [110] axis of the Cu is parallel to the [010] axis of the Si. This orientation results in a 6% misfit at the interface which is low to allow epitaxy, but high enough to produce a highly dislocated interface. This effect is illustrated in Figure 8.1 and Figure 8.2, which shows x-ray pole figures of the (111) peaks of both Si and Cu on the same (001) sample showing the expected four-fold symmetry. It can be seen from this figure that the Cu lattice is rotated by 45° with respect to the Si lattice in the plane of the interface.

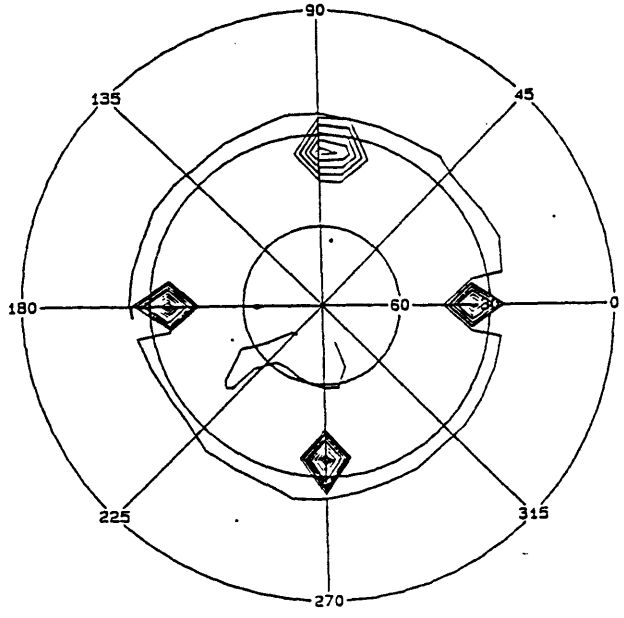

Figure 8.1 Si (111) pole figure

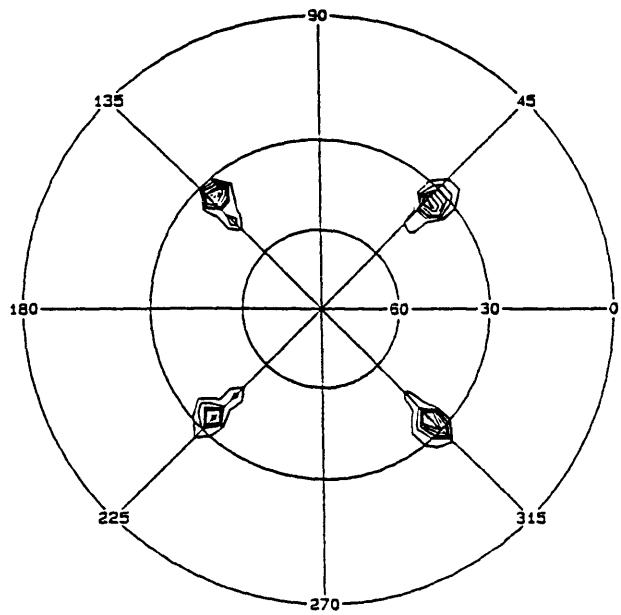

Figure 8.2 Cu (111) pole figure

8.2 SILICIDE FORMATION

It is well known that Cu and Si react readily to form copper silicide.[68,69,70,71,72,73,74] Cu diffuses extremely rapidly in Si.[70] A portion of the Cu-Si phase diagram, shown in Figure 8.3, shows several intermetallic phases. The silicide most often observed at room temperature is the orthorhombic phase η"-Cu_3Si.[71,72] In the case of a Cu deposition on a Si wafer, the deposition conditions determine which type, if any, silicide will form. At low (<200°C) temperatures, the silicide that forms is Cu_3Si. Bai et al.[71] and Li et al.[72] both observed the formation of η"-Cu_3Si (a = 76.76Å, b = 7.00Å, c = 21.94Å)[70] in the Cu/Si (111) and Cu/Si (100) system respectively. It is interesting to note that although there exist several other phases between pure Cu and Cu_3Si, they do not form at low temperatures.[70] At higher temperatures, there tends to be some of the cubic Cu_5Si phase forming in the Cu_3Si matrix.[73] Chang[68] observes the formation of the tetragonal phase (a = 7.267Å, c = 7.892Å) η'-Cu3Si at about 200°C. Chang also notes that the Cu-Si reaction is significantly faster for (100) oriented films than for (111) films, as determined by Rutherford backscattering spectroscopy (RBS).[68]

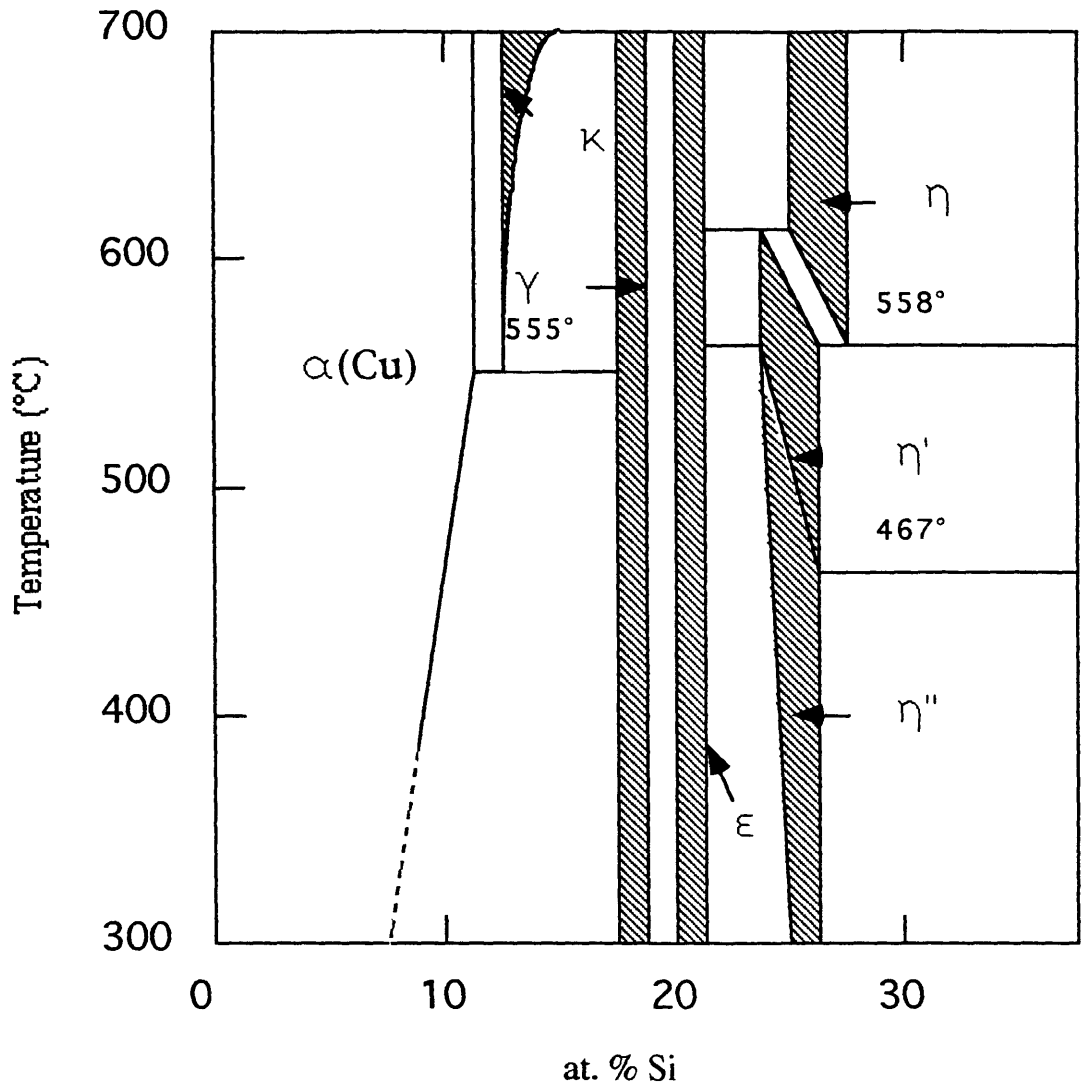

Figure 8.3 Cu-Si phase diagram

There is general agreement that rapid silicide formation begins at 150° - 200°C. The films in this work were all deposited at room temperature in order to inhibit silicide formation. Figure 8.4 shows a cross-sectional TEM micrograph of the Cu/Si interface in the as-deposited state. It can be seen that the interface is sharp, with the Cu growing epitaxially on the Si in the (100) orientation.

Our observations indicate that although the film is initially epitaxial, silicide formation occurs at room temperature over a moderate period of time (on the order of months), and at elevated temperature (>100°C) within hours, to a maximum thickness of

about 100Å. Several of the peaks for the orthorhombic phase are present in a standard theta-two theta x-ray diffraction pattern.

8.3 OXIDE GROWTH

It has been shown by some researchers[73,74,75,76] that the presence of the silicide tends to enhance the oxidation of the silicon according to the reaction

$$Cu_3Si + 2O \rightarrow SiO_2 + 3Cu.$$

The extent of the oxidation reaction seems to be limited only by the thickness of the silicide. Harper, et al.[5] observed oxide growth as thick as 2μm.

Experimental evidence shows that the presence of the Ni layer has an effect on the interfacial reaction behavior. Measurements were made using a wafer curvature measurement system available to us at Harvard University.[77] The system uses reflection of a laser from the wafer surface to measure curvature in the same manner as the Tencor commercial system discussed in Chapter 6. Like the Tencor system, the capability exists for heating the sample and monitoring the curvature during the anneal. In this case, however, the wafer is actually inside a vacuum chamber, reducing the likelihood of oxidation during anneal. The chamber is evacuated to 10^{-6} Torr and backfilled with He during the anneal.

It was suspected from high temperature radius of curvature measurements performed using this equipment that the presence of the Ni overlayer affected either silicide formation or subsequent Si oxidation. Figure 8.7 and Figure 8.8 show plots of radius of curvature versus time for Cu/Si and for 100Å Ni/Cu/Si. The relaxation of the film with the Ni overlayer shows the expected relaxation of the compressive strain

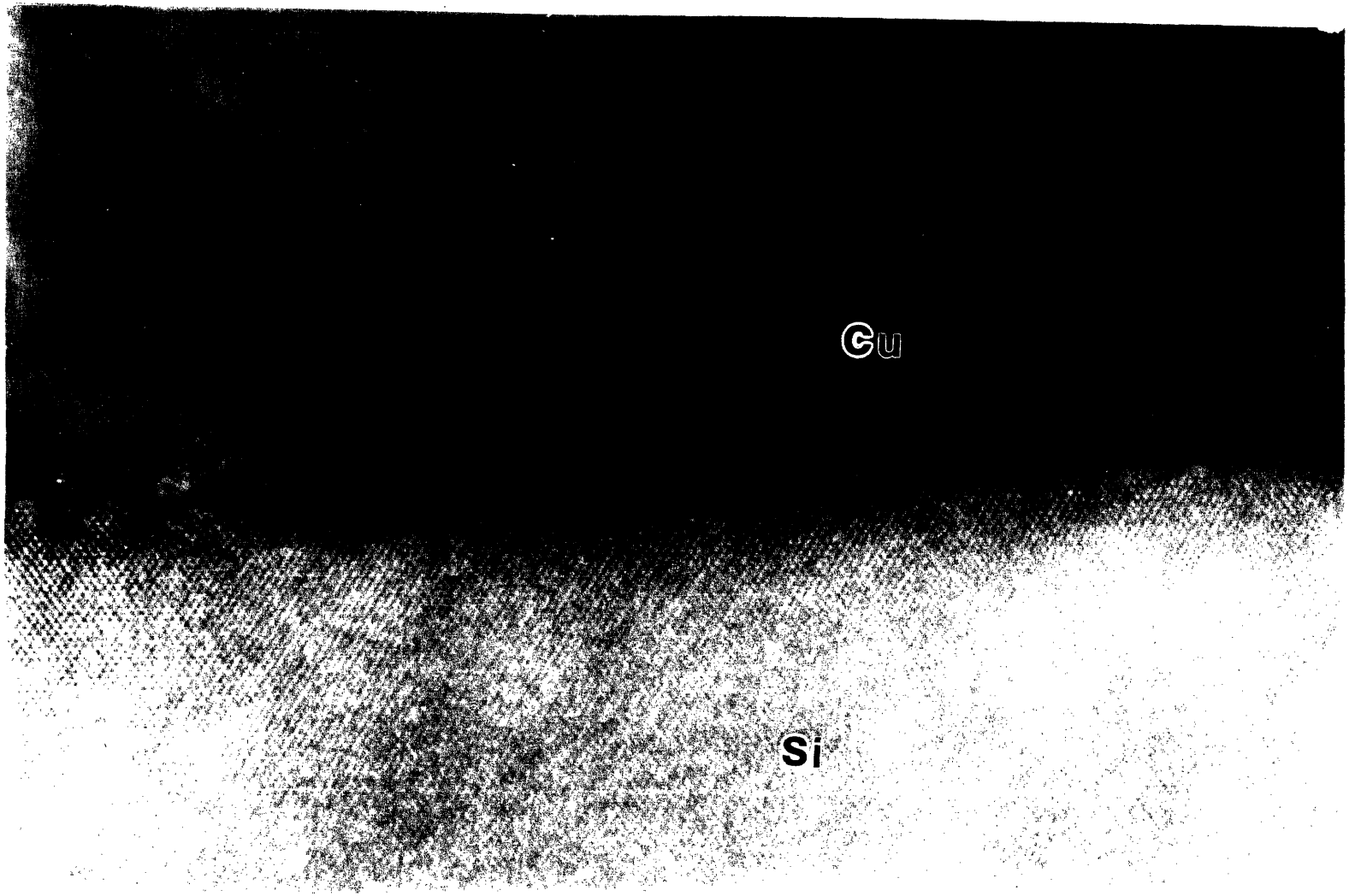

Figure 8.4 Cross-sectional TEM of as-deposited Cu/Si interface. No evidence of silicide is present.

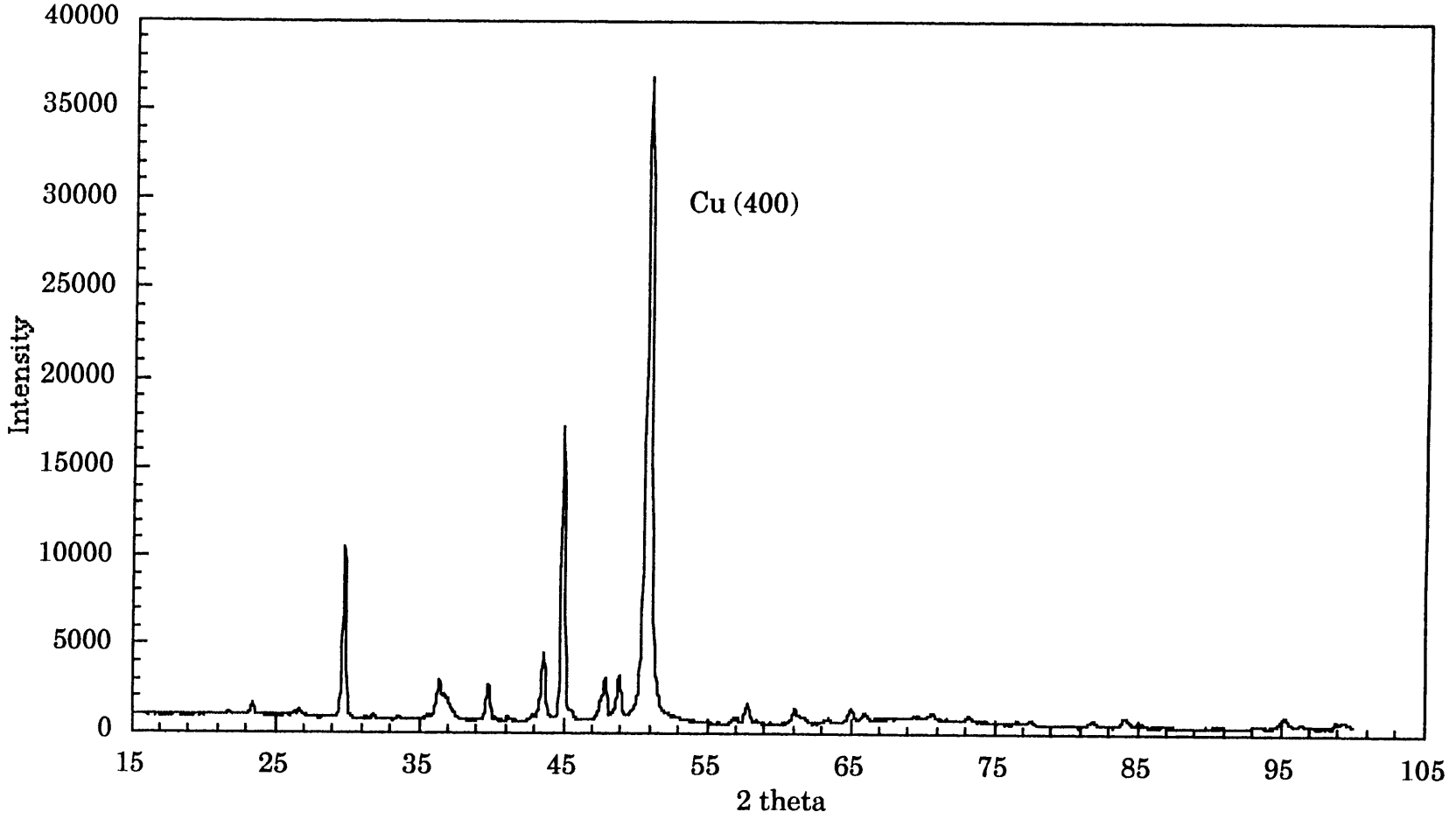

Figure 8.5 X-ray diffraction pattern of annealed Cu/Ni/Cu/Si

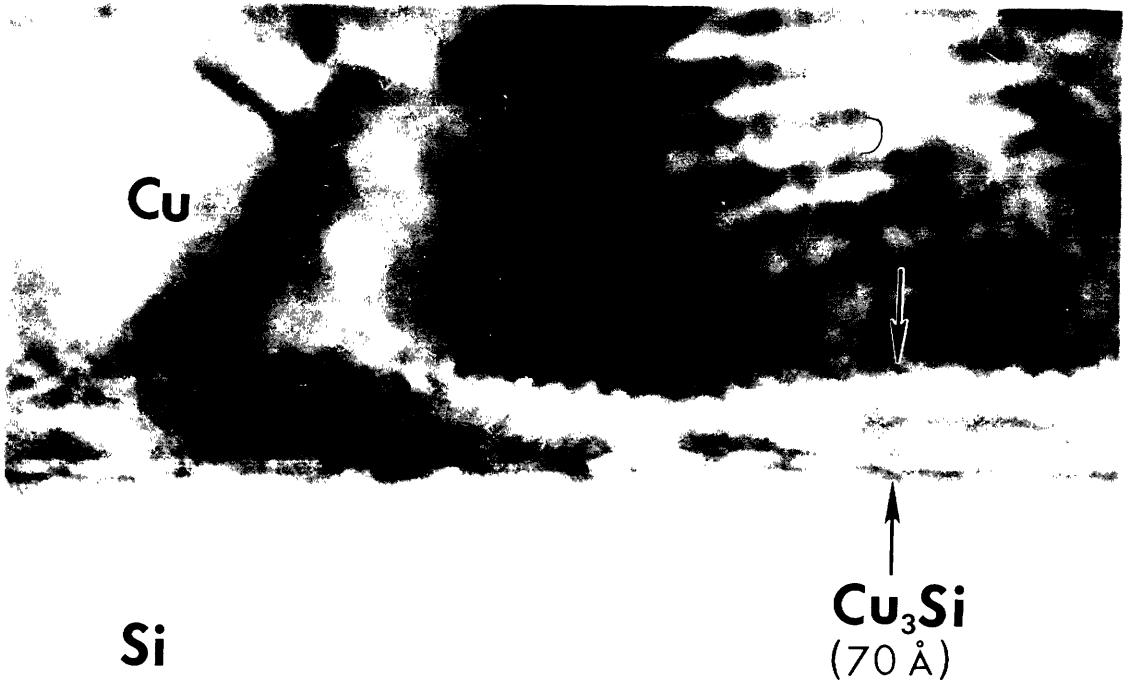

Figure 8.6 Cross sectional TEM of Cu/Si interface showing silicide region

induced by thermal expansion as discussed in Chapter 6. The relaxation of the Cu/Si sample, however is different. The strain begins decreasing toward zero as expected, but becomes more compressive after about 6 hours. This increase in strain is due to a possible phase change. The increase in strain energy must be offset by some other energy drop, and the most likely candidate is silicide formation and subsequent oxidation.

Rutherford backscattering spectroscopy (RBS) is an experimental technique whereby a collimated beam of MeV ^{4}He ions is scattered off a sample. A semiconductor nuclear particle detector is used to detect the energy of the scattered ions. The ions are scattered from the target atom via Coulomb repulsion. The energy of the scattered ion is therefore dependent on the mass of the target atom. In the case of scattering from a thin film, the RBS spectrum will have a peak at the energy associated with the target material, and the peak-width will be proportional to the thickness of the film.

An experiment was performed in which a film of 2000Å Cu was deposited on one Si wafer and 50Å Ni/2000ÅCu was deposited on another. RBS was performed on these wafers shortly after deposition[78] and the results are shown in Figure 8.9 and Figure 8.10. Peaks corresponding to the film and Si substrate can be seen. No detectable intermixing between the layers occurred. The wafers were then reintroduced to the vacuum chamber and annealed simultaneously at 150°C for a period of several hours. The RBS spectra were again acquired and the results are shown in Figure 8.11 and Figure 8.12. Intermixing (silicide formation) is evident in both samples via a broadening of the Si and Cu peaks. However, an oxygen peak is clearly visible in the spectrum of the Cu/Si sample and not present in that of the Ni/Cu/Si sample. This result shows inhibition of the oxide formation at the Cu/Si interface by the presence of the Ni film. It is important to realize that the samples were annealed in vacuum and allowed to cool before removal from the chamber. The oxidation took place, therefore, at room temperature after the silicide had formed.

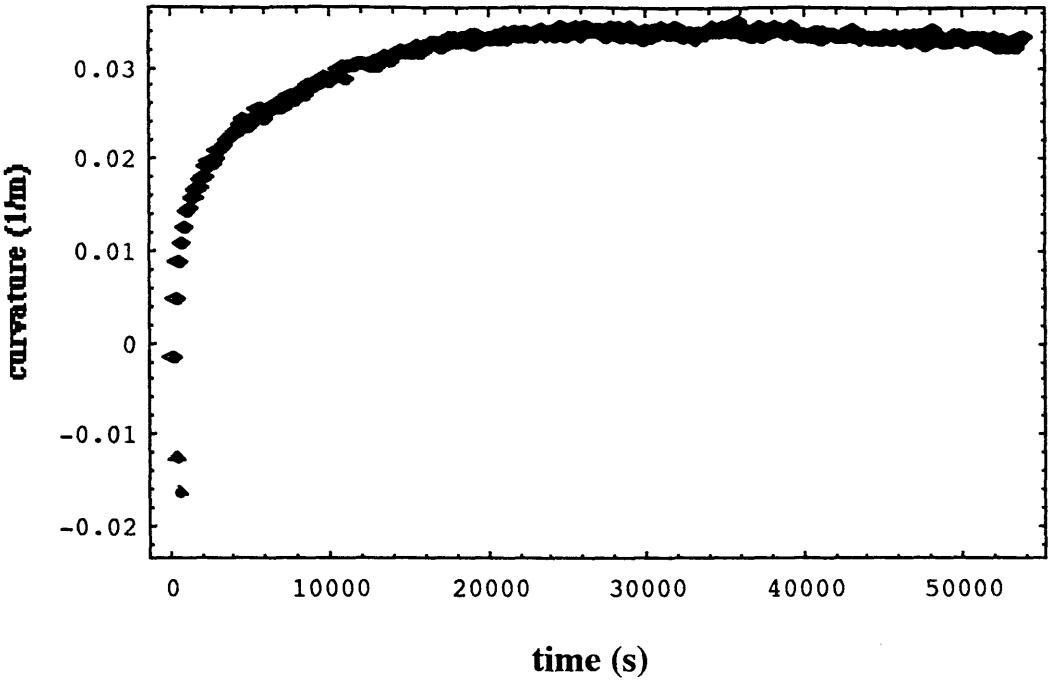

Figure 8.7 Relaxation over time at 150°C of Ni/Cu/Si

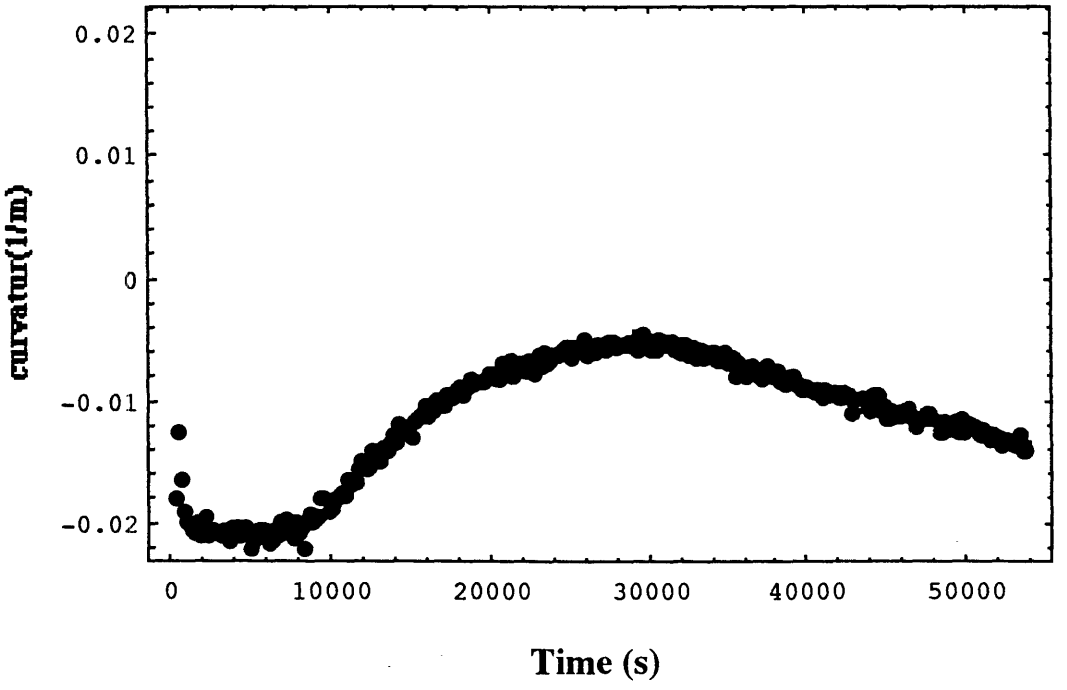

Figure 8.8 Relaxation over time at 150°C of Cu/Si

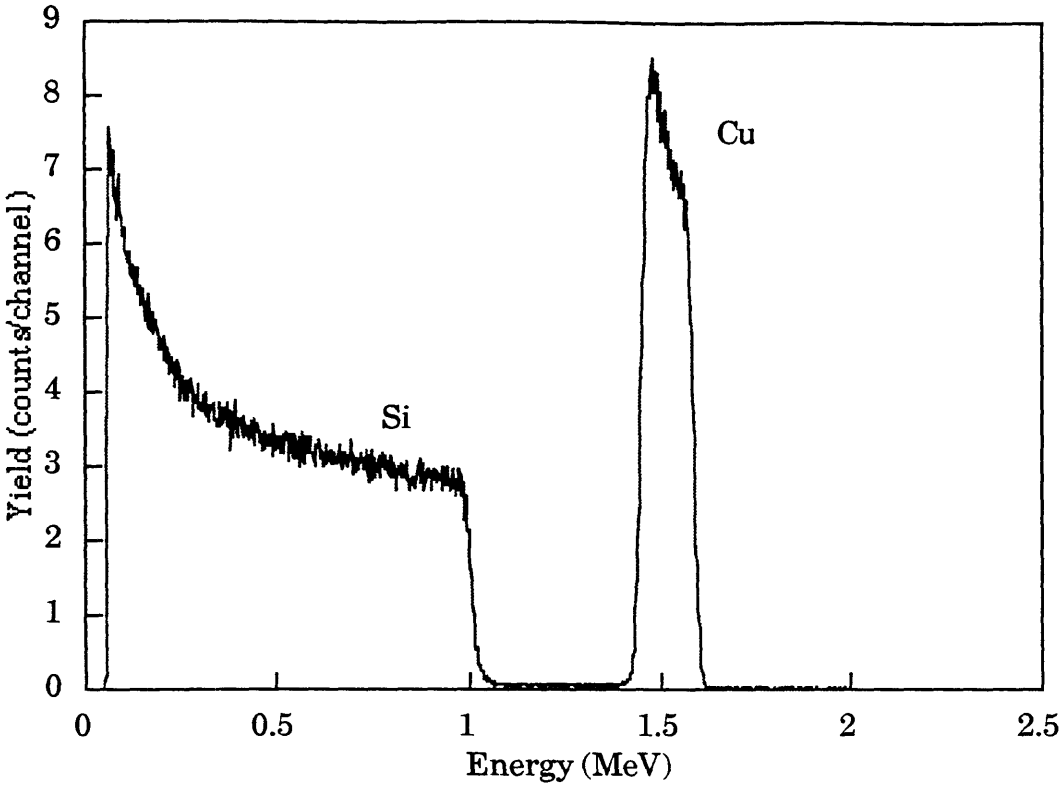

Figure 8.9 RBS of Cu/Si as deposited

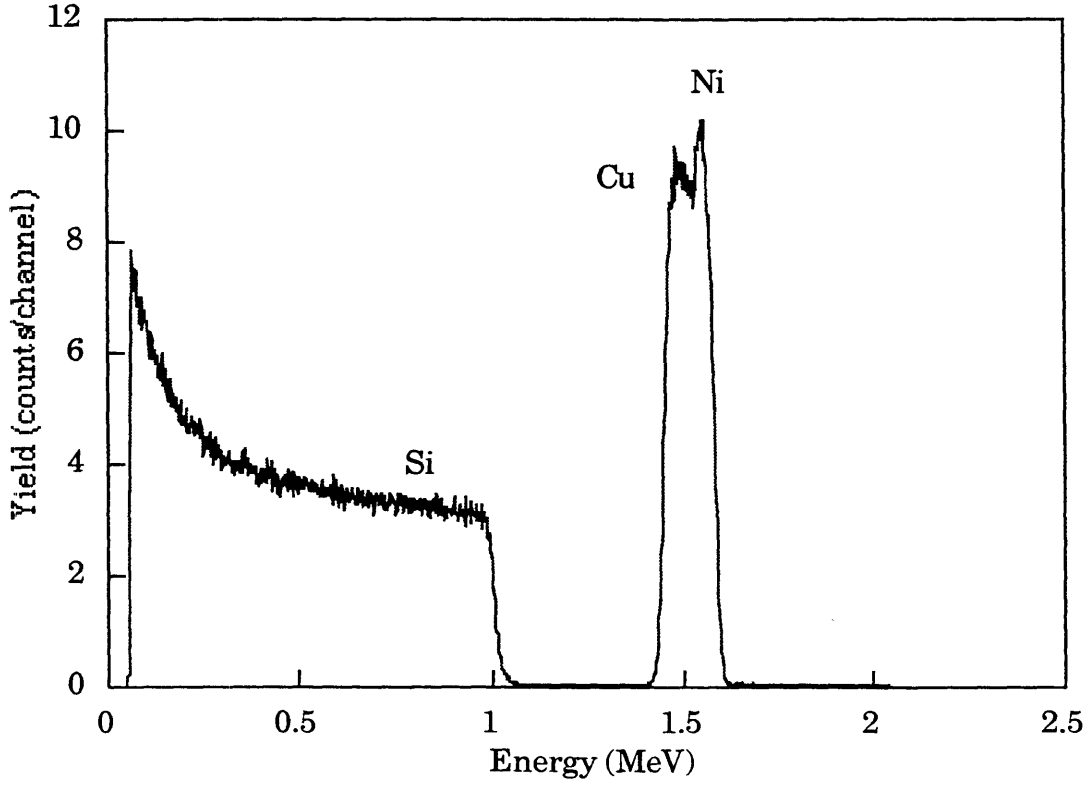

Figure 8.10 RBS of 100Å Ni/Cu/Si as deposited

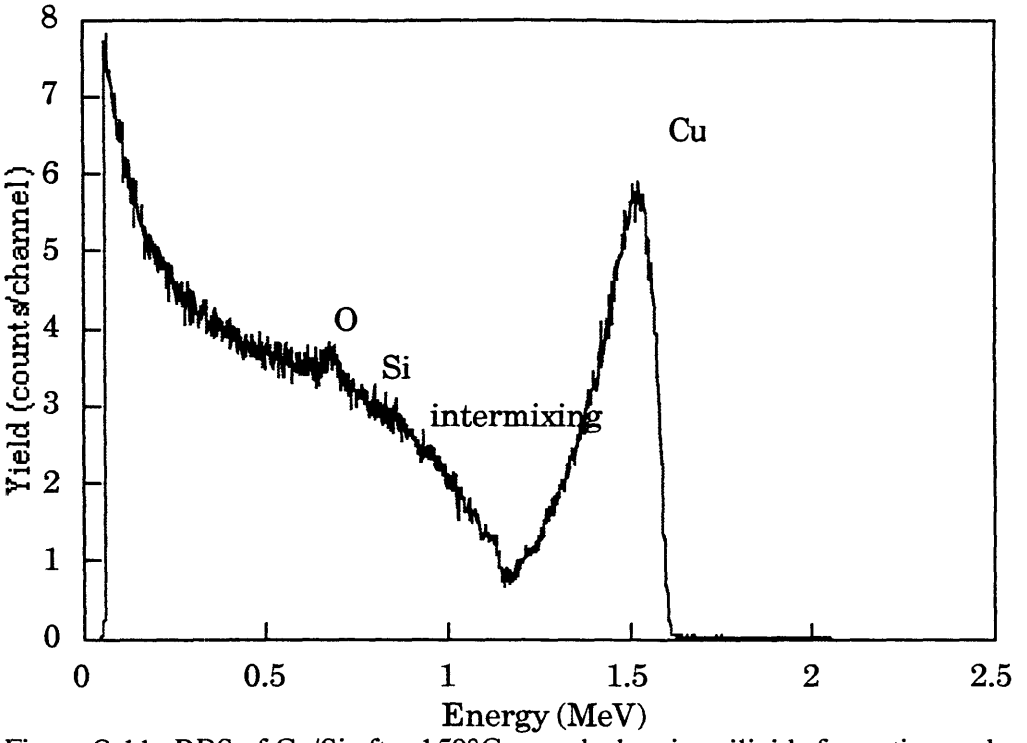

Figure 8.11 RBS of Cu/Si after 150°C anneal, showing silicide formation and oxidation

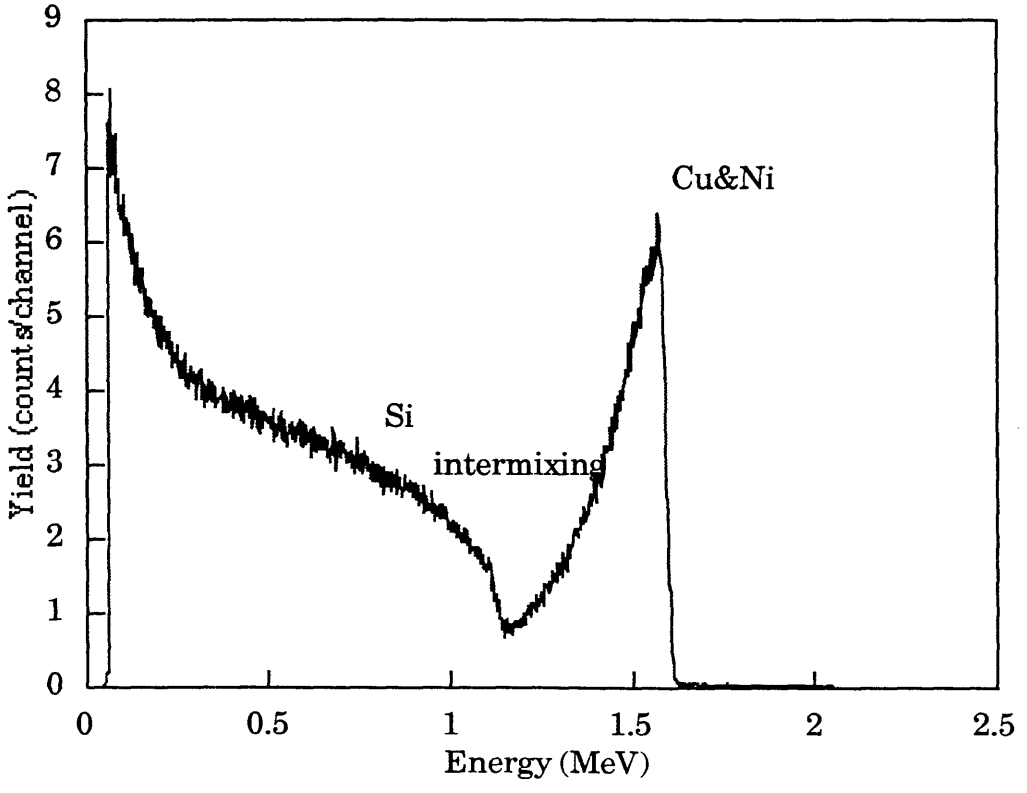

Figure 8.12 RBS of 100Å Ni/Cu/Si after 150°C anneal, showing silicide formation, but no oxidation

8.4 DISCUSSION

This investigation into the nature of the Cu/Si interface produced some interesting results. The enhancement of oxidation of Si in the presence of a Cu film has been observed by a few researchers, but is poorly understood. The main question is the mechanism by which the oxygen reaches the interface. Diffusion of Cu through Cu_2O is quite slow at room temperature.[65] This transport mechanism could not be the active one in this system since the epitaxial Cu layer appears undisturbed. Diffusion of oxygen through Cu at room temperature is virtually zero, as measured in bulk systems.[65] Another possible transport path is along the interface itself, starting from the edge of the wafer. The discovery that the presence of the Ni apparently inhibits oxidation at the Cu_3Si/Si interface is evidence, however, that the oxygen arrives at the interface from the surface.

Several steps were taken to minimize the effect of silicide/oxide formation on the strain state of the system. First, as indicated before, the films were deposited at room temperature. The samples were kept at or below room temperature during processing for TEM sample preparation. Additionally, the Cu layer was grown to a thickness of 2000Å. Since the silicide thickness observed was on the order of 100Å, 2000Å was sufficiently thick to ensure a relaxed Cu surface. Also, the curvature change of Cu/50Å Ni/Cu/Si films during anneal were compared to the curvature change of a Cu/10Å Ni/Cu/Si film annealed under the same conditions rather than to the curvature change of a Cu/Si film for the strain measurements discussed in Chapter 6.

REFERENCES

[1] I. J. Fritz, S. T. Picraux, L. R. Dawson, T. J. Drummond, W. D. Laidig, and N. G. Anderson, *Appl. Phys. Lett.* **46**, 967 (1985).

[2] G. J. Whaley and P. I. Cohen, *Appl. Phys. Lett.* **57**, 144 (1990).

[3] G. Bochi, Ph. D. thesis, MIT, 1995.

[4] R. Hull and J. C. Bean, *Appl. Phys. Lett.* **54**, 925 (1989).

[5] G. Springholtz, N. Frank, and G. Bauer, *Appl. Phys. Lett.* **64**, 2970 (1994).

[6] F. G. Celii, L. A. Files-Sesler, E. A. Beam III, and H. Liu, *J. Vac. Sci. Technol. A* **11**, 1796 (1993).

[7] S. Yang, M. Yu, G. Meigs, X. H. Feng, and E. Garfunkel, *Surface Science* **205**, L777-L785 (1988).

[8] C. P. Flynn, *Journal of Physics F* **18**, L195-L200 (1988).

[9] C.-A. Chang, *Surface Science Letters* **237**, L417-420 (1990).

[10] D. W. Gidley, *Phys. Rev. Lett.* **62**, 811-814 (1989).

[11] A. Chambers and D. C. Jackson, *Thin Solid Films* 1357-1371 (1975).

[12] S. A. Chambers, H. W. Chen, I. M. Vitomirov, S. B. Anderson, and J. H. Weaver, *Phys. Rev. B* **33**, 8810-8813 (1986).

[13] P. F. A. Alkemade, H. Fortuin, R. Balkenende, F. H. P. M. Habraken, and W. F. v. d. Weg, *Springer Series in Surface Science* (edited by p. 443-449. Springer Verlag, New York (1987).

[14] J. W. Matthews and J. L. Crawford, *Thin Solid Films* **5**, 187-198 (1970).

[15] E. R. Thompson and K. R. Lawless, *Appl. Phys. Lett.* **9**, 138-140 (1966).

[16] L. H. Bennet, L. J. Swartzendruber, D. S. Lashmore, and R. Oberle, *Phys. Rev. B* **40**, 4633-4637 (1989).

[17] R. Jungblut, M. T. Johnson, J. a. d. Stegge, A. Reinders, and F. J. A. d. Broeder, *J. Appl. Phys.* **75**, 6424 (1994).

[18] J. Tersoff and L. M. Falicov, *Phys. Rev. B* **26**, 6186-6200 (1982).

[19] L. R. Sill, M. B. Brodsky, S. Bowen, and H. C. Hamaker, *J. of Appl. Phys.* **57**, 3663-3665 (1985).

[20] J. Voigt, X. L. Ding, R. Fink, G. Krausch, B. Luckscheiter, R. Platzer, U. W_hrmann, and G. Schatz, *J. of Mag. and Magnetic Mater.* **93**, 341-344 (1991).

[21] R. Naik, C. Kota, J. S. Payson, and G. L. Dunifer, *Phys. Rev. B* **48**, 1008-1013 (1993).

[22] J. W. Matthews, S. Mader, and T. B. Light, *J. Appl. Phys.* **41**, 3800 (1970).

[23] J. Y. Tsao, *Materials Fundamentals of Molecular Beam Epitaxy*, p. .Academic Press, Boston (1993).

[24] B. W. Dodson, *J. Cryst. Growth* **111**, 376 (1991).

[25] S. Jang, H. Kim, and R. Reif, *Appl. Phys. Lett.* **61**, 315-317 (1992).

[26] B. J. Spencer, P. W. Voorhees, and S. H. Davis, *J. of Appl. Phys.* **73**, 4955-4970 (1993).

[27] B. W. Dodson and J. Y. Tsao, *Appl. Phys. Lett.* **51**, 1325 (1987).

[28] S. Chickazumi, *Physics of Magnetism*, p. . Robert E. Krieger Publishing Company, Malabar, Florida (1964).

[29] L. Neél, *J. Phys. Radium* **15**, 227 (1954).

[30] D. S. Chuang, MIT Ph.D. thesis (1994).

[31] G. H. Olsen and J. C. Botha, *J. Appl. Phys.* **43**, 3581-3583 (1972).

[32] P. F. A. Alkemade, H. Fortuin, R. Balkenende, and F. H. P. M. Habraken, *Surface Science* **225**, 307-318 (1990).

[33] A. Kidron, *Phys. Rev. Lett.* **22**, 774-776 (1969).

[34] B. Mozer, D. T. Keating, and S. C. Moss, *Phys. Rev.* **175**, 868-876 (1968).

[35] R. A. Oriani and W. K. Murphy, *Acta Metall.* **8**, 23-25 (1960).

[36] G. H. Olsen and J. C. Botha, *J. Appl. Phys.* **43**, 3581-3583 (1972).

[37] J. Vrijen and S. Radelaar, *Phys. Rev. B* **17**, 409-421 (1978).

[38] *ASM Binary Phase Diagrams*, T. B. Massalski, ed.

[39] P. B. Hirsch, A. Howie, R. B. Nicholson, D. W. Pashley, and M. J. Whelan, *Electron Microscopy of Thin Crystals*, p.156-206.Butterworths, Washington (1965).

[40] J. W. Menter, *Advances in Physics: A Quarterly Supplement of the Philosophical Magazine* **7**, 299-348 (1958).

[41] J. Weertman and J. R. Weertman, *Elementary Dislocation Theory* (The MacMillan Company, New York, 1964), p. 93.

[42] J. M. Bonar, R. Hull, J. F. Walker, and R. Malik, *Appl. Phys. Lett.* **60**, 1327 (1992).

[43] M. Albrecht, H. P. Strunk, P. O. Hansson, and E. Bauser,*Mater. Res. Soc. Symp. Proc.* **238,** 79 (1992).

[44] C. A. Volkert, E. A. Fitzgerald, R. Hull, Y. H. Xie, and Y. J. Mii, *J. of Elec. Mater.* **20**, 833 (1991).

[45] E. P. Kvam, D. M. Maher, and C. J. Humphreys, *J. Mater. Res.* **5**, 1900 (1990).

[46] R. Hull and J. C. Bean, *J. Vac. Sci. Technol. A* **7**, 2580 (1989).

[47] R. Hull, J. C. Bean, L. J. Peticolas, B. E. Weir, K. Prabhadaran, and T. Ogino, *Appl. Phys. Lett.* **65**, 327 (1994).

[48] J. Washburn, E. P. Kvam, and Z. Liliental-Weber, *J. of Elec. Mater.* **20**, 155 (1991).

[49] J. Narayan and S. Sharan, *Mat. Sci. and Eng. B* **10**, 261-267 (1991).

[50] E. A. Fitzgerald, D. G. Ast, P. D. Kirchner, G. D. Pettit, and J. M. Woodall, *J. Appl. Phys.* **63**, 693 (1988).

[51] K. H. Chang, P. K. Bhattacharya, and R. Gibala, *J. Appl. Phys.* **66**, 2993 (1989).

[52] F. R. N. Nabarro, *Theory of Crystal Dislocations*, p. 26.Dover Publications, Inc., New York (1987).

[53] W. A. Jesser and J. H. v. d. Merwe, *J. Appl. Phys.* **75**, 872 (1994).

[54]J. Washburn, G. Thomas, and H. J. Queisser, *J. Appl. Phys.* **35**, 1909 (1964).

[55] H. E. Inglefield, C. A. Ballentine, G. Bochi, S. S. Bogomolov, R. C. O'Handley, and C. V. Thompson,*Mater. Res. Soc. Conf. Proc.* **308,** 765 (1993).

[56] W. D. Nix, *Met. Trans. A* **20A**, 2217-2245 (1989).

[57] Gronet, as reported in W. D. Nix, *Met. Trans. A* **20A**, 2217-2245 (1989).

[58] G. G. Stoney, *Proc. Royal Soc. London* **A82**, 172 (1909).

[59] M. Ohring, *The Materials Science of Thin Films*

[60] J. Tao, L. H. Lee, and J. C. Bilello, *J. of Elec. Mater.* **20**, 819 (1991).

[61] D. I. Westwood and D. A. Woolf, *Journal of Applied Physics* **73**, 1187 (1993).

[62] D. Jiles, *Magnetism and Magnetic Materials*, p. 57 .Chapman and Hall, New York (1991).

[63] G. Bochi, C. A. Ballentine, H. E. Inglefield, S. S. Bogomolov, C. V. Thompson, and R. C. O'Handley,*Mater. Res. Soc. Symp. Proc.* **313,** 309 (1993).

[64] C. A. Ballentine, Ph.D., University of Texas at Austin (1989).

[65] W. D. Kingery, H. K. Bowen, and D. R. Ullman, *Introduction to Ceramics*, 2, p. 58 .John Wiley and Sons, New York (1976).

[66] C. K. Kim, Ph. D. MIT, 1991.

[67] I. Hashim, B. Park, and H. A. Atwater, (1992).

[68] C.-A. Chang, *Journal of Applied Physics* **67**, 566-568 (1990).

[69] J. Li, Y. Shacham-Diamand, and J. W. Mayer,*Materials Science Reports* **9**, 1-51 (1992).

[70] G. Weber, G. Billot, and P. Barret, *Physica Status Solidi a* **75**, 567-576 (1983).

[71] P. Bai, G. Yang, L. You, T. Lu, and D. B. Knorr, *J. Mater. Res.* **5**, 989-997 (1990).

[72] J. Li, J. W. Mayer, L. J. Matienzo, and F. Emmi, *Materials Chemistry and Physics* **32**, 390-393 (1992).

[73] J. M. E. Harper, A. Charai, L. Stolt, F. M. D'Heurle, and P. M. Fryer, *Appl. Phys. Lett.* **56**, 2519-2521 (1990).

[74] J. Li, J. W. Mayer, L. J. Matienzo, and F. Emmi, *Materials Chemistry and Physics* **32**, 390-393 (1992).

[75] M. Setton, J. V. d. Spiegel, and B. Rothman, *Appl. Phys. Lett.* **57**, 357-359 (1990).

[76] S. H. Corn, J. L. Falconer, and A. W. Czanderna, *Journal of Vacuum Science and Technology A* **6**, 1012-1016 (1988).

[77] work done in association with Jennifer Mullin and Frans Spaepen at Harvard University.

[78] collaboration with Dr. K. Das Chowdhury, MIT.